SAND79-1026
Unlimited Release
UC-62

Receiver Assembly Design Studies for 2-m 90° Parabolic-Cylindrical Solar Collectors

Arthur C. Ratzel

Prepared by Sandia Laboratories, Albuquerque, New Mexico 87185
and Livermore, California 94550 for the United States Department
of Energy under Contract DE-AC04-76DP00789

Printed September 1979

Sandia Laboratories

SF 2900 Q(7-73)

Issued by Sandia Laboratories, operated for the United States Department of Energy by Sandia Corporation.

Printed in the United States of America

Available from
National Technical Information Service
U. S. Department of Commerce
5285 Port Royal Road
Springfield, VA 22161
Price: Printed Copy **$6.00**; Microfiche $3.00

Distribution
Category UC-62

SAND79-1026

RECEIVER ASSEMBLY DESIGN STUDIES FOR 2-m 90° PARABOLIC-CYLINDRICAL SOLAR COLLECTORS

Arthur C. Ratzel
Fluid Mechanics & Heat Transfer Division II - 5512
Sandia Laboratories

ABSTRACT

This report presents results from a parametric study of the Sandia Laboratories' second-generation 2-m, 90° parabolic-cylindrical solar collector design. A computer simulation was developed to provide cumulative all-day performance results or instantaneous solar-noon results for three annular solar receiver assemblies: 2.223-, 2.54-, and 3.175-cm-o.d. tubes with concentric glass jackets. Representative clear spring, summer, and winter conditions for Albuquerque, NM, were modeled. Design problems considered in the analysis included misalignment of the receiver assembly from the focal line, reflector trough tracking bias, variation in receiver tube operating temperature, and variation in the reflector trough one-dimensional slope errors and two-dimensional mirror errors. Changes in collector material radiative properties and wind effects are also summarized, and comparative performance results for evacuated versus nonevacuated annular receivers are given. Summarized performance results for all studies are provided graphically.

For operating receiver-tube temperatures < 475 K, the 3.175-cm receiver tube provides the best overall collector performance results. For higher operating temperatures where detrimental receiver heat losses become more significant, the smaller 2.54-cm tube is more effective for solar energy collection.

ACKNOWLEDGMENTS

Appreciation is expressed to F. Biggs, 4237, who assisted in modifying the simulation code EDEP used in the parametric study and to S. B. Martin, 2323, who initiated the problem and served as consultant during development and interpretation of simulation results.

TABLE OF CONTENTS

ILLUSTRATIONS

TABLES

RECEIVER ASSEMBLY DESIGN STUDIES FOR 2-m 90° PARABOLIC-CYLINDRICAL SOLAR COLLECTORS

Introduction

An effective device for the collection of solar energy that has received widespread attention is the so-called parabolic-cylindrical solar collector. In this device, a circular receiver tube, with suitable selective coating, is enclosed by a concentric glass envelope and situated along the focal line of a parabolic trough reflector. The reflector trough is positioned so that the incident solar radiation will be reflected to the receiver assembly. This energy is absorbed by a working fluid circulating through the receiver tube and can be used to produce electricity, process steam, air conditioning, or even hot water.

Significant efforts have addressed optimizing the components of the parabolic-cylindrical collector. Studies to improve the performance characteristics of annular solar receiver, for example, have considered effects of receiver tube and glass envelope eccentricity and have considered different heat-loss reduction techniques including evacuation of the annulus gas and replacement of the gas with high molecular-weight fill gases.[2,3] Material technology improvements have included developing thin sagged glass reflector mirror panels[4] and durable black-chrome absorbing coatings for receiver tubes.[5] As a result of these and other improvements in reflector support structure, tracking, and receiver assembly design, it is expected that more economic parabolic-cylindrical solar-collector systems will be produced in the future.

In order to assess the overall performance of a collector system, however, the components must be considered together. Tradeoffs to

optimize the design must be based on both the operating constraints and design weaknesses of each component. This work reports on such a study developed to optimize a 2-m, 90° parabolic-cylindrical solar collector to be used at the Sandia/Department of Energy (DOE) Midtemperature Solar Systems Test Facility (MSSTF). Results to be presented have been obtained from a computer simulation developed to model east-west (E-W)-oriented parabolic collector troughs with annular receiver assemblies.

Although specific design constraints have been selected for this work, off-design effects are considered to provide sensitivity data and to present additional results useful for designing collectors for different applications (other than production of 589 K Therminol-66 (T-66) required at the MSSTF). Three annular solar receivers (2.223-, 2.54-, and 3.175-cm receiver tubes with appropriate glass jackets) are compared in this study, assuming that the trough aperture is fixed at 2-m. In addition, the trough is assumed to be aligned on an E-W axis in Albuquerque, NM. Representative clear spring, summer, and winter conditions are modeled. Off-design factors that are specifically addressed include (1) horizontal and vertical misalignment of the receiver assembly, (2) tracking bias, (3) variation of operating temperature, and (4) variation of reflector trough one-dimensional slope errors and two-dimensional mirror errors. Results are presented graphically for all conditions studied.

Computer Simulation

Analysis of parabolic-cylindrical solar collectors under varied operating constraints was performed using a general-purpose computer simulation to model both instantaneous solar-noon and cumulative all-day collector performances. Maximum collector performance results are obtained from solar-noon studies. The E-W orientation of the collector dictates cumulative studies as well since collector errors

associated with solar radiation path-lengths increase at off-solar-noon conditions, reducing collector performance. In addition, all-day results are more useful for sizing solar collector systems.

The computer simulation has two major components--a solar radiation deposition model and a receiver heat-loss model. Each component is described in the following two sections, respectively. A third section describes the simulation organization. In addition, the organization section specifies the input parameters required and defines the collector efficiency to be used in interpreting collector performance results.

Solar-Energy Deposition Model

The computer simulation uses a modified version of a solar-energy deposition program created by F. Biggs, known as EDEP.[6] This subroutine package, first used in collector rim-angle optimization studies,[7] computes absorbed solar flux distributions on a cylindrical receiver positioned above a parabolic trough. The model assumes that the errors associated with redirecting the solar radiation from the trough to the receiver may be treated statistically, conforming to normal error distributions. Inputs required by EDEP include:

- Geometry data for the trough and receiver assembly
- Collector radiative properties
- Collector errors associated with tracking and with the reflector trough and receiver
- Solar radiation magnitude and incidence angle

Figure 1 is a schematic of the trough and receiver assembly modeled by EDEP. Absorbed solar radiation distributions for both the glass and receiver tube can be obtained by appropriate use of the model. EDEP computes the collected energy as a function of position on the tubes and uses material radiative property subroutines to calculate the absorbed fraction of solar radiation as a function of the incidence

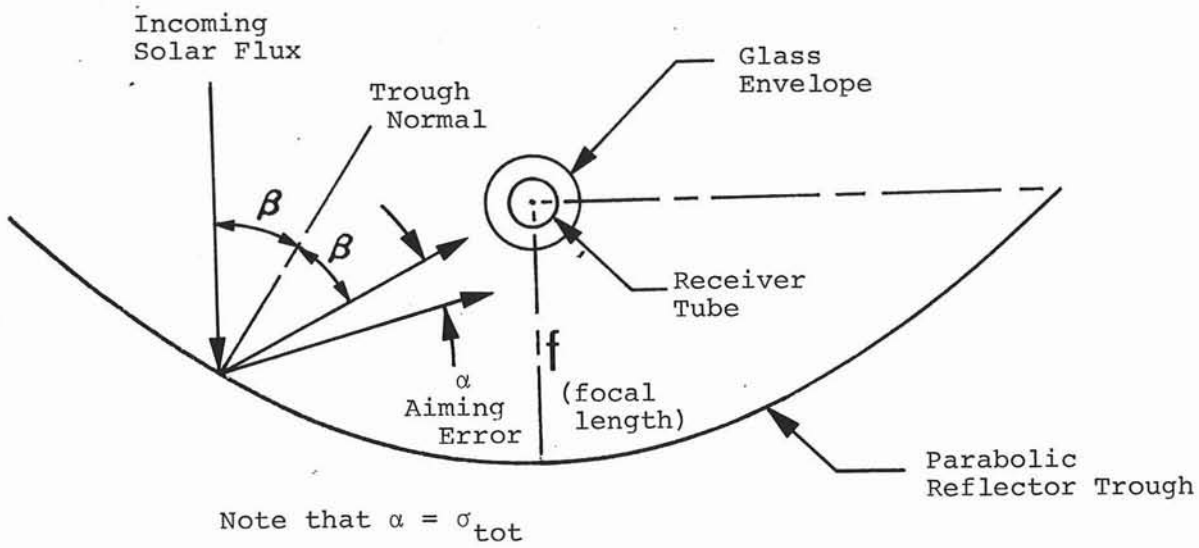

FIG. 1. PARABOLIC-CYLINDRICAL COLLECTOR TROUGH MODELED BY EDEP.

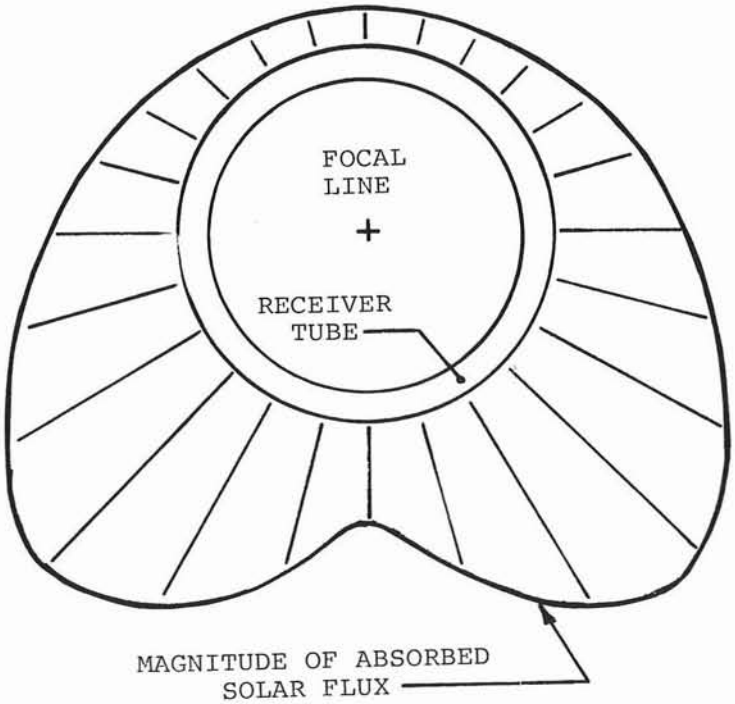

FIG. 2. SCHEMATIC OF A TYPICAL ABSORBED SOLAR FLUX DISTRIBUTION ON A RECEIVER TUBE.

angle. Transmission of solar radiation through the glass jacket is also accounted for as a function of the incidence angle. Figure 2 shows a representative symmetric solar flux distribution on a receiver tube positioned at the focal line of a collector trough.

Errors associated with redirection of the incident solar radiation from the reflector trough are divided into two classes for EDEP use: one- and two-dimensional errors. Figure 3 shows examples of each type of error. One-dimensional errors are assumed to be independent of the direction of the solar radiation. Examples of possible one-dimensional error sources are errors associated with the reflector support structure, known as slope errors (σ_s), and errors associated with random misalignment of the collector, such as random receiver errors (σ_r) and random trough tracking errors (σ_t). The total one-dimensional error (σ_{1D}) is given in Eq. (1) using the root-mean square relation

$$\sigma_{2D} = \sqrt{\sigma_s^2 + \sigma_t^2 + \sigma_r^2} \quad . \tag{1}$$

Two-dimensional errors are solar-radiation path-length dependent and are hence functions of the solar-radiation incidence angle on the trough. Examples of this type of error include errors associated with reflector-trough specularity (σ_m) and with finite sun-shape effects (σ_{sun}). Note that the error sources are all assumed to conform to normal (Gaussian) error distributions. It is thought that the sun-shape error conforms more to a "pillbox" (i.e., square wave) depending upon circumsolar effects.[6] However, for the purposes of statistical blending of the error sources, EDEP treats the sun shape as a comparable normal error. Equation (2) presents the two-dimensional error (σ_{2D}) model used with EDEP to account for radiation path-length effects.

$$\sigma_{2D} = \sqrt{\sigma_{sun}^2 + \sigma_m^2} \Big/ \cos \gamma \quad , \tag{2}$$

where γ = radiation incidence angle on the trough .

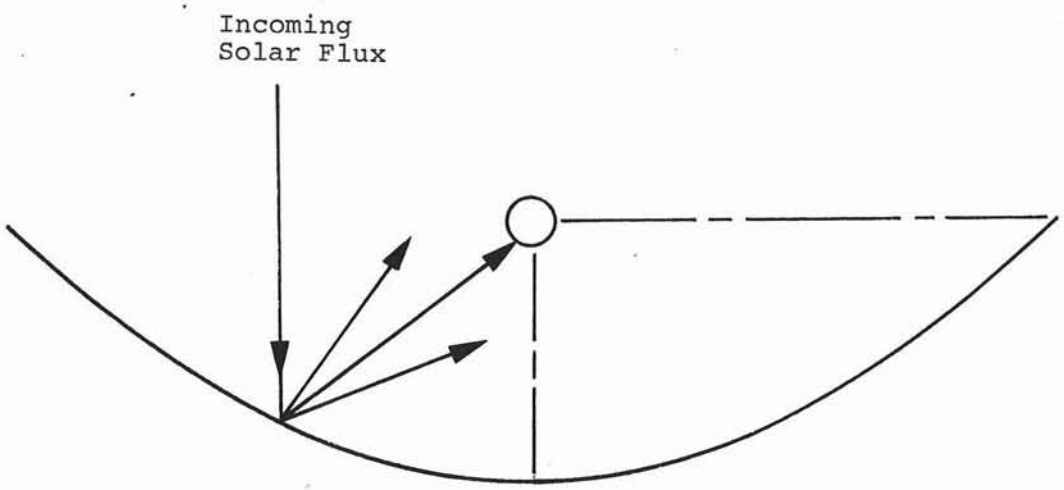

(a)

Example of a One-Dimensional Error
(Associated with Tracking, Slope, and
Receiver Errors)

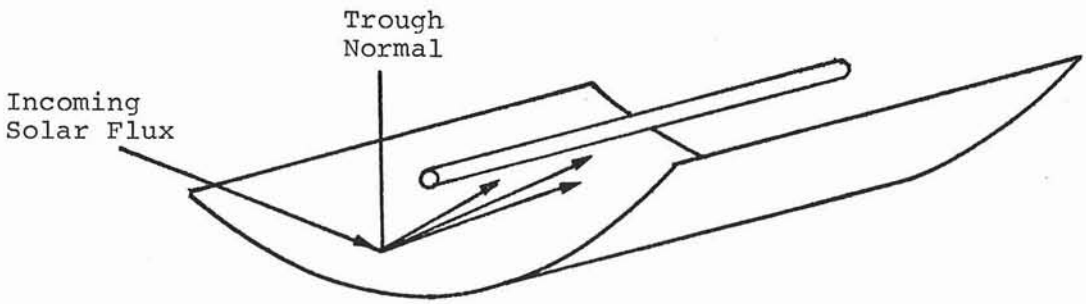

(b)

Example of a Two-Dimensional Error
(Associated with Sun and Mirror Errors)

FIG. 3. ONE- AND TWO-DIMENSIONAL ERROR TYPES.

EDEP has been modified for all-day-collector performance modeling by inclusion of the solar radiation incidence angle effect. For E-W-oriented collector fields, the solar radiation incidence angle (γ) varies according to the sun elevation (α) and azimuthal (β) angles and the declination angle (δ), all of which depend upon the collector location and time and day of year. Equations (3) through (6) present these angular relations. Reference 8 contains additional detail on the development of the incidence angle expression.

$$\gamma = \cos^{-1} [\cos (\alpha) \cos (\beta)] - 90^{\circ} \tag{3}$$

$$\alpha = 90^{\circ} - \cos^{-1} [\sin (\phi) \sin (\delta) + \cos (\phi) \cos (\delta) \cos (\omega)] \tag{4}$$

$$\beta = \tan^{-1} \left[\sin (\delta) \cos (\phi) - \cos (\delta) \sin (\phi) \cos (\omega) - \cos (\delta) \sin (\omega) \right] \tag{5}$$

$$\delta = 23.4523 \sin [2\pi(d-80)/365] \quad , \tag{6}$$

where

d = day of year (80 = March 21)

ϕ = latitude of location

ω = hour angle (15t)

t = solar time with respect to solar noon (times before solar noon are negative) .

Typical variations in the solar radiation incidence angle for E-W-oriented troughs range from 60° to 70° at operating times near sunrise (or sunset) to normal incidence (0°) at solar noon. Thus, the two-dimensional error can vary by a factor of two to three times within a day (see Eq. (2)).

EDEP combines the two error types, again using the root mean square relation, to form a total collector error (σ_{tot}) shown in Eq. (7). The variation of this total error

$$\sigma_{tot} = \sqrt{\sigma_{1D}^2 + \sigma_{2D}^2} \tag{7}$$

may result in significant performance reductions at off-solar noon conditions, depending upon the magnitude of the one-dimensional error. To ensure that significant fractions of the solar energy are always intercepted, receiver tube size may need to be increased. However, enlarging the receiver also increases the detrimental heat-loss characteristics of the design. Thus, off-solar noon modeling becomes important for optimizing collector performance, given known constraints of operating temperature and collector error-budget.

Additional descriptions on EDEP and on the nature of the error sources are available in References 6 and 7. Typical error magnitudes are provided in the Definition of Problem Parameters section, (p. 24) as are the radiative property models generated for use in this study.

Receiver Assembly Heat Loss-Model

Receiver assembly heat-loss modeling incorporates work previously described.[3,9] The model considers one-dimensional (radial) energy exchange assuming that (1) the receiver tube surface temperature is known, and (2) the solar radiation absorbed by the glass is uniformly distributed. Heat-loss results are obtained after solving the coupled energy balance equations for the surface temperatures of the glass. Figure 4 shows the schematic energy transfer between the receiver tube and glass and between the glass and environment. The notation used in Fig. 4 is defined below:

$Qo_{i-j_{IR}}$ = thermal radiative energy leaving surface i and incident on j

$Q_{conv_{i-j}}$ = energy transferred from surfaces i to j by by conduction or convection

Q_{glass} = solar radiation absorbed by the glass

The surface designators (and temperatures) are given as follows:

1 - receiver-tube surface (T_1)

2 - glass-jacket inner surface (T_2)

3 - glass-jacket outer surface (T_3)

a - ambient (T_a)

s - blackbody sky (T_s)

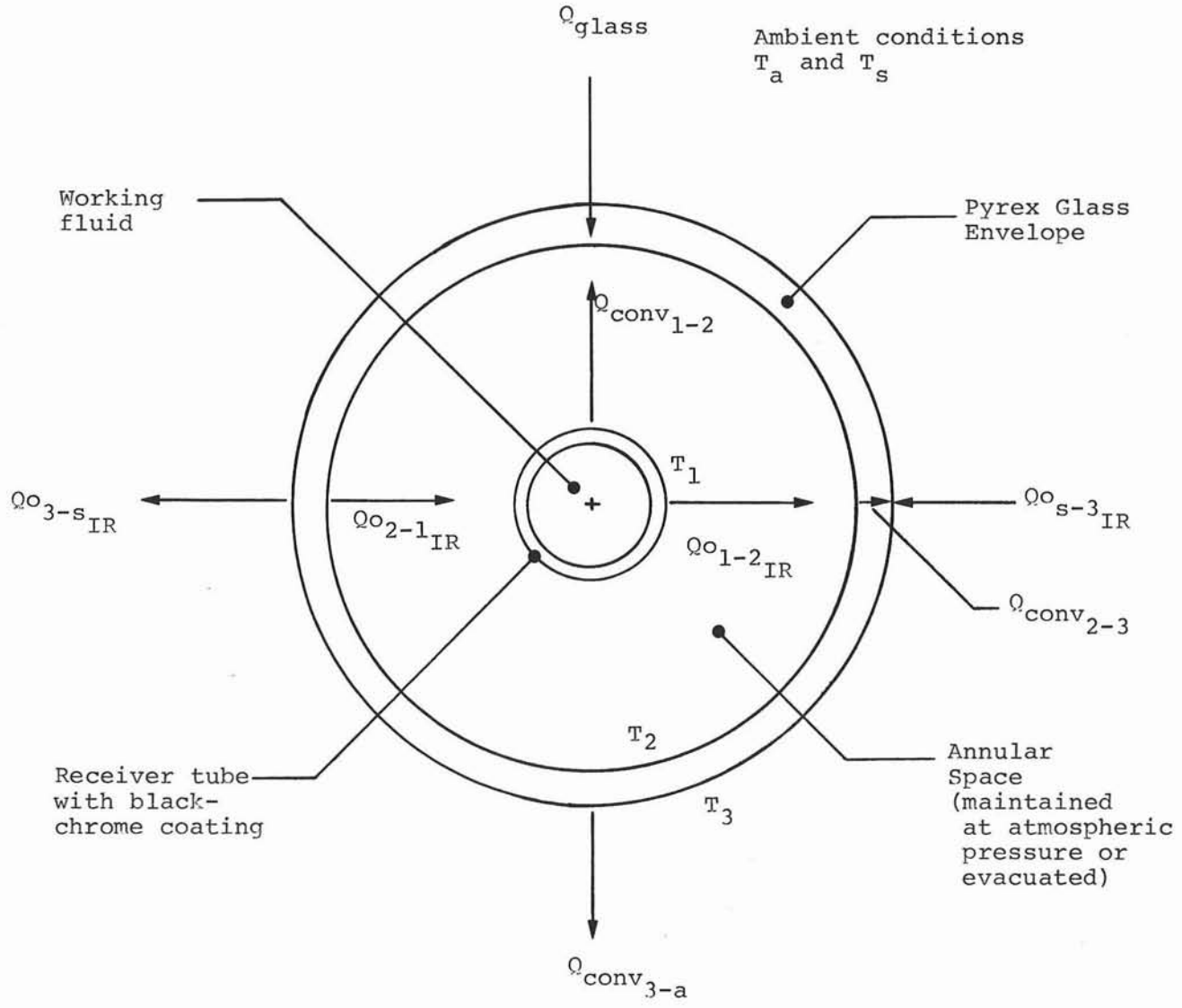

FIG. 4. SCHEMATIC OF ENERGY EXCHANGE FOR THE RECEIVER ASSEMBLY HEAT LOSS CALCULATION

A Newton-Raphson iteration method described in Siegel and Howell[10] is used to solve the coupled nonlinear energy balance equations. This method also allows for use of temperature-dependent conduction, convection, and radiation coefficients. The overall receiver heat loss (Q_{HL}) calculation uses the previously calculated outer surface glass temperature (T_3) and ambient temperature conditions (T_a, T_s), as shown in Eq. (8).

$$Q_{HL} = A_3[h_{3a}(T_3 - T_a) + \varepsilon_{3_{IR}}\sigma(T_3^4 - T_s^4)] \quad , \tag{8}$$

with

A_3 = glass outer surface area

h_{3a} = convection coefficient for energy transfer to ambient

$\varepsilon_{3_{IR}}$ = glass thermal emissivity

σ = Stefan-Boltzmann constant

Further assumptions used in the analysis include that (1) the glass is thermally opaque, (2) all surfaces are gray and diffuse, (3) the environment acts as a blackbody at a reduced temperature ($T_s = T_a - 6K$), and (4) glass and receiver tubes are concentric. Correlations used in the simulation for the heat-transfer coefficients are functions of the geometry, pressure, temperature, and ambient conditions and are given in Reference 9.

Simulation Organization

The computer simulation organization for both instantaneous solar-noon and all-day performance studies is summarized in Fig. 5. Separate calculations for the absorbed solar radiation distributions and the receiver heat loss are performed using data on the insolation and ambient conditions taken from computer weather tapes. Specific problem inputs include:

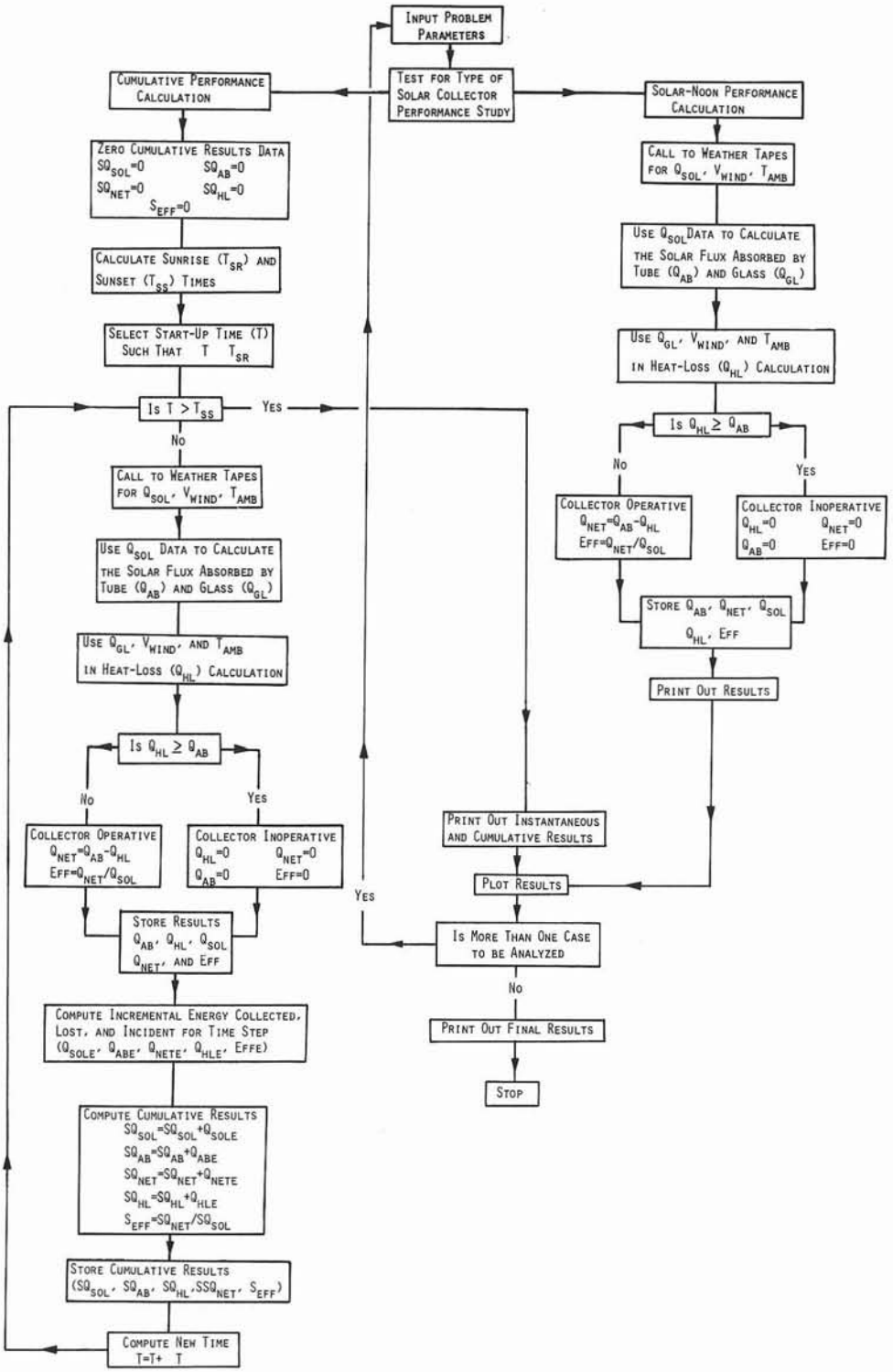

FIG. 5. COMPUTER SIMULATION OPERATION SEQUENCE

- Geometry data for the trough and receiver
- Day and site of study
- Type of study (solar-noon or cumulative analysis)
- Receiver-tube surface temperature
- Annulus gas and pressure
- Solar-noon one- and two-dimensional collector errors
- Collector solar and thermal radiative properties

Cumulative collector performance analyses model the parabolic-cylindrical collector from sunrise to sunset. The total direct normal solar energy incident on the reflector trough is thus accounted for. Cumulative collector efficiency results are based on the total possible solar energy available as opposed to using only that direct normal solar energy incident while the collector is operational. The computer simulation assumes that a collector will operate so long as the energy absorbed by the receiver tube (Q_{AB}) is greater than the receiver assembly heat loss (Q_{HL}). For the case where

$$Q_{AB} < Q_{HL} \quad , \tag{9}$$

the receiver heat loss and absorbed solar energy are zeroed in the analysis.

The simulation determines the cumulative solar energy collection in discrete time increments (1200 s used in the parameter study). Ambient conditions and insolation (Q_{SOL}) are assumed constant over the time step. Instantaneous collector efficiency (η) is defined in terms of the net absorbed radiation (Q_{NET}), and is given in Eq. (10)

$$\eta = Q_{NET}/Q_{SOL} \quad , \tag{10}$$

with

$$Q_{NET} = Q_{AB} - Q_{HL} \quad . \tag{11}$$

This instantaneous efficiency may be redefined in terms of an optical efficiency (η_{opt})

$$\eta = \eta_{opt} - Q_{HL}/Q_{SOL} \quad , \tag{12}$$

where

$$\eta_{opt} = Q_{AB}/Q_{SOL} \quad . \tag{13}$$

Note that the optical efficiency is obtained solely from EDEP results and is independent of the receiver-tube operating temperature.

Cumulative performance results are obtained by numerical integration of the instantaneous collector results. A trapezoidal-rule integration scheme is used, assuming that the heat loss and solar energy absorbed are constant over each time step. The simulation thus considers the transient solar energy collection as a series of discrete steady-state miniproblems.

Collector performance results (Q_{AB}, Q_{HL}, and Q_{NET}) are given in terms of collector-trough aperture area (W/m^2 and $W\text{-}hr/m^2$). The simulation neglects receiver end-effects in off-solar-noon modeling and also assumes that there is no reflector trough shadowing other than that by the receiver tube. Note also that the anaysis fixes the receiver tube surface temperature. The bulk fluid temperature (and working-fluid mass flow rate) are not considered in this work. Additional information on the computer simulation is given in Reference 11, which provided preliminary parametric results for the 2-m collector-trough design.

Definition of Problem Parameters

The intent of the parametric study has been to optimize the design of an E-W-oriented, 2-m, 90^{o} parabolic-cylindrical solar collector. This collector, to be used at the Sandia/Department of Energy MSSTF will incorporate component design improvements developed since the installation of the first collector trough system at Sandia Laboratories in 1976. The parabolic-cylindrical collector trough will consist of thin-mirrored, sagged-glass reflector panels mounted to a honeycomb trough structure. The receiver assembly will be composed of a carbon-steel tube with an electrodeposited black-chrome selective surface and an enclosing concentric jacket of 7740 Pyrex glass. Collector-trough tracking of the sun will use electrical-thermal feedback from thin ceramic-coated nickel monitoring wires mounted to the receiver tube. The electrical resistance of these wires increases with temperature, and hence for maximum solar energy collection, the trough is positioned when the resistance is greatest.

Table I lists the baseline collector design conditions selected for the parametric study. Where feasible, radiative properties and collector error budgets reflect the optimism of the component development work. The parametric study assumes that the data given in Table I are constant unless indicated otherwise. In addition to this compilation, specific descriptions are provided for the (1) receiver geometry, (2) collector radiative properties, (3) weather and insolation conditions, and (4) collector error budget. These descriptions of the parameter study conditions are given in the following four sections, respectively.

TABLE I

Baseline Collector Trough Design Conditions

●Parabolic Trough

Solar Reflectivity of Reflector Surface: 0.95
Trough Rim Angle (Half Angle): 90^{o}
Trough Focal Length: 0.5 m
Trough Opening Aperture: 2.0 m

●Receiver Assembly

Receiver Tube o.d.: Variable (see Table II)
Glass Jacket o.d.: Variable (see Table II)
Glass Thickness: Variable (see Table II)
Glass Thermal Emissivity: 0.92
Glass Solar Absorptivity: Variable (see Fig. 6)
Glass Solar Transmissivity: Variable (see Fig. 6)
Receiver Tube Solar Absorptivity: Variable (see Fig. 7)
Receiver Tube Emissivity: Variable
$\varepsilon(373\ K) = 0.15$
$\varepsilon(589\ K) = 0.25$
(Emissivity linear between and outside these limits)

●Weather

Day Modeled: March 15, 1962
(Data for Direct Normal Insolation, Cumulative Direct Normal Solar Energy, Ambient Temperatures, and Windspeed shown in Fig. 8)
Ambient Pressure: 8.379×10^4 Pa
Sunrise: 6.127 hr (Solar Time)
Sunset: 17.873 (Solar Time)

●Operating Conditions

Location of Test: Albuquerque, NM
Receiver Tube Temperature: 589 K
Annulus Pressure: 8.379×10^4 Pa
Annulus Gas: Air
Receiver Tube and Glass Concentric
Receiver Assembly Centered in Focal Plane
Error Parameters: (see Table IV)
One-Dimensional Error Total: 6.41 mR
Two-Dimensional Solar-Noon Error Total: 2.81 mR
Reflector Trough Tracking with no Error (Bias)

Receiver Geometry

Three different-sized receiver tubes with concentric glass envelopes were selected for comparative studies with the fixed 2-m reflector-trough geometry. Table II provides dimensional data for each design.

TABLE II

Geometry Data for the Three Modeled Receiver Assemblies

Receiver Tube Designator* (-)	Receiver Tube o.d. (cm)	Glass Tube o.d. (cm)	Glass Thickness (cm)
1	2.223	4.50	0.204
2	2.54	4.80	0.204
3	3.175	5.70	0.240

*Designation used in the presentation of graphical results.

The three receiver-assembly designs were selected following preliminary solar energy deposition studies on tubes varying from 1.27 to 3.81 cm o.d. The surrounding glass jackets were selected based on the criteria that (1) the glass tubing size must be of standard tubing stock, and (2) the annular space between the glass and receiver tube must minimize receiver heat loss for operating temperatures of 450 K through 650 K. The annular spaces of each receiver assembly were assumed to be filled with air at atmospheric pressure (8.379×10^4 Pa for Albuquerque) in the heat-loss minimization analyses.

Collector Radiative Properties

The reflector trough incorporates the most recent developments for glass mirrors. It is assumed that the reflectors are back-surface-

slivered, thin 0317 Corning glass ∿1.50 mm thick. Radiative property measurements have confirmed that the solar reflectivity of such mirrors is ∿0.95 for incidence angles less than 60°.[4] Because the solar radiation incidence angle is not expected to exceed 60° except near sunrise or sunset for the E-W collector orientation, angular effects on the reflectivity have been neglected in the analysis.

Figure 6 gives solar absorptivity (α_s) and transmissivity (τ_s) data for 2.04-mm-thick 7740 Pyrex glass typically used for the receiver glass envelope. Relations for these properties were derived using work by Parmelee[12] and electromagnetic theory for dielectric materials[10] and are given in Eqs. (14) and (15), respectively.

$$\alpha_s(\theta) = 1 - r - \frac{(1-r)^2 a}{1 - ra} \tag{14}$$

$$\tau_s(\theta) = \frac{(1-r)^2 a}{1 - r^2 a^2} \quad , \tag{15}$$

with

$$a = \exp-\left(\kappa \ell / \sqrt{1 - \sin^2(\theta)/n^2}\right) \tag{16}$$

$$r = 1/2 \left[\frac{\sin^2(\theta-x)}{\sin^2(\theta+x)} + \frac{\tan^2(\theta-x)}{\tan^2(\theta+x)} \right] \quad , \tag{17}$$

and

$$x = \sin^{-1}[\sin(\theta)/n] \quad , \tag{18}$$

where

κ = absorption coefficient

ℓ = glass thickness

n = index of refraction

θ = angle of incidence .

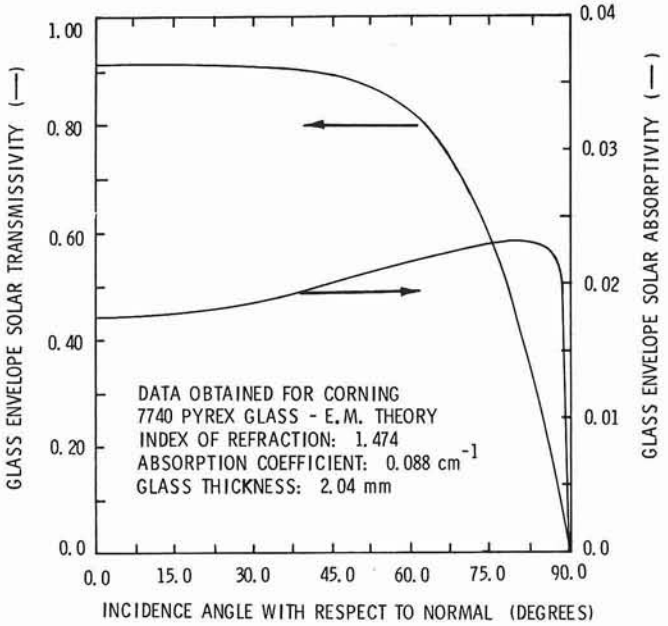

FIG. 6. SOLAR-RADIATIVE PROPERTIES FOR THE RECEIVER ASSEMBLY GLASS ENVELOPE

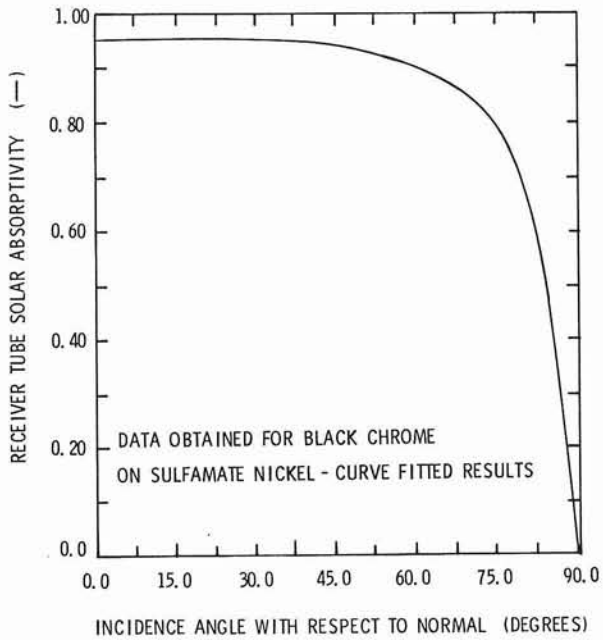

FIG. 7. SOLAR ABSORPTIVITY OF BLACK-CHROME RECEIVER TUBE SURFACE

Data on the Pyrex index of refraction and absorption coefficient were provided by Corning Glass Works. In addition, Pyrex is assumed to be thermally opaque for simplification of the heat-loss calculations. This glass is treated as a gray-diffuse material, independent of temperature, with thermal emissivity and reflectivity measurements of 0.92 and 0.08, respectively.

The modeled receiver tube surface is selectively coated with electroplated black chrome on dull sulfamate nickel. Solar absorptivity measurements by Pettit[13] for this material have been curve-fit for use with EDEP (Fig. 7). Black-chrome thermal radiative properties are assumed to vary linearly with temperature. Representative diffuse-gray thermal emissivities at 373 K and 589 K, as used in the analysis, are 0.15 and 0.25, respectively.

Weather and Insolation Conditions

March 15, June 22, and December 21, 1962, taken from the Albuquerque 1962 Weather Tapes,[14] were selected as representative clear, seasonal days for the parametric study. The three days were chosen subject to the following constraints:

- Cloud cover at any time not to exceed 10%.
- Direct normal solar-noon insolation $\geq$ 950 W/m^2
- Maximum allowable wind velocity $\leq$ 10 m/s
- Cumulative direct normal insolation conformable to Sandia Laboratories' baseline seasonal design-days[11]

Table III summarizes solar-noon and cumulative insolation data for the three days. March 15, 1962, was selected as the reference day for most of the parametric study since this day is average in length of daylight compared to the winter and summer seasonal days (June 22 and December 21 are used for seasonal variation effects, as

are summarized in Appendix A). Autumn clear-day modeling is omitted because the sun-location and length of day available for solar energy collection compare to spring-day conditions. Figure 8 summarizes graphical results for wind and ambient temperature variation and insolation conditions for March 15, 1962, in Albuquerque, NM. Weather conditions for June 22 and December 15, 1962, are summarized in Figs. A-1 and A-2 of Appendix A, respectively.

TABLE III

Seasonal Clear-Day Direct Normal Insolation*

Day (-)	Direct Normal Solar-Noon Radiation (W/m^2)	Cumulative Direct Normal Solar Energy ($W\text{-}hr/m^2$)
March 15	977	9735
June 22	977	10995
December 21	1068	8161

*Data have been obtained from Albuquerque 1962 Weather Tapes[14]

Collector Error Budget

The magnitudes of the one- and two-dimensional error sources are estimated assuming that the reflector trough structural support, glass mirror specularity, and collector tracking capablities are significantly improved over the collector design installed at the MSSTF in 1976. Work reported by Orear,[15] Treadwell,[7] and Pettit and Butler[4] has been consulted in developing the baseline error budget used in the study. Table IV summarizes the error budget breakdown. Note that the errors are treated as normal error distributions in the solar deposition model with the magnitude of each error equal to two standard deviations (2σ). Thus,

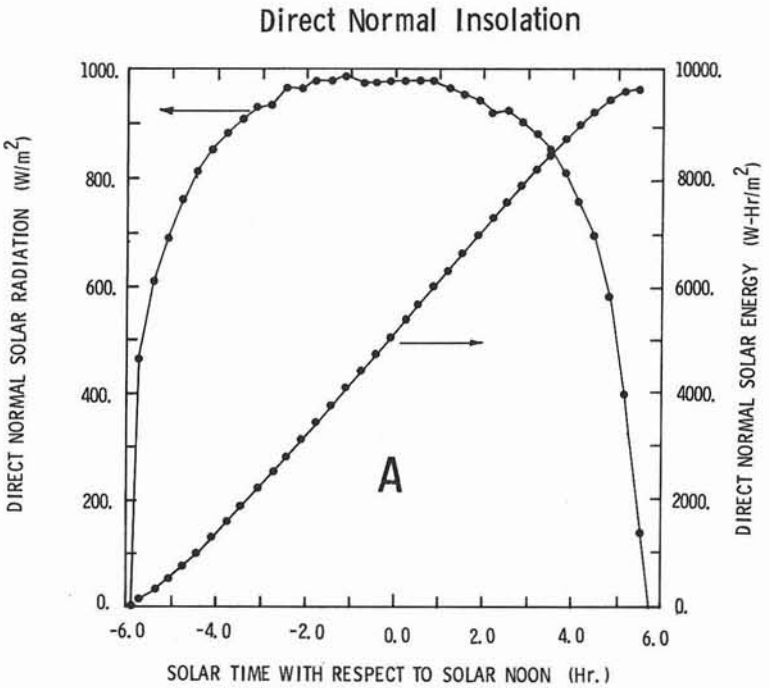

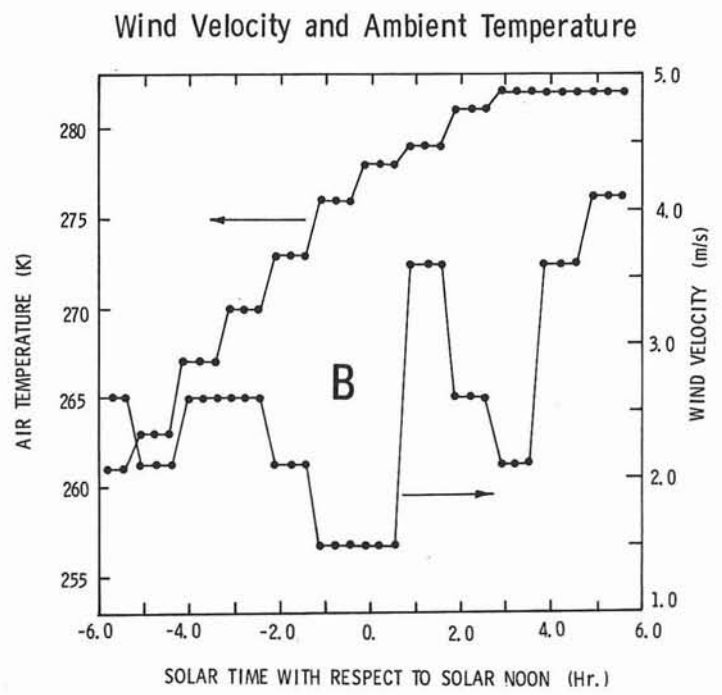

FIG. 8. DIRECT NORMAL INSOLATION AND WEATHER DATA FOR MARCH 15, 1962, IN ALBUQUERQUE, NM

95.5% of the total error under the normal error distribution curve is accounted for in the simulation.

TABLE IV

Collector Error Magnitudes

	mR
One-Dimensional Errors	
Structural-Slope (σ_s)	5.39
Random Tracking (σ_t)	2.83
Random Receiver Alignment (σ_r)	2.0
Two-Dimensional Errors at Solar Noon	
Sun-shape (σ_{sun})	2.80
Mirror Specularity (σ_m)	0.25
Total Solar-Noon Error	7.00

The two-dimensional error magnitudes are given at solar noon since the solar radiation is normal to the trough aperture. Equation (2) shows the variation of the two-dimensional error with respect to incidence angle. In addition, since the days selected for analysis are clear days, the sun statistical error is not increased to include circumsolar effects. Note that the estimation of the total collector error budget represents the greatest measure of uncertainty in the design of the collector system.

Simulation Results

Results from the computer simulation parametric study are presented graphically in Appendices A through F. The work compares the three receiver assembly designs defined in Table II. Data obtained from the study are designated on the figures using the following notation:

1. 2.223-cm receiver-tube assembly

2. 2.54-cm receiver-tube assembly

3. 3.175-cm receiver-tube assembly

The appendices provide design trade-off data using the baseline-collector parameters defined in Table I. Each appendix summarizes comparative studies concerning a specific facet of the collector design. Factors considered include

- Variation of season for collector studies (Appendix A)
- Variation of receiver-tube operating temperature (Appendix B)
- Variation of the one- and two-dimensional collector errors (Appendix C)
- Misalignment of the receiver assembly (Appendix D)
- Collector-trough tracking bias (Appendix E)

Although the results of the appendices are self-explanatory, brief summaries are provided in the following sections. The appendices should be reviewed for more detailed numerical comparisons, as the discussion of each appendix will be qualitative.

Seasonal Design-Day Variation

Appendix A summarizes performance results for the baseline collector design using weather and insolation data for June 22 and December 21, 1962. Factors varied include (1) receiver tube operating temperature, (2) one-dimensional collector error magnitude, and (3) vertical misalignment of the receiver assembly. Although the duration of the day, maximum and cumulative insolation, and other weather conditions vary drastically, the design trade-off locations for the three receivers are nearly identical for the two days. For example, in both Figs. A-3F and A-4F, the 2.223-cm receiver-tube assembly is found to be most effective for temperatures in excess of 550 K, although the magnitudes of the collector efficiency vary dramatically (< 42% for June 22 and < 54% for December 21, 1962)

The same design trade-off conditions for March 15, 1962, are omitted from Appendix A in the interest of brevity. The results, however, are presented in the other appendices and are used in studying other pertinent collector parameter variational effects. These results yield similar design trade-off locations, and indicate that the choice of a seasonal day for parametric studies can be arbitrary. Clear spring, summer, fall, or winter day studies should yield comparable performance trade-off results.

Receiver Tube Operating Temperature Variation

Appendix B summarizes results for the variation of the receiver tube operating temperature. Two annulus gas pressure conditions are modeled in this section--8.379×10^4 Pa and 1.33×10^{-2} Pa. The latter gas pressure limits the annular space heat-loss mechanism to radiation heat transfer. The higher pressure, atmospheric pressure for Albuquerque, NM, results in combined conduction and radiation across the annular space. The annular spaces of each receiver have previously been sized to minimize convection heat transfer with the annulus pressure maintained at atmospheric pressure.

The smaller two receiver-tube assemblies yield the best performance results for temperatures > 550 K with the annular space maintained at atmospheric pressure. When the annular space is evacuated, other factors (such as the one-dimensional collector error magnitude) must also be considered. A comparison of Figs. B-4C and B-4E, for example, indicates that the error magnitude increase causes the largest receiver-tube assembly to have the highest efficiency up to temperatures of ∿575 K. This occurs because the overall increased heat loss of the 3.175-cm tube is less than the difference in total solar energy collection between the different tubes. In addition, at operating temperatures < 500 K, the selection of the optimal receiver design is less clear, although the larger tubes appear most effective since the

net collected energy, defined in Eq. (11), is greater because of the smaller heat-loss magnitudes. Note also that this design modeling assumes random errors (see Table IV) for receiver alignment and reflector tracking. Changes in these parameters also affect the selection of the optimal receiver as a function of temperature.

Collector Error Magnitude Variation

Appendix C gives one- and two-dimensional error magnitude variation results. Figure 3, discussed previously, illustrates the types of errors modeled. The sun-shape error is assumed fixed throughout these analyses at 2.80 mR. Annulus gas pressure conditions and receiver-tube operating temperatures are also varied in Appendix C to provide additional design data.

Variation of the two-dimensional error is presented with the one-dimensional error fixed at 6.41 mR, as prescribed in Table I. From the cumulative results shown in Figs. C-2, it appears that the variation in mirror specularity would have to be over an order of magnitude greater than the 0.25 mR baseline estimate to reduce collector performance significantly. In fact, for a larger one-dimensional error, an increased mirror specularity error would probably be undetectable, owing to the manner in which EDEP combines the error sources, shown in Eq. (7). Circumsolar-related errors may also be assumed to act as a two-dimensional error source. Results shown in Fig. C-2C indicate, however, that a total two-dimensional error (sun shape included) variation from 2.81 to 5.73 mR at solar noon would only decrease the cumulative collector performance for the 2.54-cm receiver by 2.5 percentage points (47.0% to 44.5%). Hence, it is not expected that circumsolar effects should be anymore detrimental to collector performance than would increased one-dimensional error variation or even receiver assembly misalignment.

One-dimensional error variation studies reveal that the 2.223-cm receiver-tube-assembly performance degrades so rapidly with increasing error that its use is not advised. The intermediate tube assembly (2.54-cm tube) is optimal for $\sigma_{1D} \leq 9.0$ mR for operating temperatures > 589 K. At 477 K, the trade-off between using the 2.54 cm or 3.175 cm receiver-tube assembly depends upon the annulus gas pressure. If σ_{1D} > 8.0 mR and the receiver is maintained below 477 K, then the 3.175-cm receiver assembly should be used, regardless of the annulus gas pressure.

Receiver Assembly Misalignment

Appendix D summarizes data on the effects of misalignment of the receiver assembly from the focal line of the parabolic trough. Figure 9 presents the possible misalignment conditions considered. In this study, it is assumed that the entire receiver assembly is misplaced from the focal line, with the glass and receiver tubes remaining concentric. In addition, it is assumed that the misalignment is with respect to the trough location. As the trough repositions for tracking, the misalignment (d) is a fixed distance off the trough focal length (f) shown previously in Fig. 1.

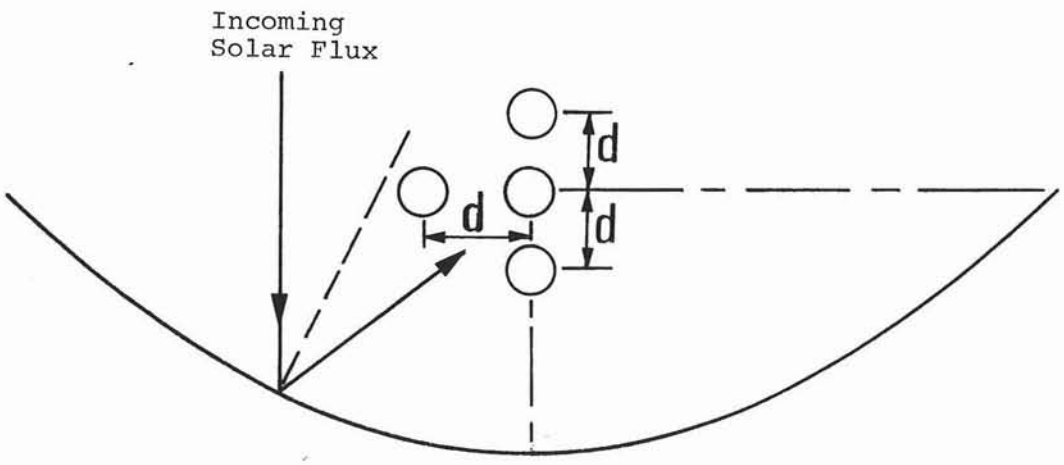

FIG. 9. MISALIGNMENT CONDITIONS CONSIDERED IN THE PARAMETRIC STUDY

Misalignment of the receiver assemblies degrades the performance of the two smaller receivers much more significantly than it does the 3.175-cm receiver. The 2.223-cm receiver design should not be considered for use since small misalignments $\leq$ 4.0 mm can reduce instantaneous and cumulative efficiencies by 2.0 percentage points. The 2.54-cm receiver-tube assembly should probably be used if misalignments > 6.0 mm can be avoided and if the one-dimensional collector error magnitude is $\sim$6.41 mR. For larger one-dimensional errors, the 3.175-cm tube will maintain the best performance characteristics over the range of possible misalignment conditions.

Note that although the figures on vertical misalignment appear symmetric, the absorbed solar energy distributions on the receiver tubes are drastically different. Figure 10 shows some typical solar-noon absorbed solar-flux distributions for the three misalignment conditions and also for a typical tracking bias condition. Results are obtained using a 2.54-cm receiver tube. Two curves are shown in each figure. One corresponds to the baseline absorbed flux distribution and the second corresponds to an extreme misalignment or tracking bias condition.

The heat-loss model assumes that the absorbed solar energy can be uniformly distributed to provide the required heat-loss results. Although this one-dimensional model can provide estimates on the heat loss fairly accurately, it will not provide maximum receiver-tube temperature variations. Two-dimensional (radial and circumferential) receiver assembly heat-loss and energy-collection studies have been completed and are currently being documented.[16] This work should be consulted to ensure that the various misalignment scenarios will not lead to black-chrome and/or T-66 degradation.

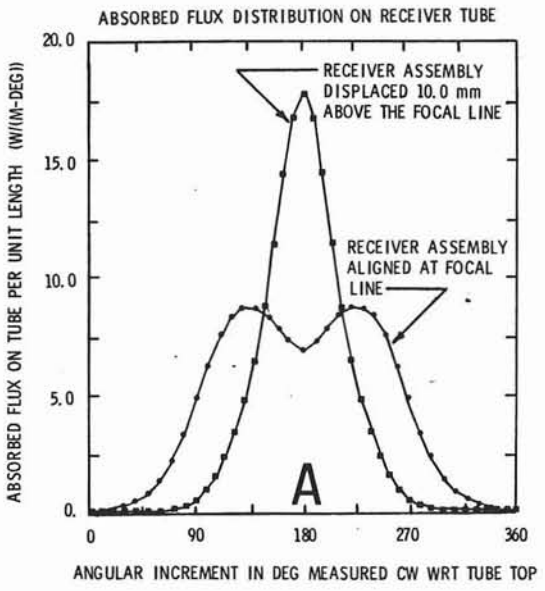

Misalignment Above the Focal Line

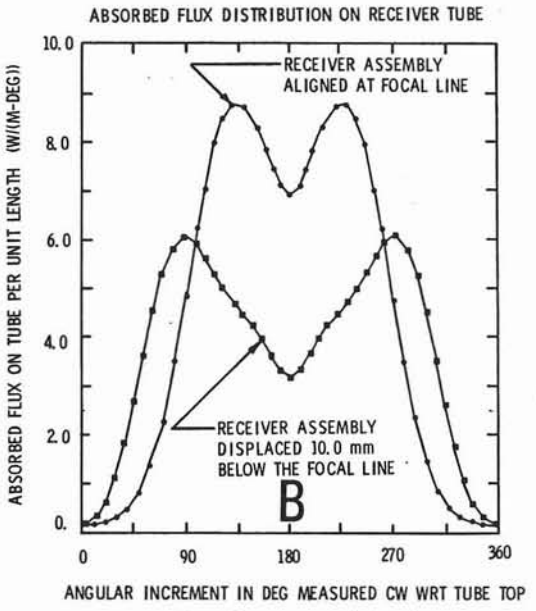

Misalignment Below the Focal Line

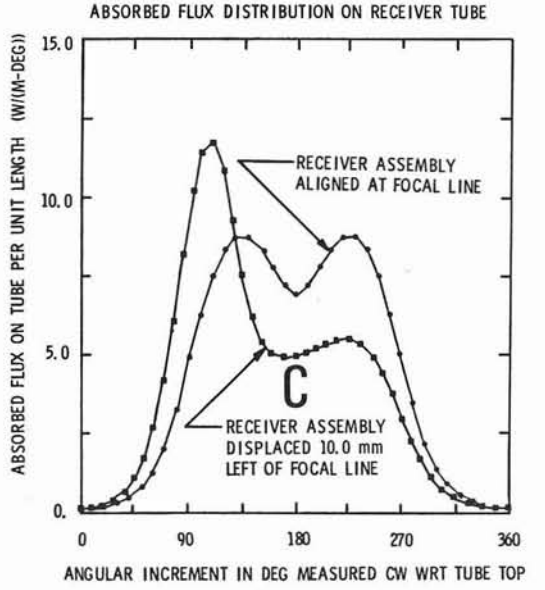

Misalignment to the Left of the Focal Line

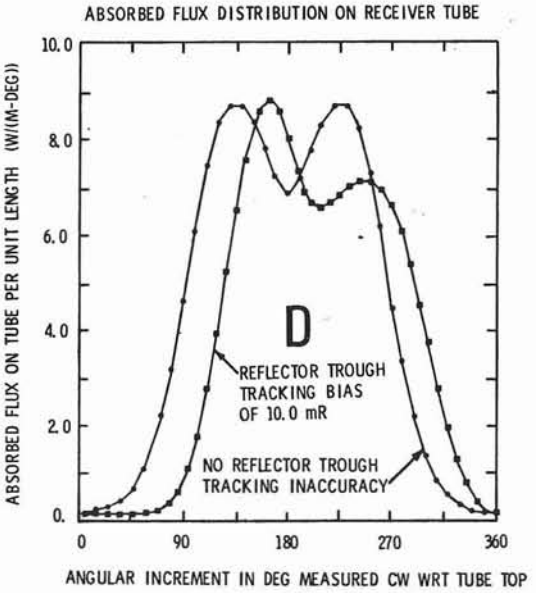

Collector-Trough Tracking Error

FIG. 10. SOLAR-NOON ABSORBED FLUX DISTRIBUTION FOR DIFFERENT MISALIGNMENT AND RECEIVER TRACKING BIAS CONDITIONS - 2.54-cm RECEIVER-TUBE ASSEMBLY MODELED

Collector-Trough Tracking Variation

Collector-trough tracking is designed to follow the sun's movement so that the energy is normal to the trough aperture in one plane at all times during the day. If the tracking mechanism fails, the incident energy would strike the trough at some bias angle (β) from the normal (Fig. 11). The reflected solar energy would also be biased

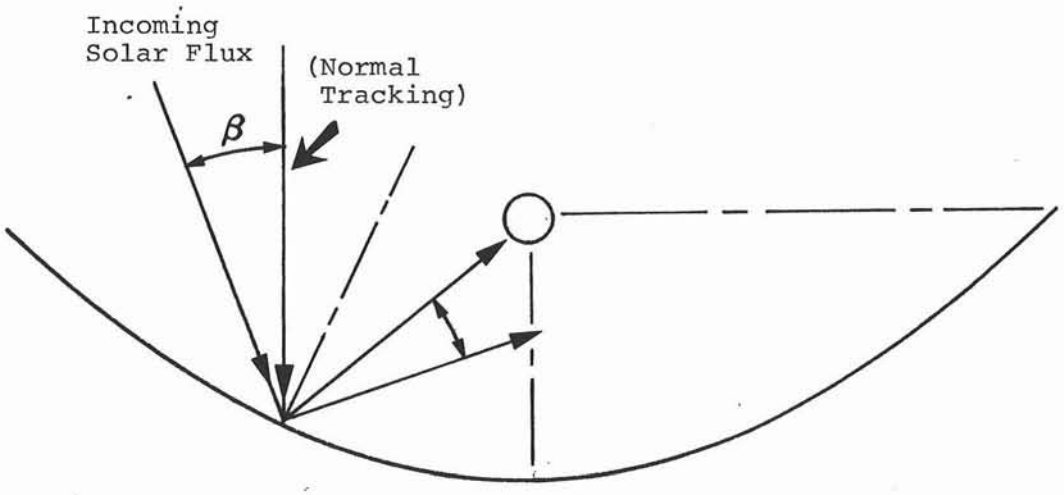

FIG. 11. ERROR ASSOCIATED WITH TRACKING BIAS

by this angular error and would either (1) miss the receiver tube entirely, or (2) intercept the receiver at some off-set position. The absorbed flux distribution on the receiver would thus be asymmetric (Fig. 10). Additional description on this asymmetric energy collection effect on the receiver heat-loss calculation is provided in Reference 16.

Appendix E presents results from the variation of tracking bias study. The performance results yield the same trends summarized in the previous misalignment section as would be expected since horizontal misalignment and tracking errors yield comparable absorbed solar-flux distributions (see Fig. 10). The smallest tube design is still unacceptable from a design standpoint, so long as there is any possibility that the tracking bias could exceed 3.0 mR. The 2.54-cm

receiver-tube assembly appears optimal for tracking bias < 6.0 mR so long as the one-dimensional collector error is ∿6.41 mR. For one-dimensional collector errors ≥ 8.55 mR, the 3.175-cm receiver-tube assembly will be least affected by tracking bias. This has also been the case for other misalignment conditions modeled.

Conclusions

The results presented in Appendices A through E are difficult to summarize, since so many different receiver-collector configurations have been modeled. Nonetheless, since the purpose of this work was to optimize the performance of a 2-m, 90° E-W-oriented parabolic trough under the conditions given in Table I, use of the 2.54-cm receiver-tube assembly is recommended. The following comments justify this selection:

1. The receiver-tube operating temperature range prescribed for the MSSTF is ∿475 K to 589 K. Over this temperature range, the 2.54-cm receiver tube will collect nearly the same quantity of solar energy as the 3.175-cm tube. Because of smaller heat losses, it will also operate more efficiently.

2. Variation of the one-dimensional collector error above 6.41 mR reduces the performance of the 2.223-cm receiver tube much more significantly than that of the 2.54-cm tube. One-dimensional errors in excess of 8.0 mR, with the annulus gas maintained at atmospheric pressure, are required to cause the 3.175-cm receiver design to be more efficient than the 2.54-cm receiver design.

3. Vertical and horizontal misalignment effects (for the baseline one-dimensional error of 6.41 mR) favor use of the 2.54-cm tube design over the larger receiver design for misalignment errors ranging from 5.0 to 7.0 mm, depending upon the receiver operating temperature. In addition, the 2.54-cm tube is superior to the 3.175-cm tube so long as the tracking error does not exceed 5.0 mR.

Additional simulation results for the 2.54-cm receiver-tube assembly are provided in Appendix F, using the baseline collector conditions of Table I. Included in this appendix are figures showing the effects of varying the radiative properties associated with the black chrome, sagged mirrors, and Pyrex glass envelopes. The results for the solar-radiative property variation account for angular incidence variation of the black-chrome absorptivity and glass transmissivity. Scaling factors are applied to the curves in Figs. 6 and 7 so that the new normal incidence data are obtained. Also, Figs. F-6 are included to show the effect of a constant normally directed wind velocity on the receiver assembly heat loss. Evacuation of the annulus gas may be considered as a practical way to reduce the detrimental effects of wind, as is shown in these figures.

It should be pointed out that the selection of a 2.54-cm receiver-tube assembly was based on the conditions of Table I. Selection of the larger 3.175-cm receiver-tube assembly can also be justified, especially if there are uncertainties in the collector error budget or if collector tracking capabilities are suspect. The larger receiver design, a more conservative choice, will maintain nearly constant performance characteristics over a greater range of parameter variation owing to its greater surface area for solar energy collection. At operating temperatures < 475 K, the 3.175-cm receiver-tube assembly

should certainly be considered optimal since the receiver heat loss is reduced. Evacuation of the annular space of the 3.175-cm receiver assembly would also improve performance characteristics. Evacuation results are provided in the Appendices B and C if such an option is considered for implementation at the MSSTF.

As a final note, the cumulative and solar-noon performance studies yielded comparable results for selecting an optimal receiver assembly. This interesting conclusion was initially somewhat surprising since the two-dimensional collector error varies so significantly during daily operation. Because the one-dimensional collector error is so large, however, the path-length dependence effects become less significant. Also at times near sunrise and sunset, the direct normal insolation is small and hence there is less possible energy collection available to be affected by the two-dimensional error. Since the trends presented in the appendices are comparable for the two analyses, the solar-noon calculation is preferred because computational cost is minimized.

References

1. C. E. Hickox and D. K. Gartling, The Effects of Nonuniformities on Natural Convection in Annular Receiver Geometries, SAND 77-1641, Sandia Laboratories, Albuquerque, NM, December, 1977.

2. A. C. Ratzel, C. E. Hickox, and D. K. Gartling "Techniques for Reducing Thermal Conduction and Natural Convection Heat Losses in Annular Receiver Geometries," Trans. ASME, J. Heat Transfer, Vol. 101, 1979, pp 108-113.

3. A. C. Ratzel and C. E. Simpson, Heat Loss Reduction Techniques for Annular Solar Receiver Designs, SAND78-1769, Sandia Laboratories, Albuquerque, NM, February, 1979.

4. R. B. Pettit and B. L. Butler, "Laser Ray Trace and Bi-Directional Reflectometry Measurements of Various Solar Concentrators," presented at ERDA Concentrating Solar Collector Conference, Georgia Institute of Technology, Atlanta. GA, September 26-28, 1977, (Paper 6.5) (also SAND77-1466).

5. R. R. Sowell and R. B. Pettit, "The Influence of Bath Composition on Thermal Stability of Electroplated Black-Chrome Solar Coating," Plating and Surface Finishing, Vol. 65, (10), October, 1978, pp 42-43.

6. F. Biggs, EDEP: A Computer Program for Modeling the Parabolic Trough Solar Concentrator, SAND76-0106, Sandia Laboratories, Albuquerque, NM, (to be published).

7. G. W. Treadwell, Design Considerations for Parabolic - Cylindrical Solar Collectors, SAND76-0032, Sandia Laboratories, Albuquerque, NM, March, 1976.

8. A. F. Veneruso, Tracking Angles and Rates for Single Degree of Freedom Solar Collectors, SAND76-0027, Sandia Laboratories, Albuquerque, NM, March, 1976.

9. A. C. Ratzel, Evaluation of the Evacuated Solar Annular Receivers Employed at the Midtemperature Solar Systems Test Facility, SAND78-0983, Sandia Laboratories, Albuquerque, NM, August, 1979.

10. R. Siegel and J. R. Howell, Thermal Radiation Heat Transfer, New York, McGraw-Hill Book Co., 1972, pp 385-387.

11. A. C. Ratzel, "Thermal Parametric Studies for the Second-Generation Sandia Ninety-Degree Parabolic Collector," Internal Memorandum RS 1262/1008, Sandia Laboratories, Albuquerque, NM, June, 1978.

12. G. V. Parmelee, "Transmission of Solar Radiation through Flat Glass," ASHVE Trans. Vol. 51, 1945, pp 317-350.

13. R. B. Pettit and R. R. Sowell, "Solar Absorptance and Emmittance Properties for Several Solar Coatings," J. Vac. Sci. Technol. Vol. 13, No.2, March/April, 1976, pp 596-602.

14. "SOLDATALBQ62," 1962 Albuquerque Ten Minute Weather Data Tape, provided by E. C. Boes, Sandia Laboratories, Albuquerque, NM.

References Cont.

15. L. Orear, Sensitivity of Slope Measurements on Parabolic Solar Mirrors to Positioning and Alignment of the Laser Scanner, SAND 78-0700, Sandia Laboratories, Albuquerque, NM, May, 1978.

16. A. C. Ratzel and C. E. Sisson, Annular Solar Receiver Thermal Characteristics, SAND79-1010, Sandia Laboratories, Albuquerque, NM (in preparation).

APPENDIX A

Seasonal Clear-Day Effects on Collector Performance

Solar-noon and cumulative performance results are provided for the baseline design of the parabolic-cylindrical collector defined in Table I using weather and insolation data for December 21 and June 22, 1962. Figures A-1 and A-2 provide the weather conditions modeled, respectively. Results for (1) variation of receiver tube operating temperature, (2) variation of one-dimensional collector error magnitude, and (3) vertical receiver assembly misalignment are presented.

Data points on the figures designate results from the computer simulation. The following notation is used:

1. 2.223-cm receiver-tube assembly
2. 2.54-cm receiver-tube assembly
3. 3.175-cm receiver-tube assembly

Results presented in the figures of Appendix A are summarized in Table A-I.

TABLE A-I

Seasonal Clear-Day Modeling - Summarized Results*

Type of Analysis	Day of Analysis	Figure Showing Results
Receiver-Tube Operating Temperature Varied	June 22	A-3
	December 21	A-4
One-Dimensional Collector Error Varied	June 22	A-5
	December 21	A-6
Receiver Assembly Vertical Misalignment Varied	June 22	A-7
	December 21	A-8

* All other conditions are fixed according to Table I

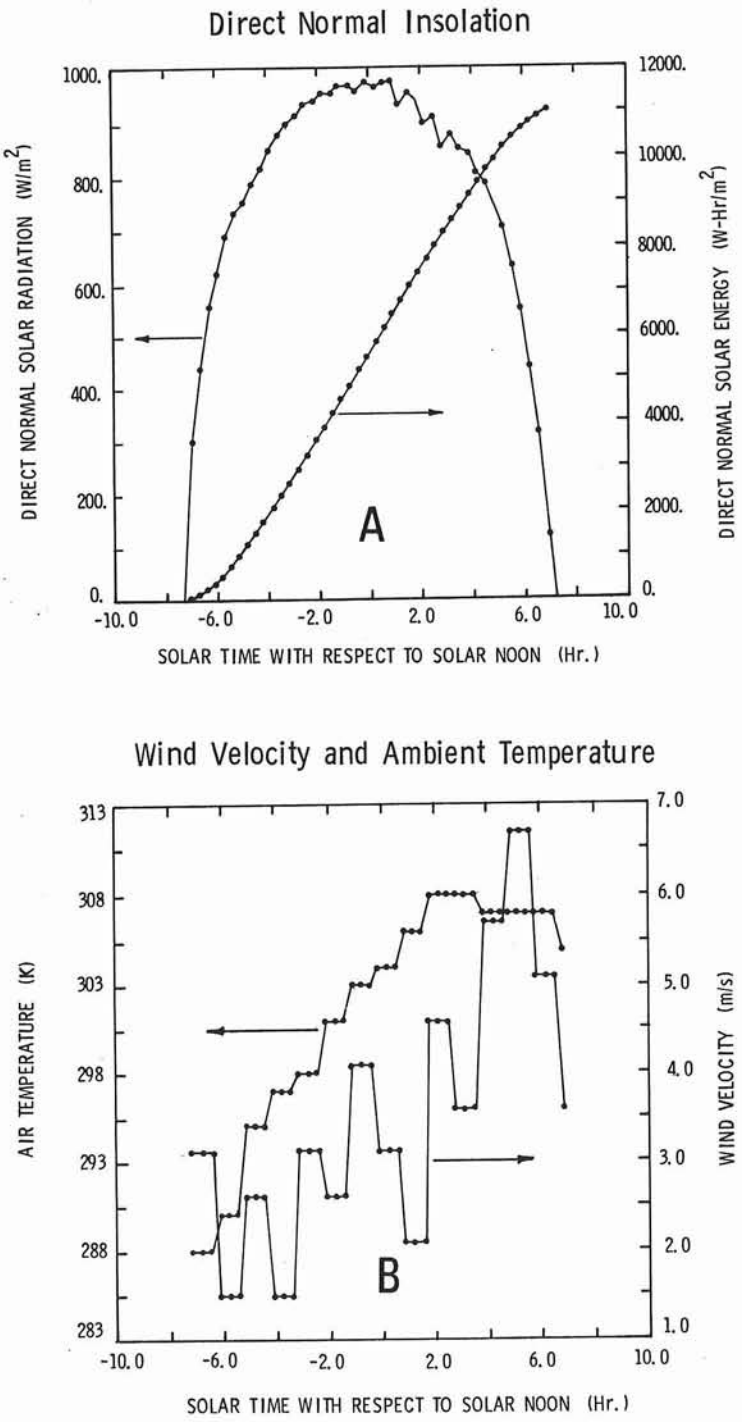

Figure A-1. Direct Normal Insolation and Weather Data for June 22, 1962 in Albuquerque, NM

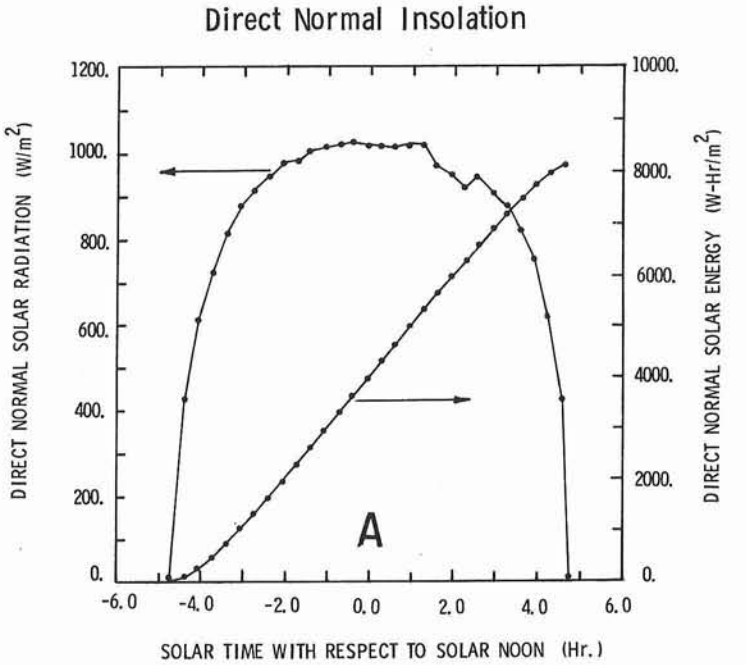

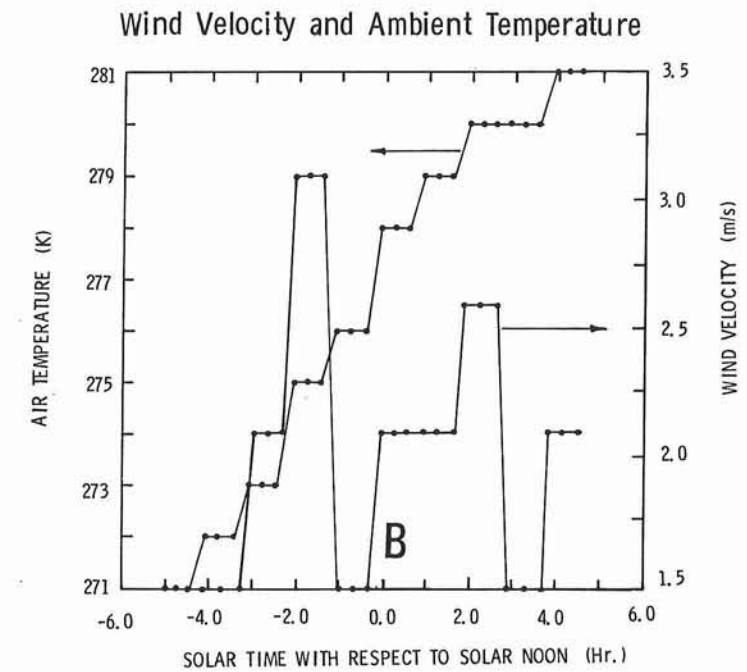

Figure A-2. Direct Normal Insolation and Weather Data for December 21, 1962 in Albuquerque, NM

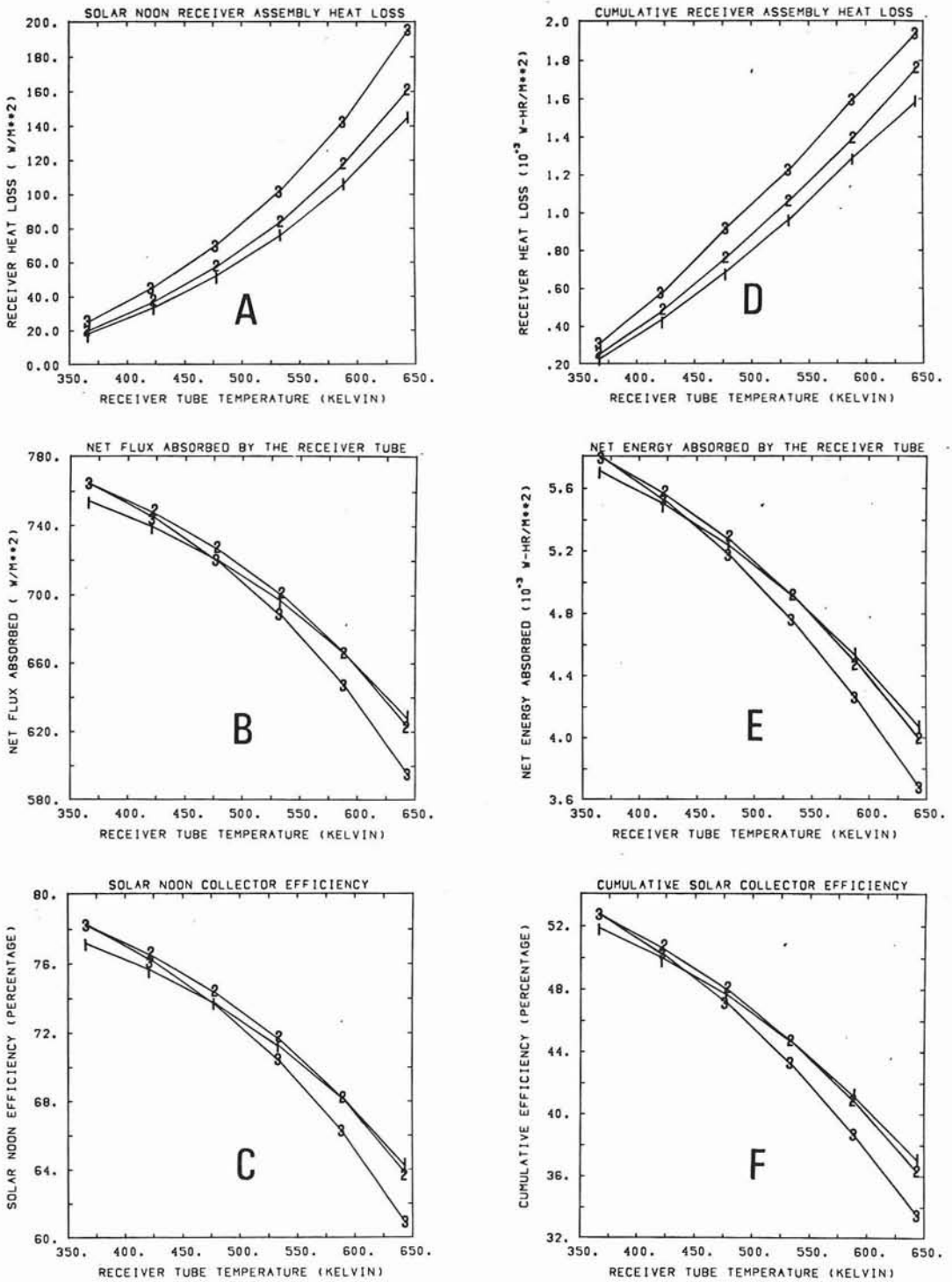

Figure A-3. Variation of Receiver Tube Operating Temperature--
June 22, 1962 Baseline Performance Results

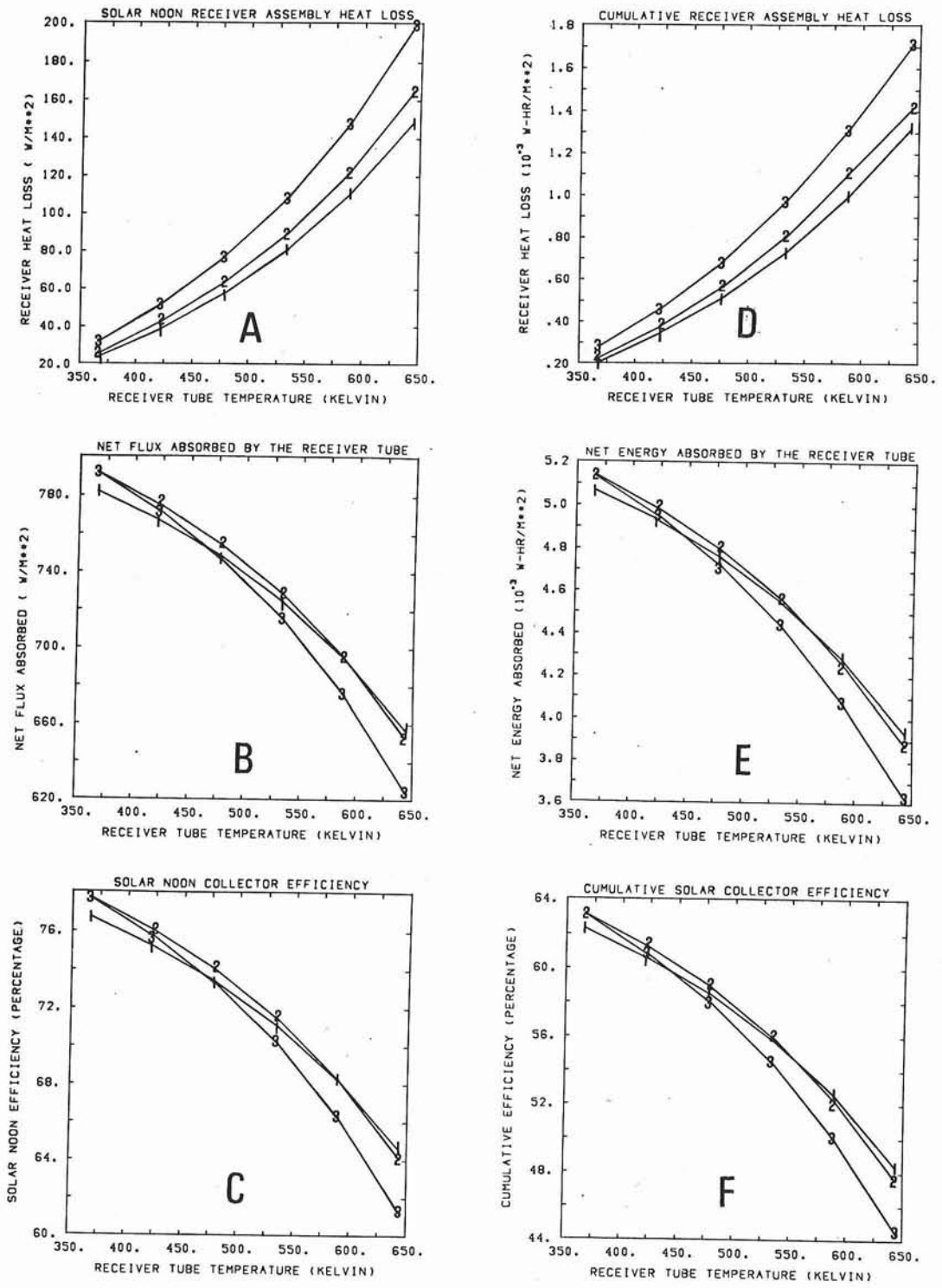

Figure A-4. Variation of Receiver Tube Operating Temperature--
December 21, 1962 Baseline Performance Results

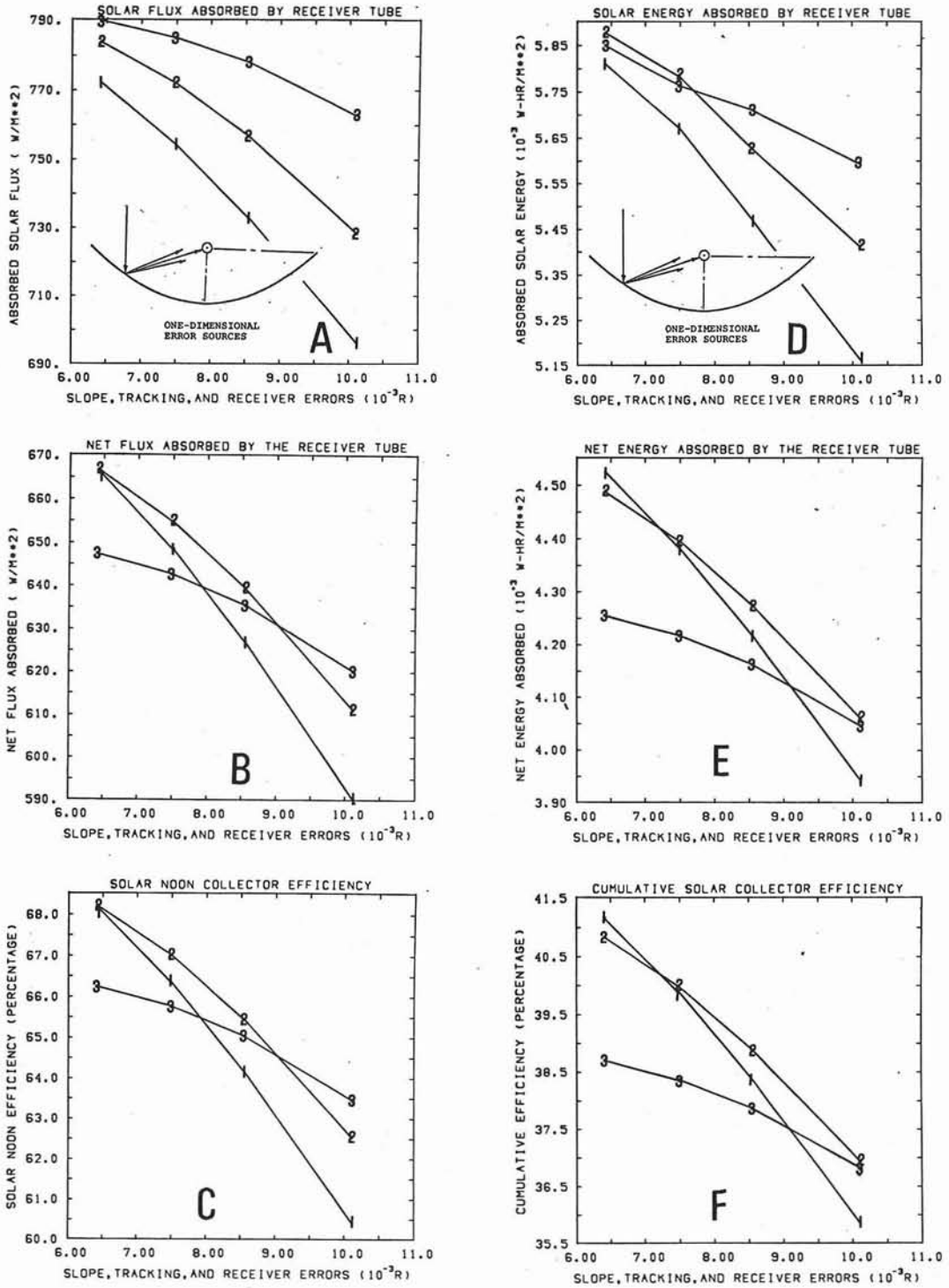

Figure A-5. Variation of One-Dimensional Collector Error Magnitude--
June 22, 1962 Baseline Performance Results

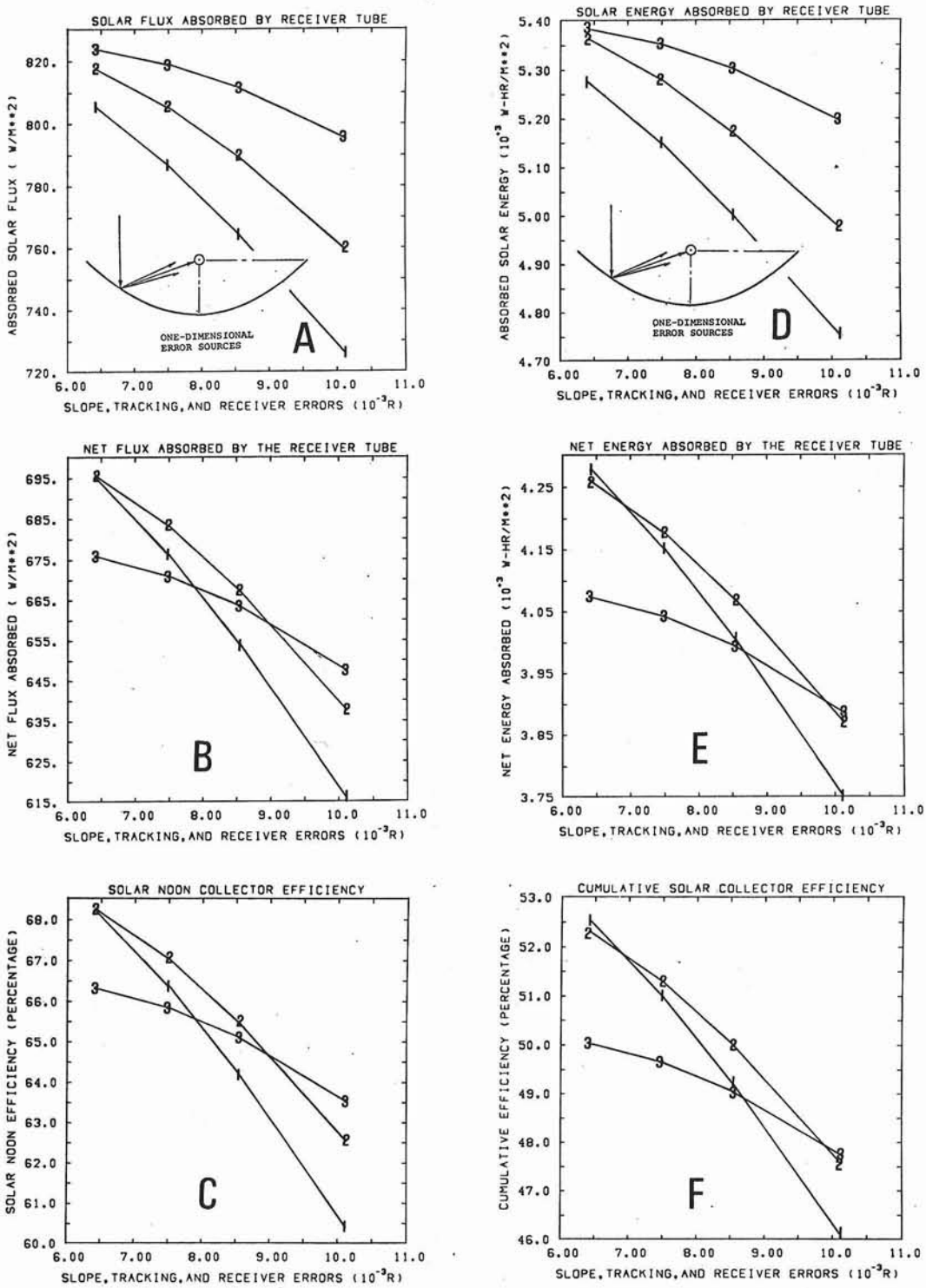

Figure A-6. Variation of One-Dimensional Collector Error Magnitude--December 21, 1962 Baseline Performance Results

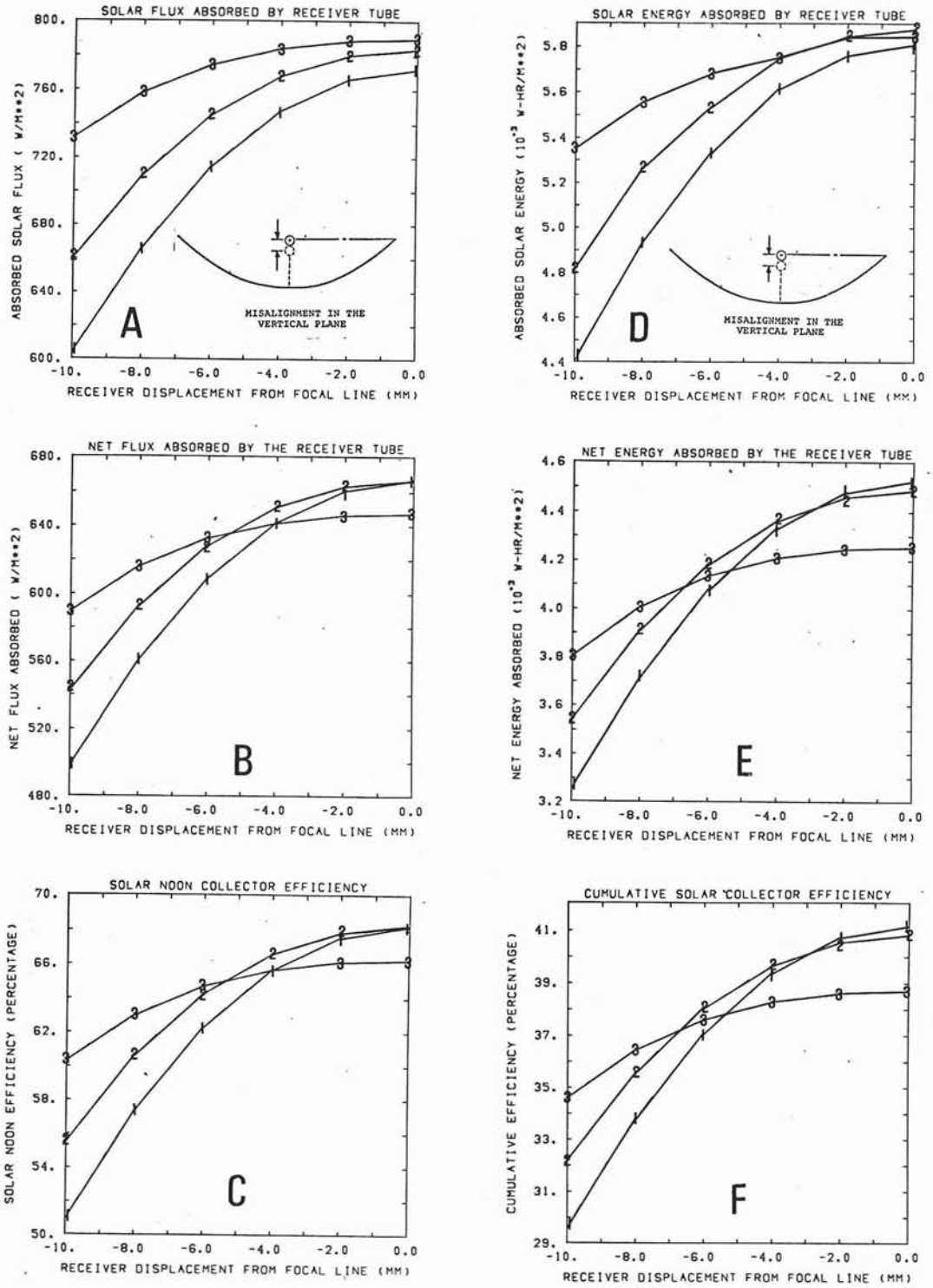

Figure A-7. Vertical Misalignment of the Receiver Assembly--
June 22, 1962 Baseline Performance Results

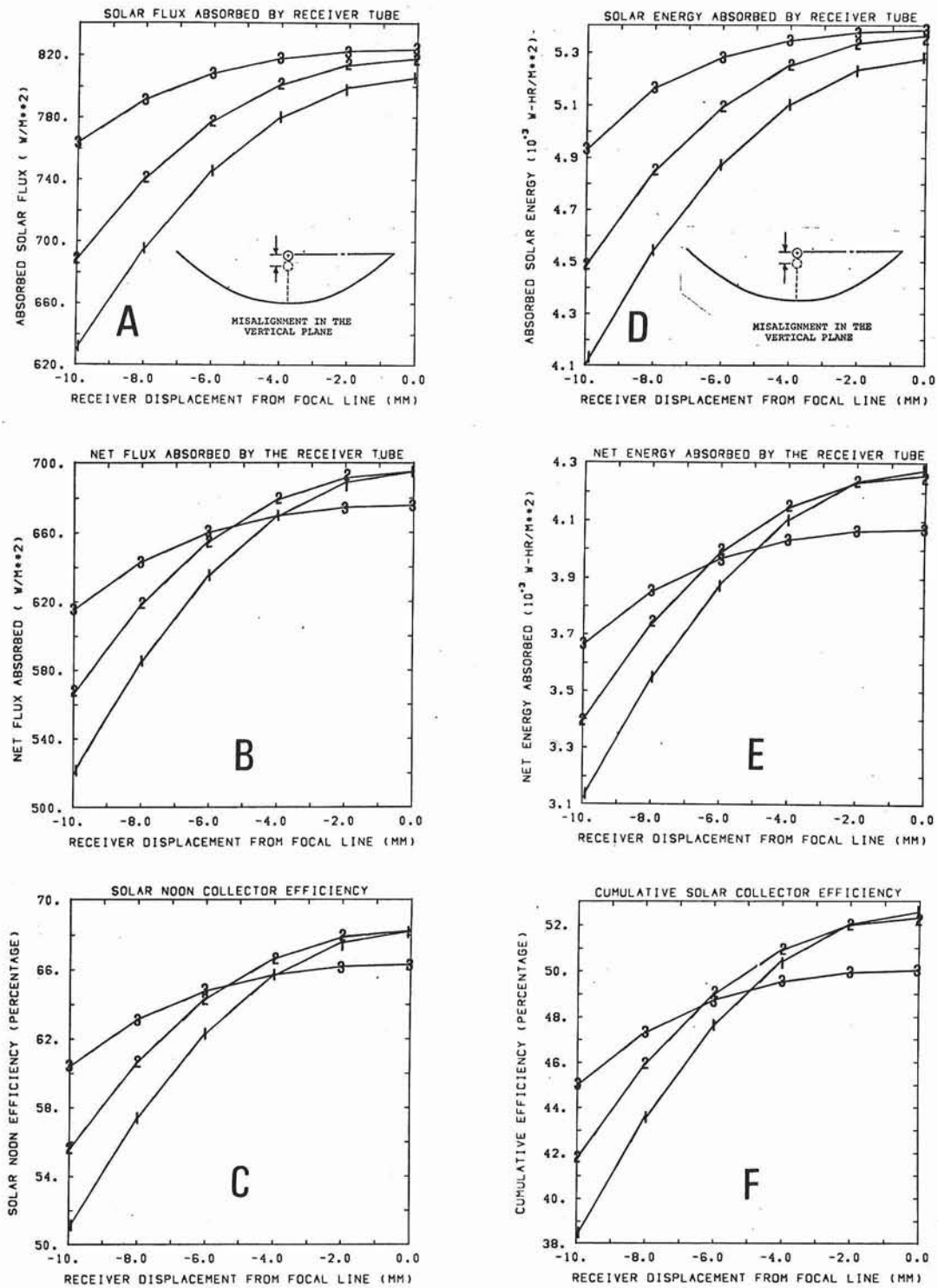

Figure A-8. Vertical Misalignment of the Receiver Assembly--
December 21, 1962 Baseline Performance Results

(Intentionally left blank)

APPENDIX B

Variation of Receiver-Tube Operating Temperature

Solar-noon and cumulative performance results are provided for the baseline parabolic-cylindrical collector, defined in Table I, as a function of receiver tube temperature. The analyses use March 15, 1962, weather and insolation conditions summarized in Figure 8 of the report. Results for two one-dimensional collector error magnitudes (6.41mR and 8.55 mR) and two annulus gas pressure conditions (8.379×10^{4} Pa and 1.33×10^{-2} Pa) are provided for comparative studies.

Data points on the figures designate results from the computer simulation. The following notation is used

1. 2.223-cm receiver-tube assembly
2. 2.54-cm receiver-tube assembly
3. 3.175-cm receiver-tube assembly

Results presented in the figures of Appendix B are summarized in Table B-I.

TABLE B-I

Receiver Tube Operating Temperature Variation - Summarized Results

Annulus Gas Pressure	One-Dimensional Collector Error (mR)	Type of Result	Figure Showing Result
Atmospheric (8.379×10^{4} Pa)	6.41 and 8.55	Solar Noon	B-1
		Cumulative	B-2
Evacuated (1.33×10^{-2} Pa)	6.41 and 8.55	Solar Noon	B-3
		Cumulative	B-4

* All other conditions are fixed according to Table I

Figure Description

A: Receiver assembly heat-loss characteristics with $P_{an} = 8.379 \times 10^4$ Pa
B: Net flux absorbed with $\sigma_{1D} = 6.41$ mR
C: Solar-noon efficiency with $\sigma_{1D} = 6.41$ mR
D: Net flux absorbed with $\sigma_{1D} = 8.55$ mR
E: Solar-noon efficiency with $\sigma_{1D} = 8.55$ mR

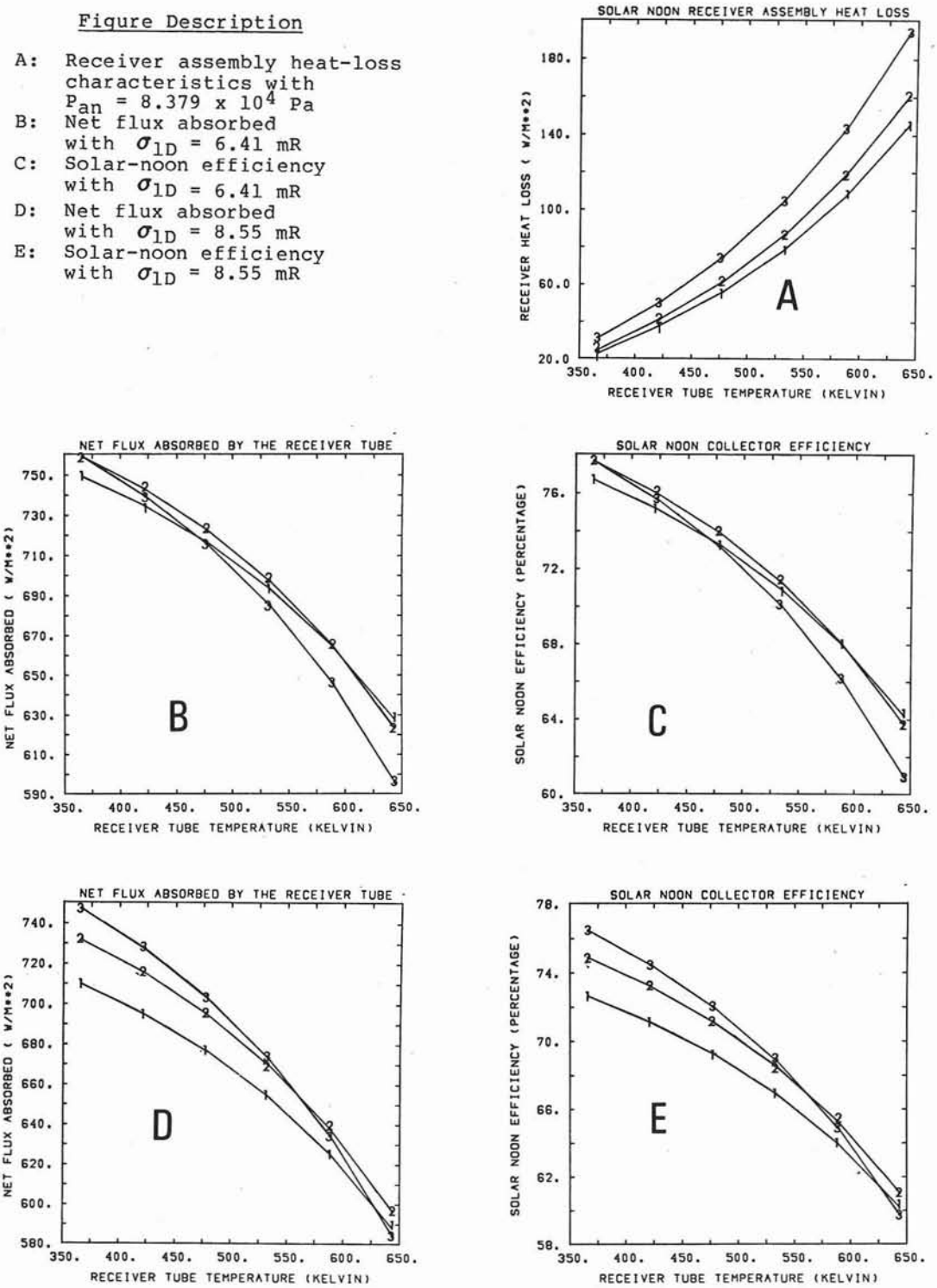

Figure B-1. Variation of the Receiver Tube Temperature with the Annular Space Maintained at Atmospheric Pressure-- Solar-Noon Results

Figure Description

A: Receiver assembly heat-loss characteristics with $P_{an} = 8.379 \times 10^4$ Pa
B: Net energy absorbed with $\sigma_{1D} = 6.41$ mR
C: Cumulative efficiency with $\sigma_{1D} = 6.41$ mR
D: Net energy absorbed with $\sigma_{1D} = 8.55$ mR
E: Cumulative efficiency with $\sigma_{1D} = 8.55$ mR

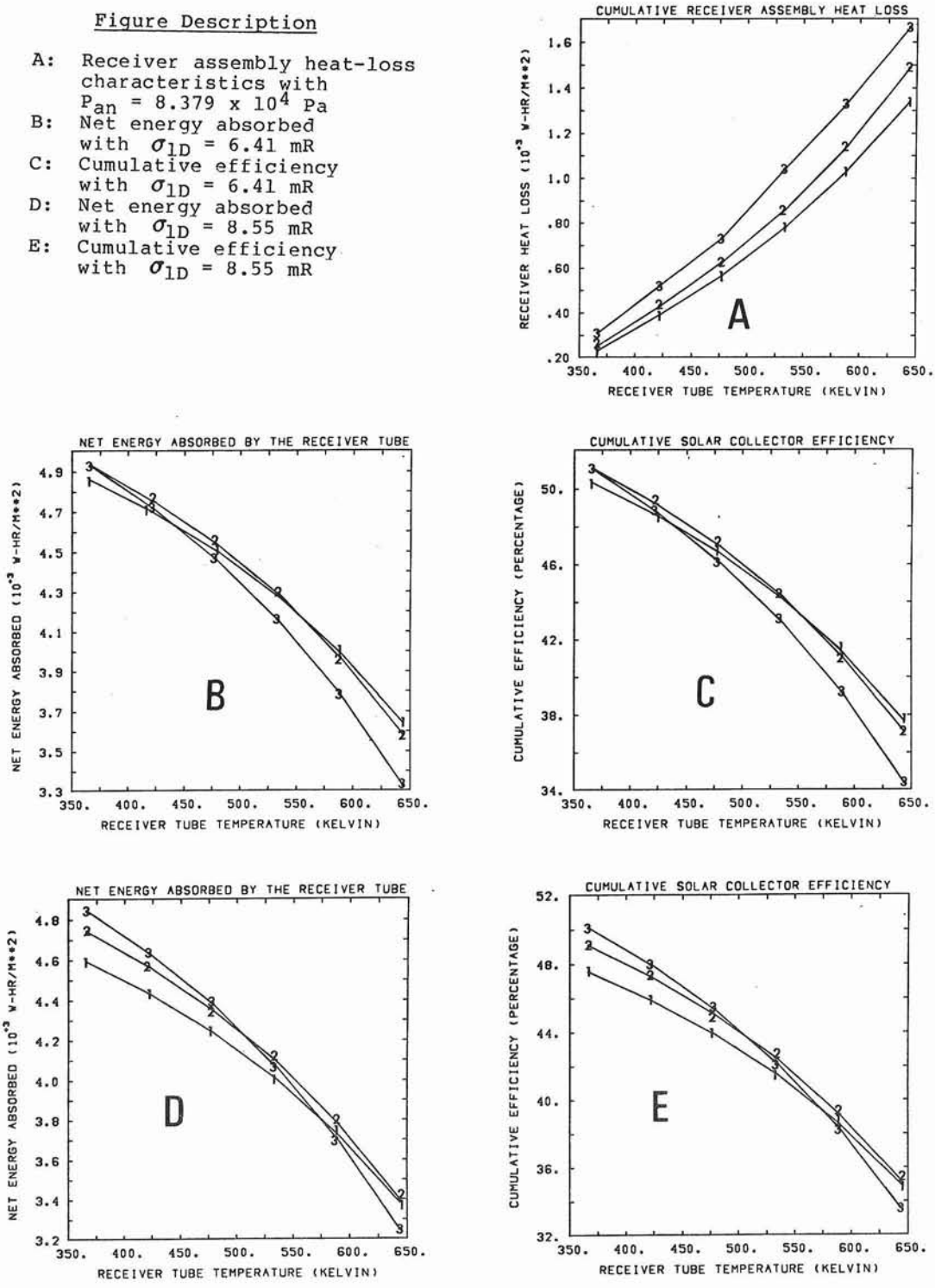

Figure B-2. Variation of the Receiver Tube Temperature with the Annular Space Maintained at Atmospheric Pressure-- Cumulative Results

Figure Description

A: Receiver assembly heat-loss characteristics with $P_{an} = 1.33 \times 10^{-2}$ Pa
B: Net flux absorbed with $\sigma_{1D} = 6.41$ mR
C: Solar-noon efficiency with $\sigma_{1D} = 6.41$ mR
D: Net flux absorbed with $\sigma_{1D} = 8.55$ mR
E: Solar-noon efficiency with $\sigma_{1D} = 8.55$ mR

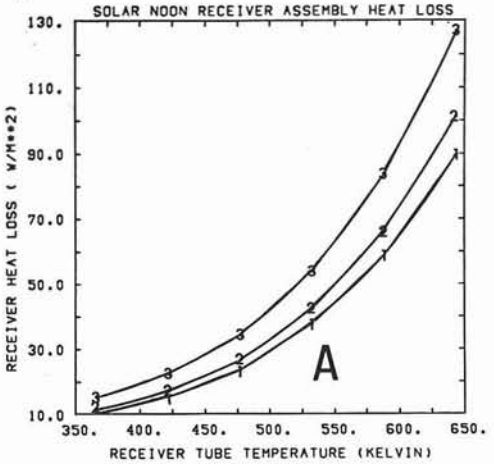

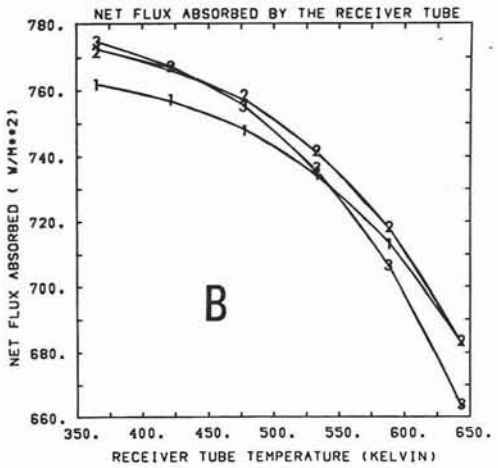

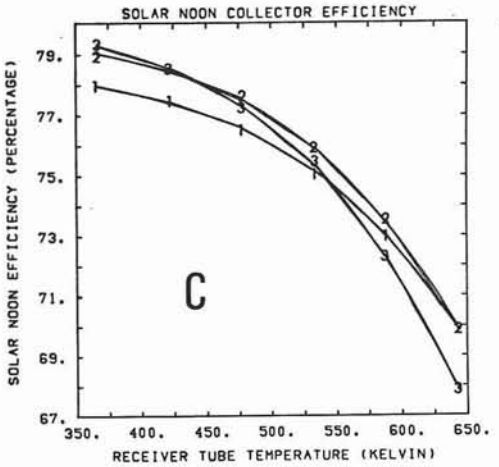

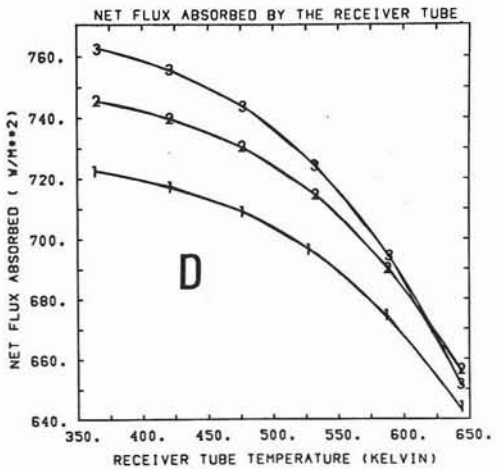

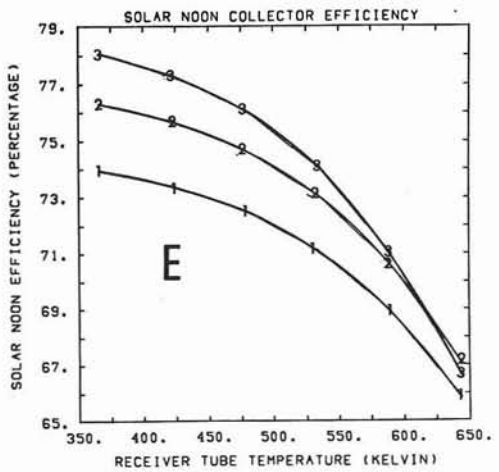

Figure B-3. Variation of the Receiver Tube Temperature with the Annular Space Evacuated to 1.33×10^{-2} Pa-- Solar-Noon Results

Figure Description

A: Receiver assembly heat-loss characteristics with $P_{an} = 1.33 \times 10^{-2}$ Pa
B: Net energy absorbed with $\sigma_{1D} = 6.41$ mR
C: Cumulative efficiency with $\sigma_{1D} = 6.41$ mR
D: Net energy absorbed with $\sigma_{1D} = 8.55$ mR
E: Cumulative efficiency with $\sigma_{1D} = 8.55$ mR

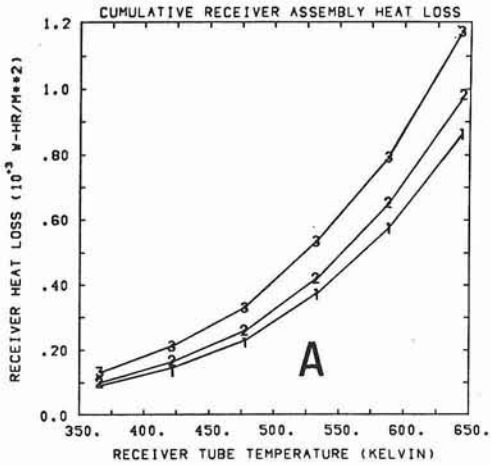

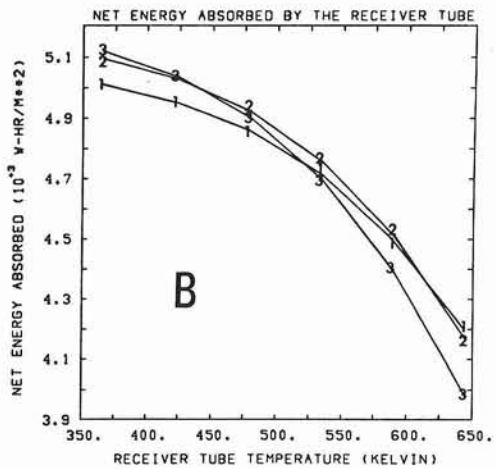

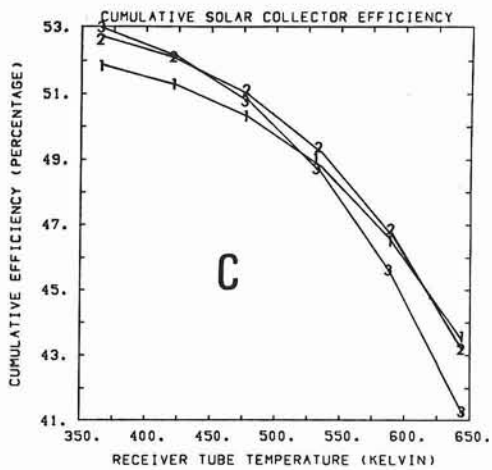

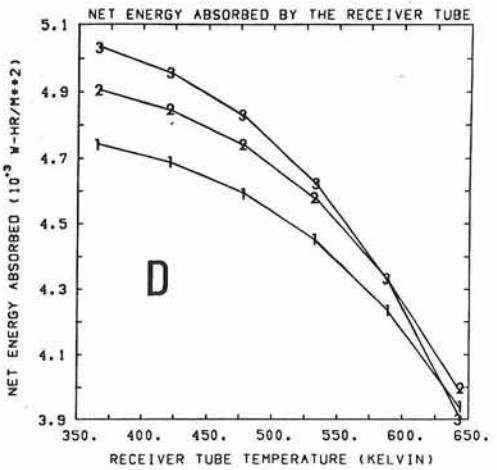

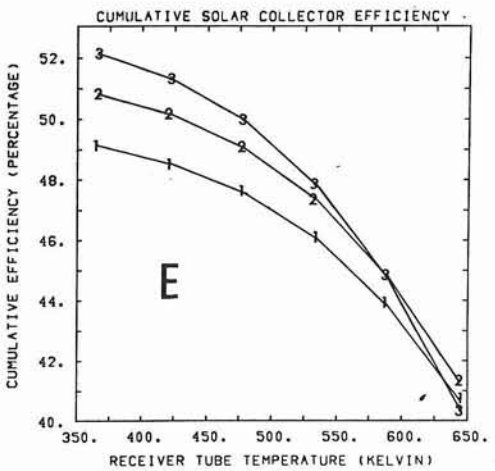

Figure B-4. Variation of the Receiver Tube Temperature with the Annular Space Evacuated to 1.33×10^{-2} Pa-- Cumulative Results

(Intentionally left blank)

APPENDIX C

One- and Two-Dimensional Collector Error Variation

Solar-noon and cumulative performance results are summarized for the baseline parabolic-cylindrical collector, defined in Table I, as a function of one- and two-dimensional collector error variation. The analyses use March 15, 1962, weather and insolation conditions, summarized in Figure 8 of the report. Results for two operating temperatures (477K and 589K) and two annulus gas pressure conditions (8.379×10^4 Pa and 1.33×10^{-2} Pa) are provided for comparative studies.

Data points on the figures designate results from the computer simulation. The following notation is used.

1. 2.223-cm receiver-tube assembly
2. 2.54-cm receiver-tube assembly
3. 3.175-cm receiver-tube assembly

Results presented in the figures of Appendix C are summarized in Table C-I.

TABLE C-I

Collector Error Magnitude Variation - Summarized Results*

Error Type Varied	Annulus Gas Pressure	Receiver Tube Temperature (K)	Type of Result	Figure Showing Results
2-D	Atmospheric (8.379×10^4 Pa)	477 and 589	Solar Noon	C-1
			Cumulative	C-2
1-D	Atmospheric (8.379×10^4 Pa) and Evacuated (1.33×10^{-2} Pa)	477	Solar Noon	C-3
			Cumulative	C-4
		589	Solar Noon	C-5
			Cumulative	C-6

*All other conditions are fixed according to Table I

Figure Description*

A: Solar flux absorbed by the receiver tube with σ_{1D} = 6.41 mR
B: Net flux absorbed with the receiver tube maintained at 477K
C: Solar-noon efficiency with the receiver tube maintained at 477K
D: Net flux absorbed with the receiver tube maintained at 589K
E: Solar-noon efficiency with the receiver tube maintained at 589K

*Note Abscissa does not include σ_{sun} = 2.80 mR

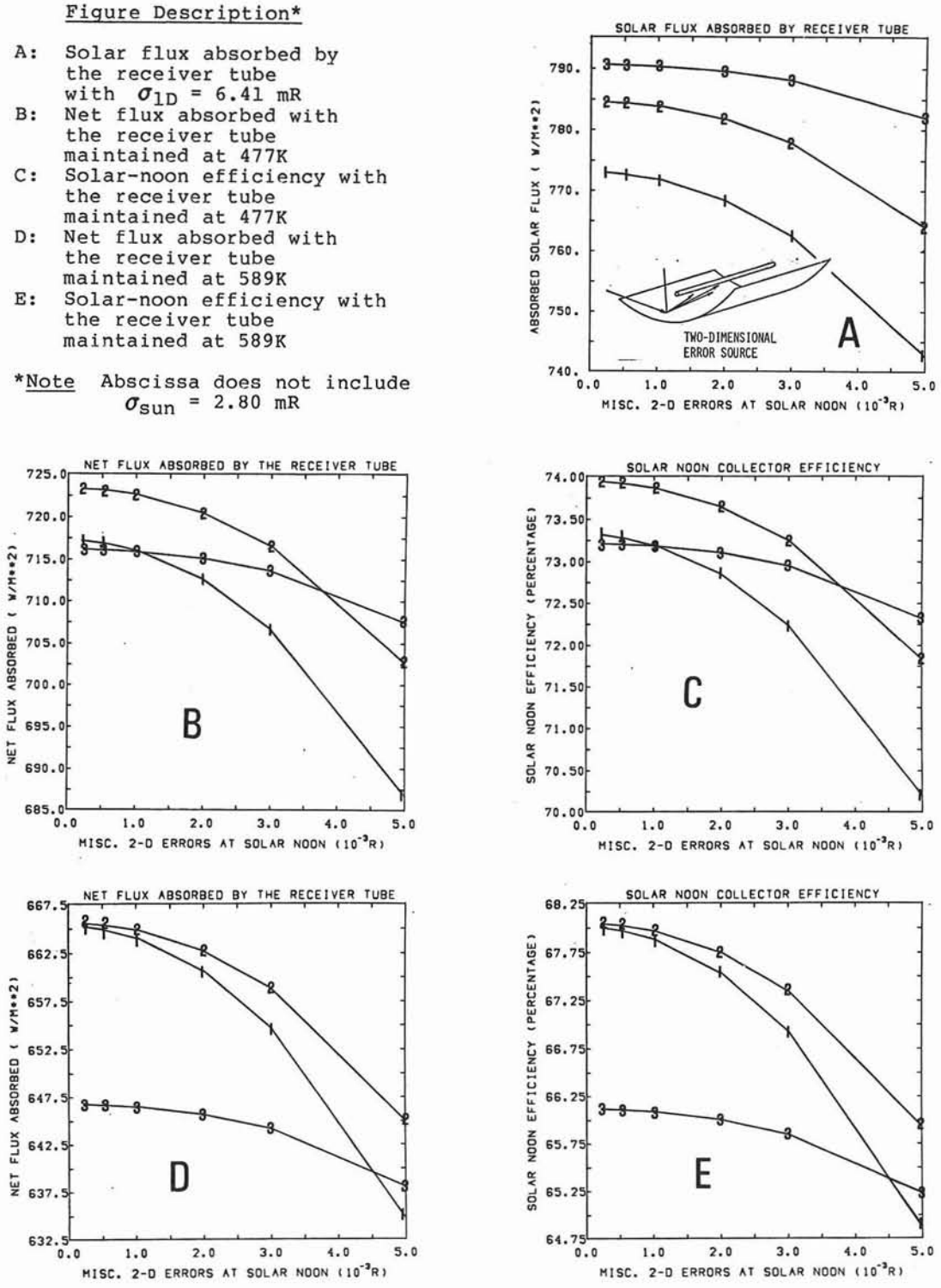

Figure C-1. Variation of Two-Dimensional Collector Error Magnitude-- Solar-Noon Results

Figure Description*

A: Solar energy absorbed by the receiver tube with σ_{1D} = 6.41 mR
B: Net energy absorbed with the receiver tube maintained at 477K
C: Cumulative efficiency with the receiver tube maintained at 477K
D: Net energy absorbed with the receiver tube maintained at 589K
E: Cumulative efficiency with the receiver tube maintained at 589K

*Note Abscissa does not include σ_{sun} = 2.80 mR

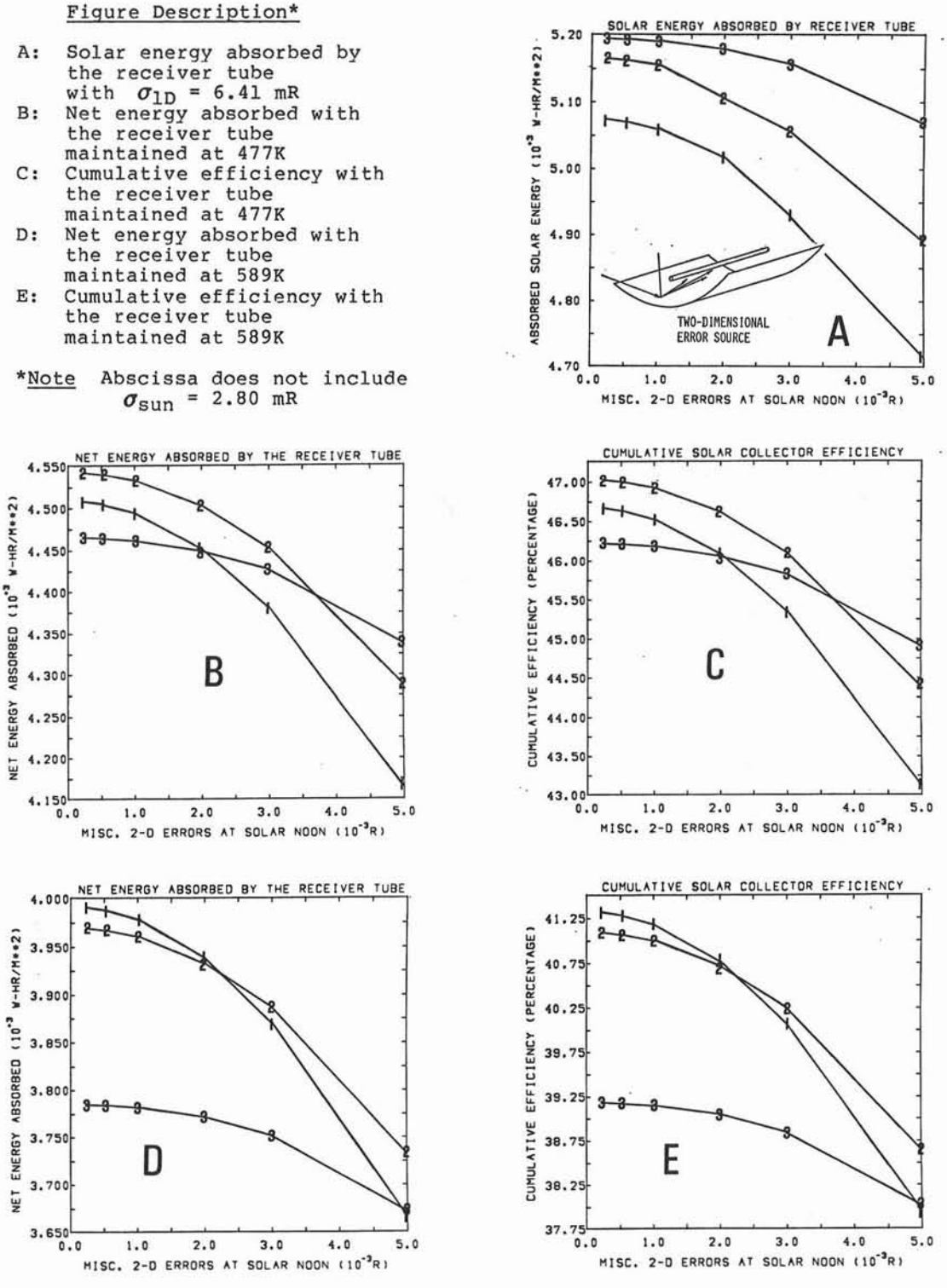

Figure C-2. Variation of Two-Dimensional Collector Error Magnitude-- Cumulative Results

Figure Description*

A: Solar flux absorbed by the receiver tube
B: Net flux absorbed by the receiver with $P_{an} = 8.379 \times 10^{4}$ Pa
C: Solar-noon efficiency with $P_{an} = 8.379 \times 10^{4}$ Pa
D: Net flux absorbed by the receiver with $P_{an} = 1.33 \times 10^{-2}$ Pa
E: Solar-noon efficiency with $P_{an} = 1.33 \times 10^{-2}$ Pa

*Note The receiver tube is maintained at 477K in this analysis

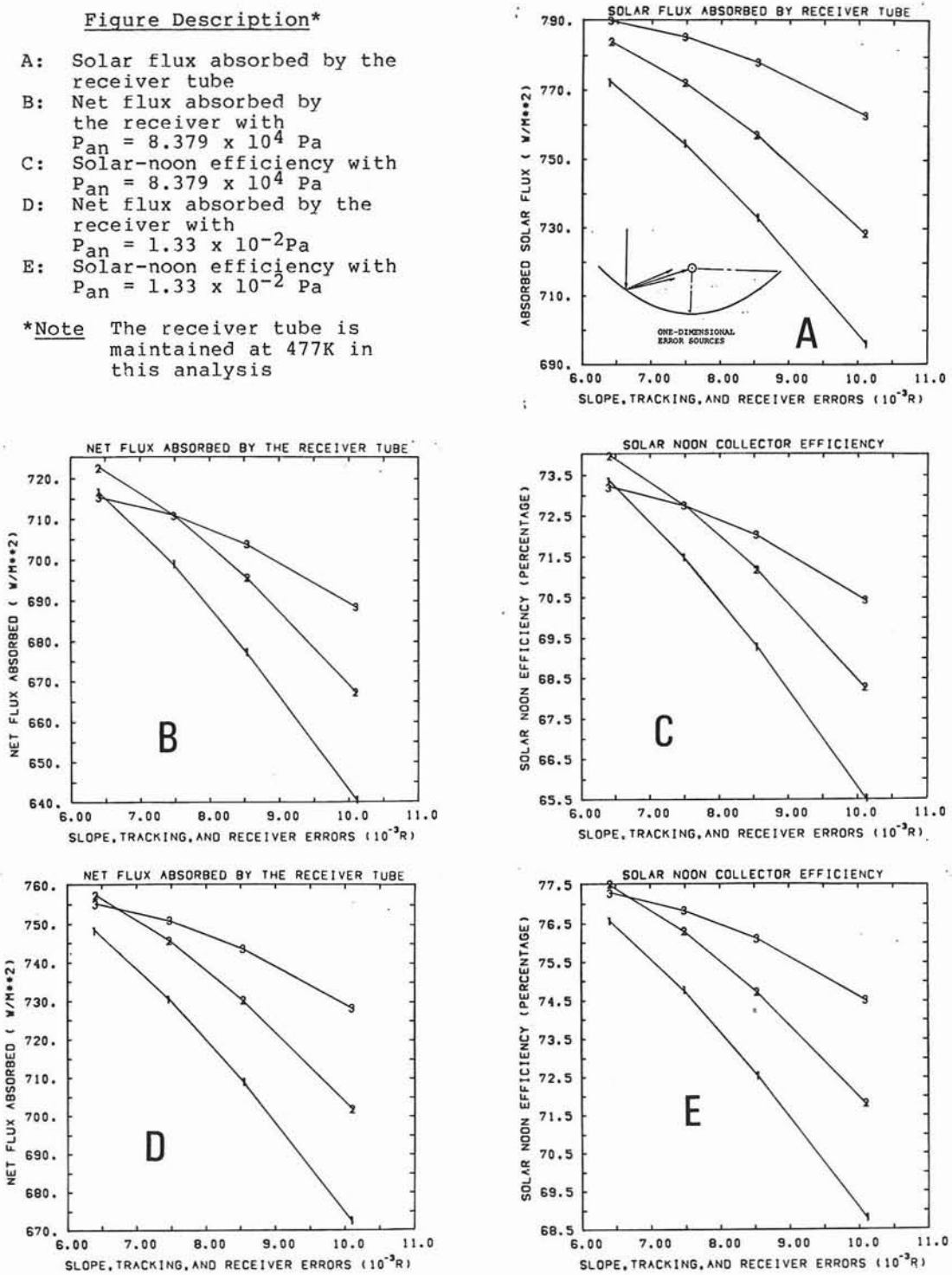

Figure C-3. Variation of One-Dimensional Collector Error Magnitude with the Receiver Tube Maintained at 477K-- Solar-Noon Results

Figure Description*

A: Solar energy absorbed by the receiver tube
B: Net energy absorbed by the receiver with $P_{an} = 8.379 \times 10^4$ Pa
C: Cumulative efficiency with $P_{an} = 8.379 \times 10^4$ Pa
D: Net energy absorbed by receiver with $P_{an} = 1.33 \times 10^{-2}$ Pa
E: Cumulative efficiency with $P_{an} = 1.33 \times 10^{-2}$ Pa

*Note The receiver tube is maintained at 477K in this analysis

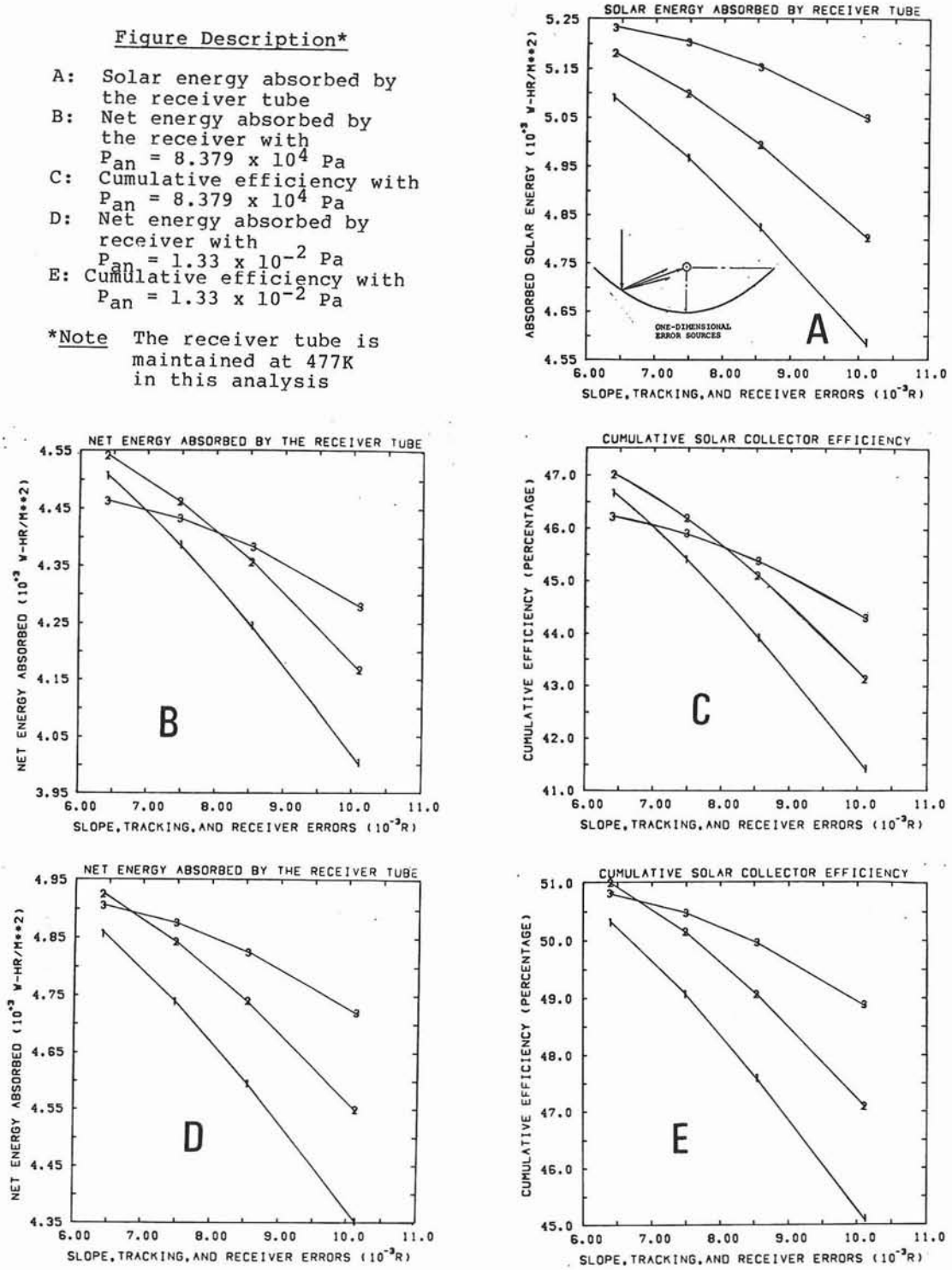

Figure C-4. Variation of One-Dimensional Collector Error Magnitude with the Receiver Tube Maintained at 477K-- Cumulative Results

Figure Description*

A: Solar flux absorbed by the receiver tube
B: Net flux absorbed by the receiver with $P_{an} = 8.379 \times 10^{4}$ Pa
C: Solar-noon efficiency with $P_{an} = 8.379 \times 10^{4}$ Pa
D: Net flux absorbed by the receiver with $P_{an} = 1.33 \times 10^{-2}$ Pa
E: Solar-noon efficiency with $P_{an} = 1.33 \times 10^{-2}$ Pa

*Note The receiver tube is maintained at 589K in this analysis

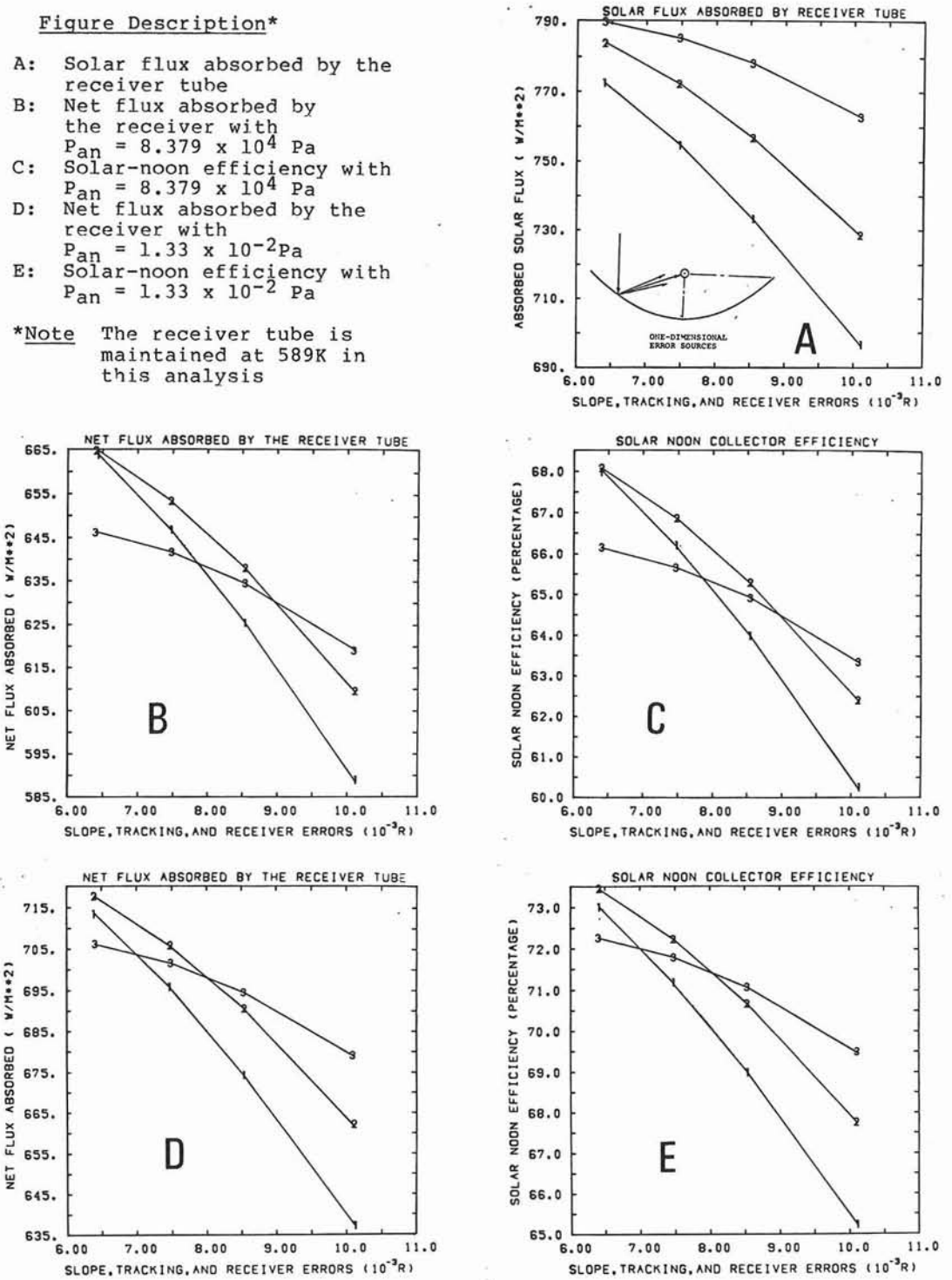

Figure C-5. Variation of One-Dimensional Collector Error Magnitude with the Receiver Tube Maintained at 589K-- Solar-Noon Results

Figure Description*

A: Solar energy absorbed by the receiver tube
B: Net energy absorbed by the receiver with $P_{an} = 8.379 \times 10^4$ Pa
C: Cumulative efficiency with $P_{an} = 8.379 \times 10^4$ Pa
D: Net energy absorbed by receiver with $P_{an} = 1.33 \times 10^{-2}$ Pa
E: Cumulative efficiency with $P_{an} = 1.33 \times 10^{-2}$ Pa

*Note The receiver tube is maintained at 589K in this analysis

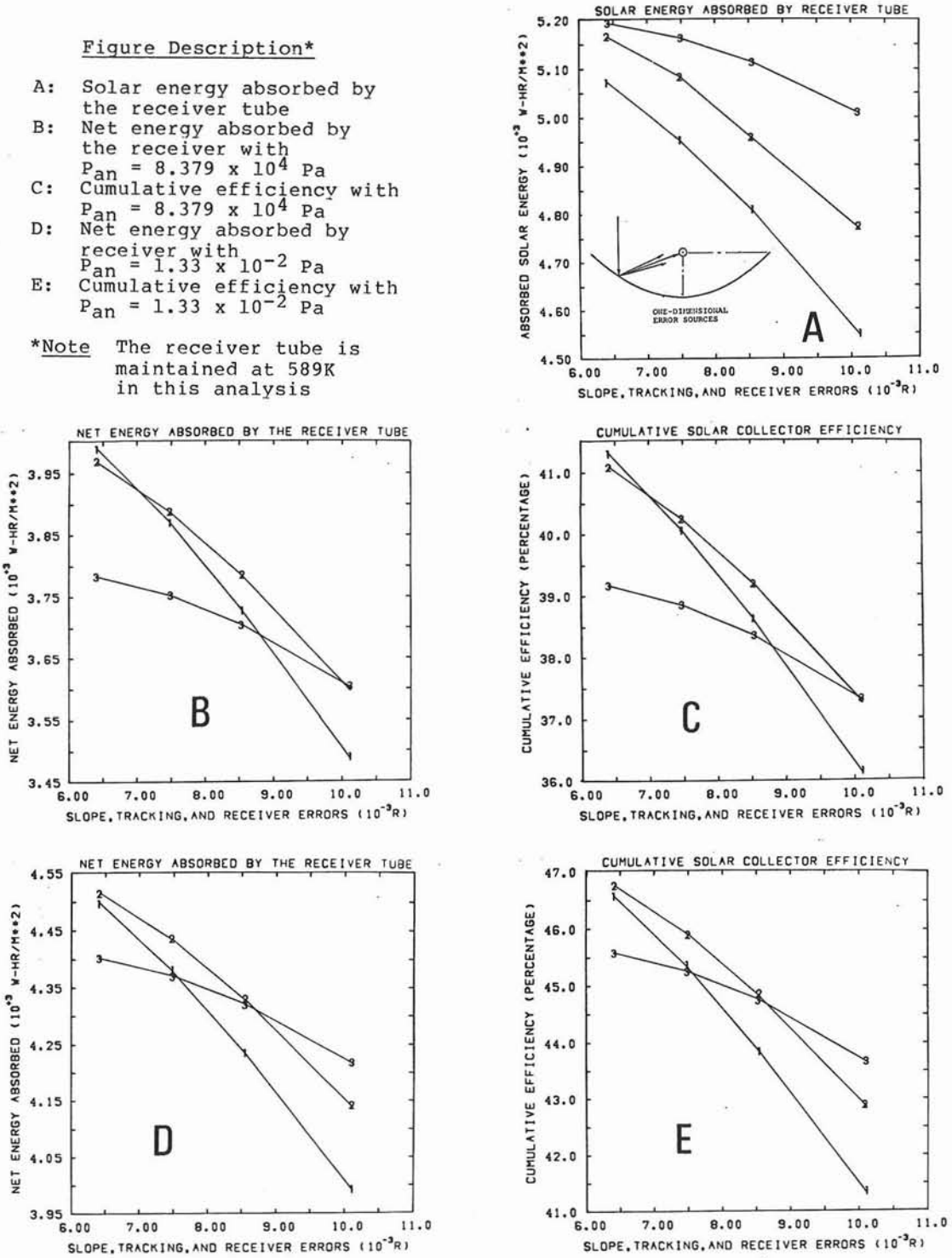

Figure C-6. Variation of One-Dimensional Collector Error Magnitude with the Receiver Tube Maintained at 589 K-- Cumulative Results

(Intentionally left blank)

APPENDIX D

Misalignment of the Receiver Assembly from the Focal Line

Solar-noon and cumulative performance results are summarized for the baseline parabolic-cylindrical collector, defined in Table I, as a function of receiver assembly position from the focal line. The analyses use March 15, 1962, weather and insolation conditions, summarized in Figure 8 of the report. Results for two operating temperatures (477K and 589K) and two one-dimensional collector error magnitudes (6.41mR and 8.55mR) are provided for comparative studies of horizontal and vertical receiver misalignment.

Data points on the figures designate results from the computer simulation. The following notation is used:

1. 2.223-cm receiver-tube assembly
2. 2.54-cm receiver-tube assembly
3. 3.175-cm receiver-tube assembly

Results presented in the figures of Appendix D are summarized in Table D-I.

TABLE D-1

Misalignment of the Receiver Assembly - Summarized Results*

Misalignment Direction	Receiver Tube Operating Temperature (K)	One-Dimensional Collector Error (mR)	Type of Result	Figure Showing Results
Vertical	477 and 589	6.41	Solar Noon	D-1
			Cumulative	D-2
		8.55	Solar Noon	D-3
			Cumulative	D-4
Horizontal	477 and 589	6.41	Solar Noon	D-5
			Cumulative	D-6
		8.55	Solar Noon	D-7
			Cumulative	D-8

* All other conditions are fixed according to Table I

Figure Description*

A: Solar flux absorbed by the receiver tube
B: Net flux absorbed with the receiver tube maintained at 477K
C: Solar-noon efficiency with the receiver tube maintained at 477K
D: Net flux absorbed with the receiver tube maintained at 589K
E: Solar-noon efficiency with the receiver tube maintained at 589K

*Note σ_{1D} = 6.41 mR is used in this analysis

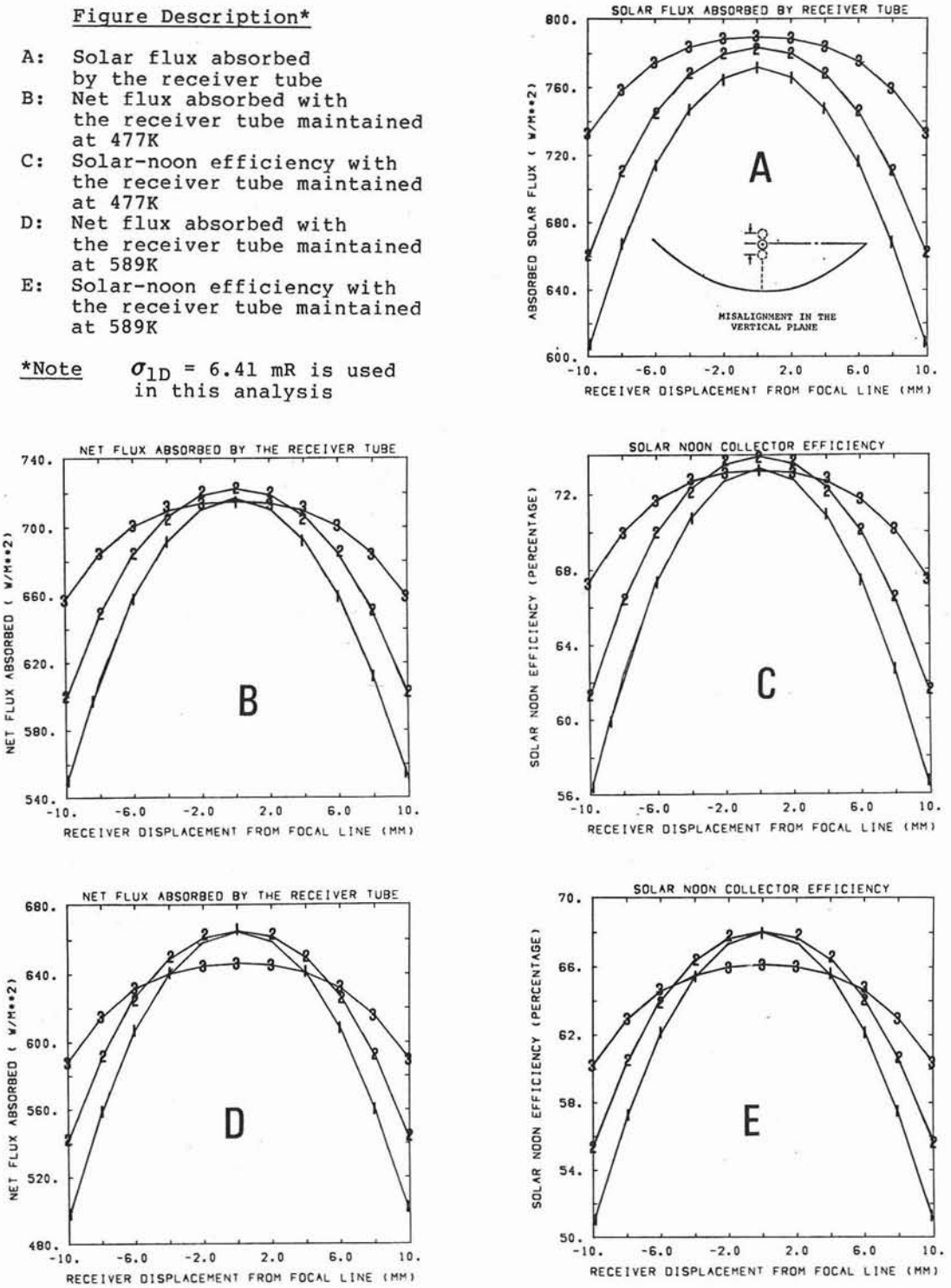

Figure D-1. Vertical Misalignment of the Receiver Assembly with the One-Dimensional Collector Error Fixed at 6.41 mR--Solar-Noon Results

Figure Description*

A: Solar energy absorbed by the receiver tube
B: Net energy absorbed with the receiver tube maintained at 477K
C: Cumulative efficiency with the receiver tube maintained at 477K
D: Net energy absorbed with the receiver tube maintained at 589K
E: Cumulative efficiency with the receiver tube maintained at 589K

*Note σ_{1D} = 6.41 mR is used in this analysis

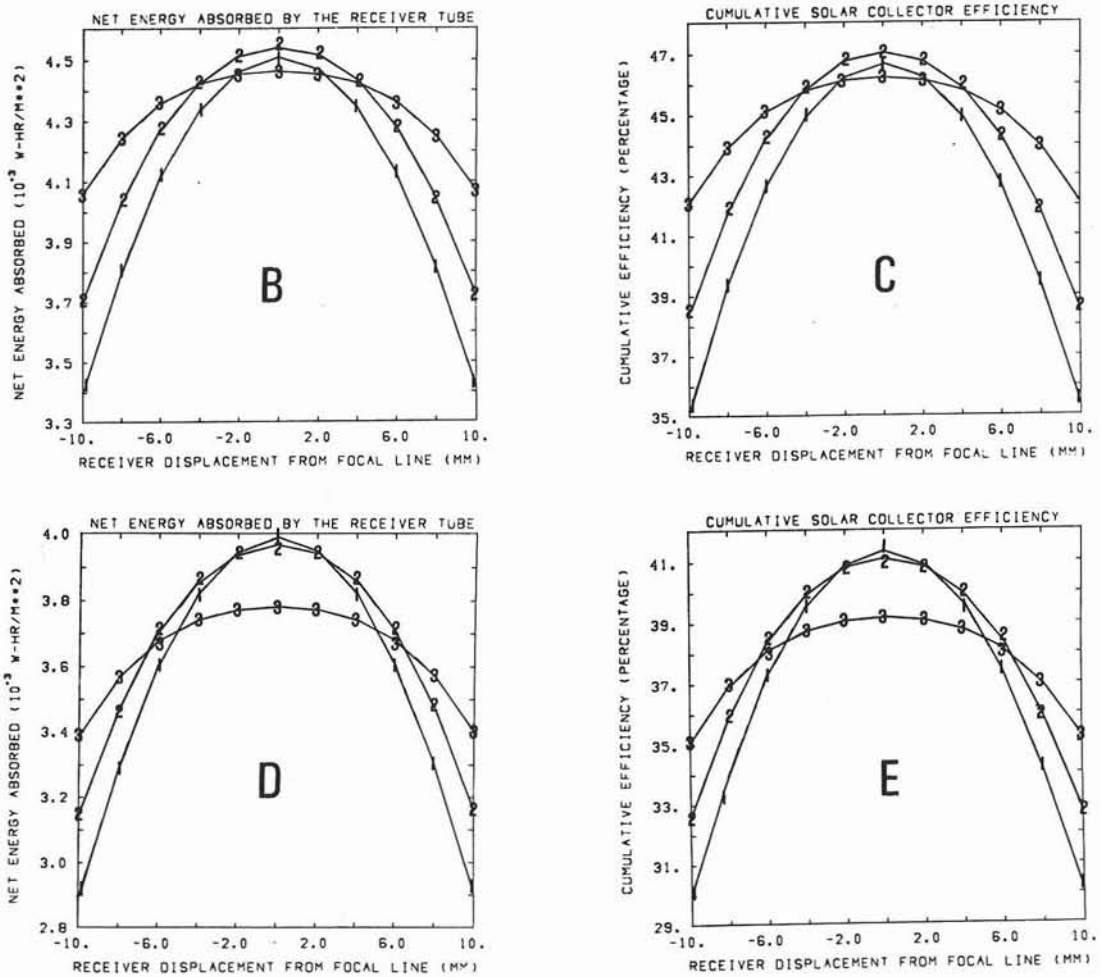

Figure D-2. Vertical Misalignment of the Receiver Assembly with the One-Dimensional Collector Error Fixed at 6.41 mR--Cumulative Results

Figure Description*

A: Solar flux absorbed by the receiver tube
B: Net flux absorbed with the receiver tube maintained at 477K
C: Solar-noon efficiency with the receiver tube maintained at 477K
D: Net flux absorbed with the receiver tube maintained at 589K
E: Solar-noon efficiency with the receiver tube maintained at 589K

*Note σ_{1D} = 8.55 mR is used in this analysis

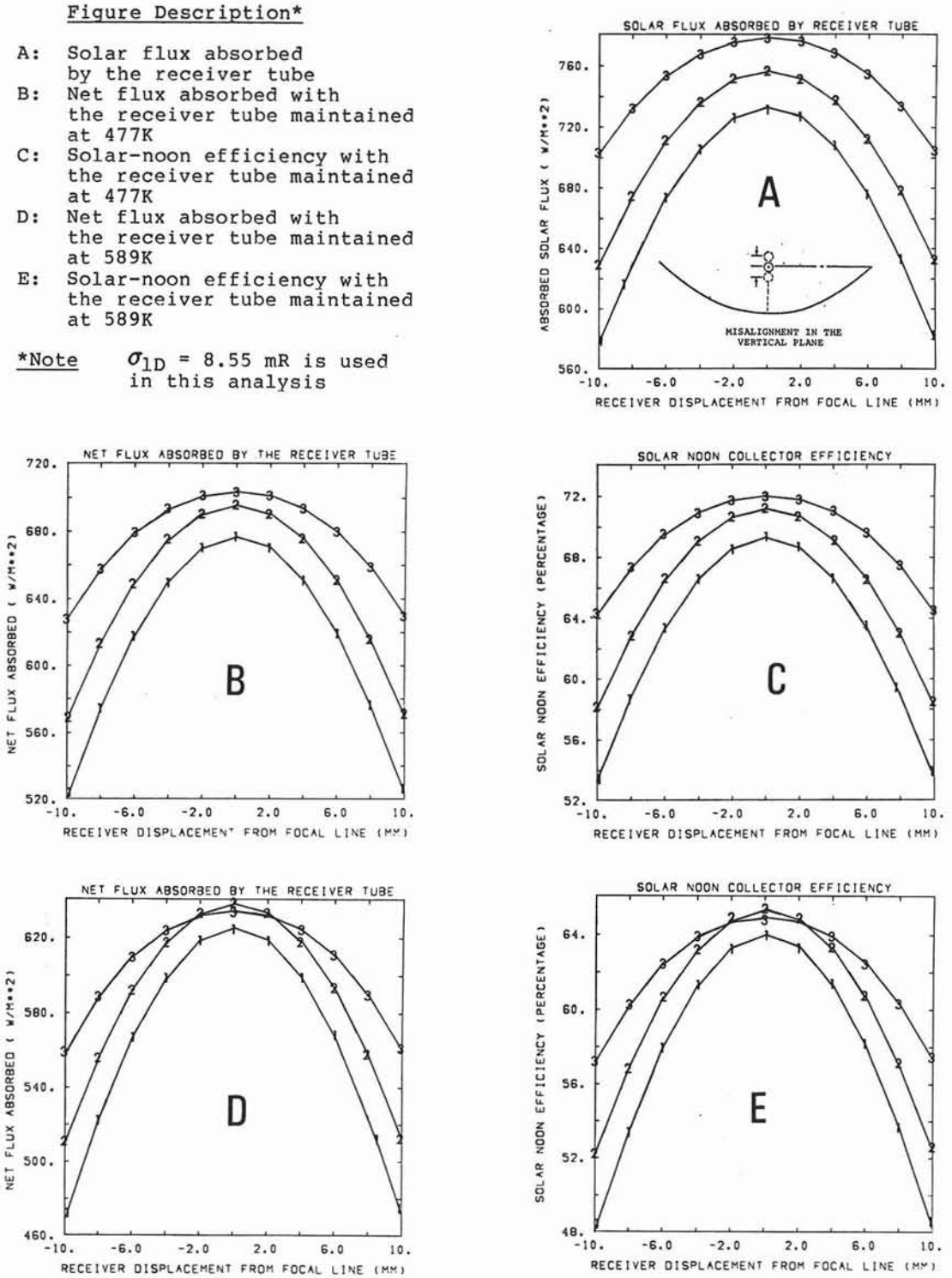

Figure D-3. Vertical Misalignment of the Receiver Assembly with the One-Dimensional Collector Error Fixed at 8.55 mR--Solar-Noon Results

Figure Description*

A: Solar energy absorbed by the receiver tube
B: Net energy absorbed with the receiver tube maintained at 477K
C: Cumulative efficiency with the receiver tube maintained at 477K
D: Net energy absorbed with the receiver tube maintained at 589K
E: Cumulative efficiency with the receiver tube maintained at 589K

*Note σ_{1D} = 8.55 mR is used in this analysis

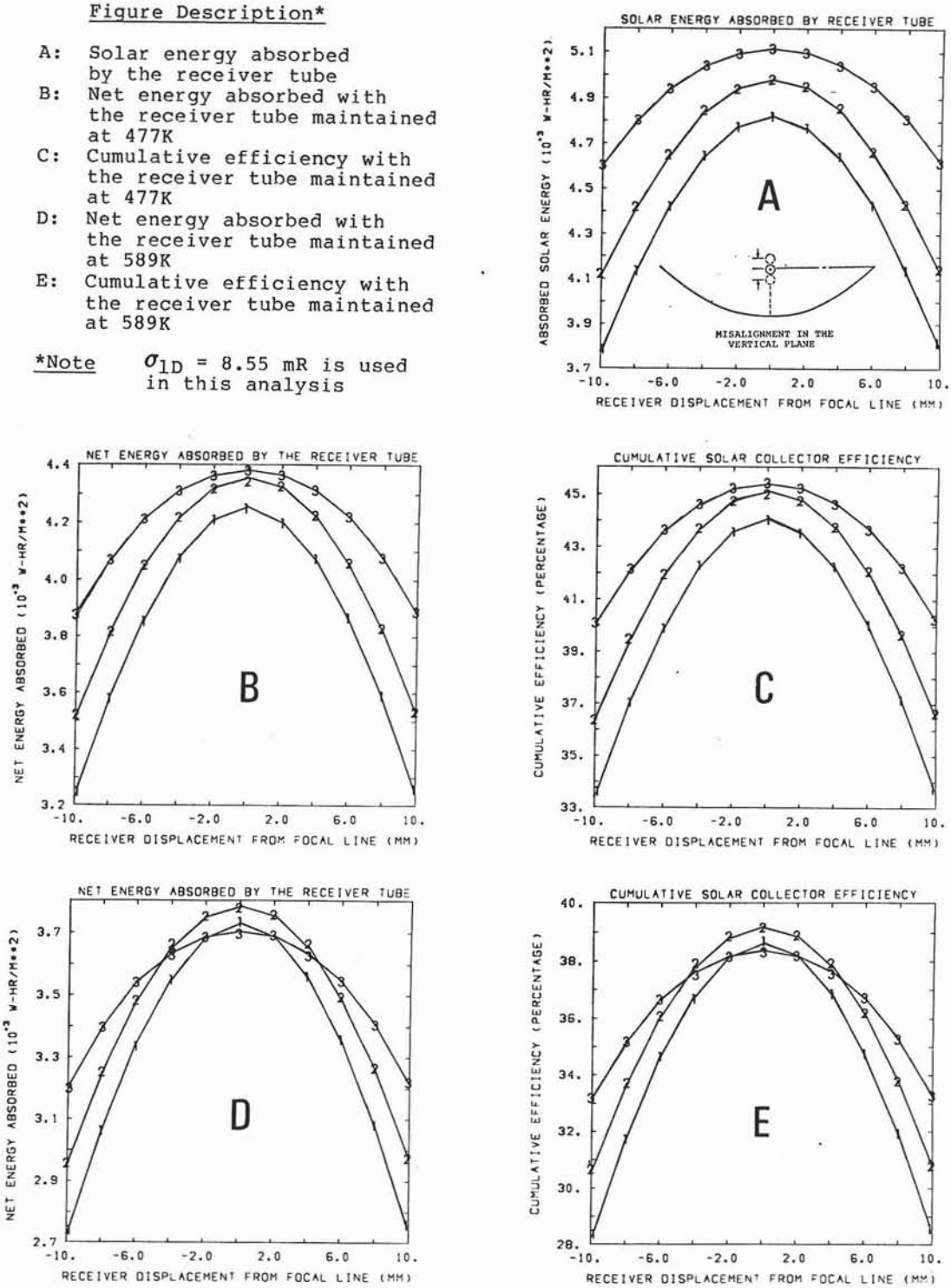

Figure D-4. Vertical Misalignment of the Receiver Assembly with the One-Dimensional Collector Error Fixed at 8.55 mR-- Cumulative Results

Figure Description*

A: Solar flux absorbed by the receiver tube
B: Net flux absorbed with the receiver tube maintained at 477K
C: Solar-noon efficiency with the receiver tube maintained at 477K
D: Net flux absorbed with the receiver tube maintained at 589K
E: Solar-noon efficiency with the receiver tube maintained at 589K

*Note σ_{1D} = 6.41 mR is used in this analysis

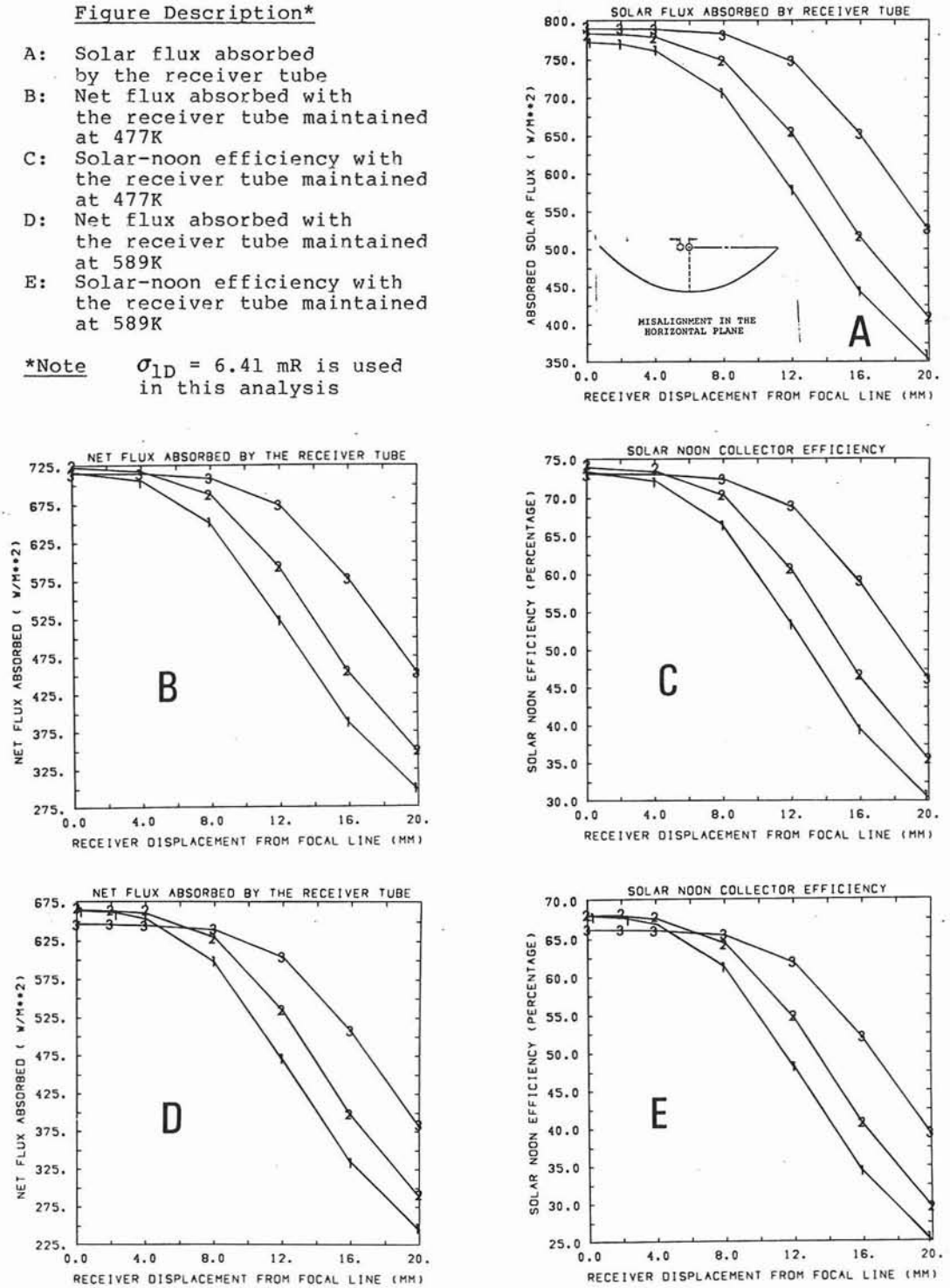

Figure D-5. Horizontal Misalignment of the Receiver Assembly with the One-Dimensional Collector Error Fixed at 6.41 mR-- Solar-Noon Results

Figure Description*

A: Solar energy absorbed by the receiver tube
B: Net energy absorbed with the receiver tube maintained at 477K
C: Cumulative efficiency with the receiver tube maintained at 477K
D: Net energy absorbed with the receiver tube maintained at 589K
E: Cumulative efficiency with the receiver tube maintained at 589K

*Note σ_{1D} = 6.41 mR is used in this analysis

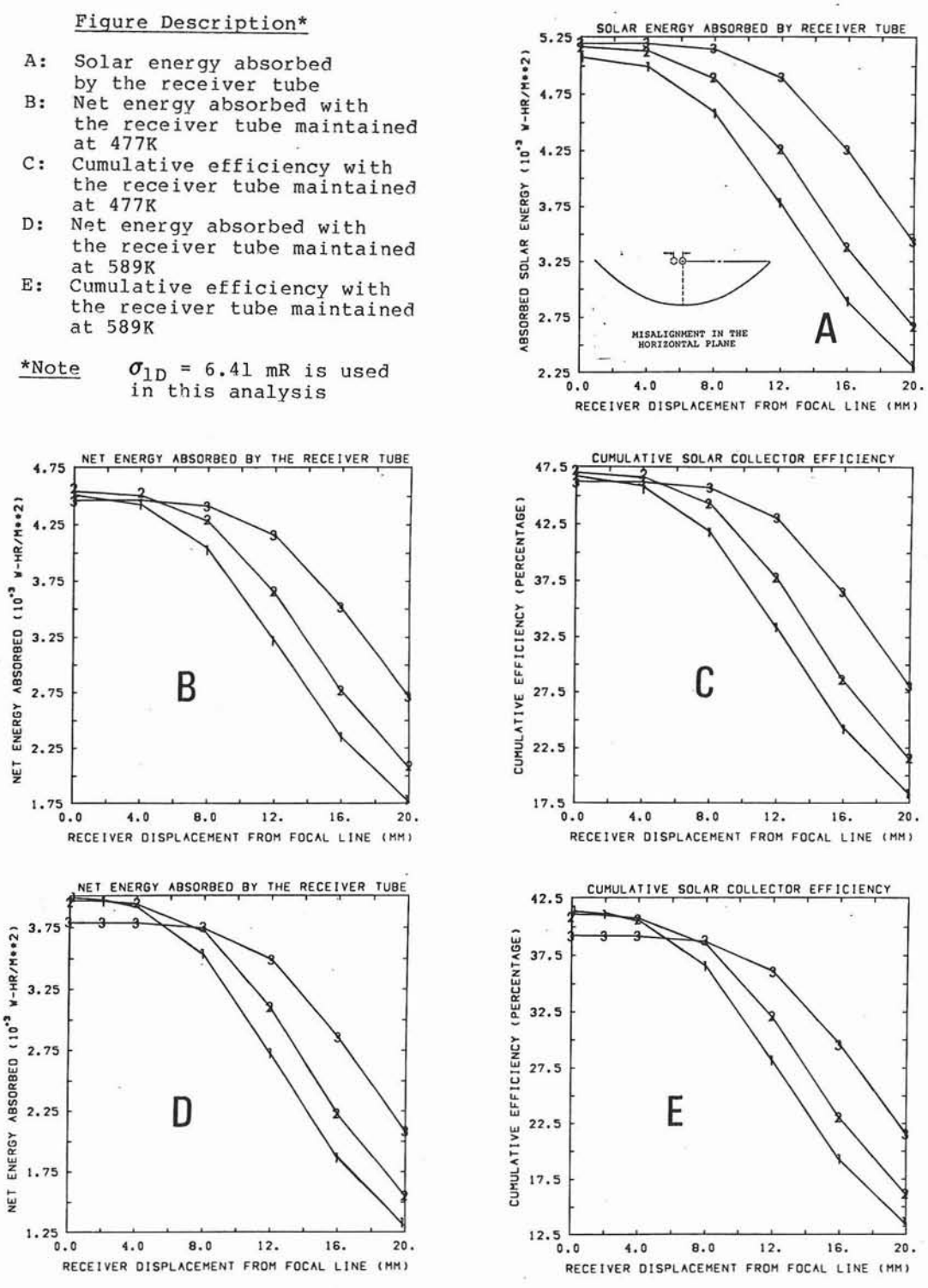

Figure D-6. Horizontal Misalignment of the Receiver Assembly with the One-Dimensional Collector Error Fixed at 6.41 mR-- Cumulative Results

Figure Description*

A: Solar flux absorbed by the receiver tube
B: Net flux absorbed with the receiver tube maintained at 477K
C: Solar-noon efficiency with the receiver tube maintained at 477K
D: Net flux absorbed with the receiver tube maintained at 589K
E: Solar-noon efficiency with the receiver tube maintained at 589K

*Note σ_{1D} = 8.55 mR is used in this analysis

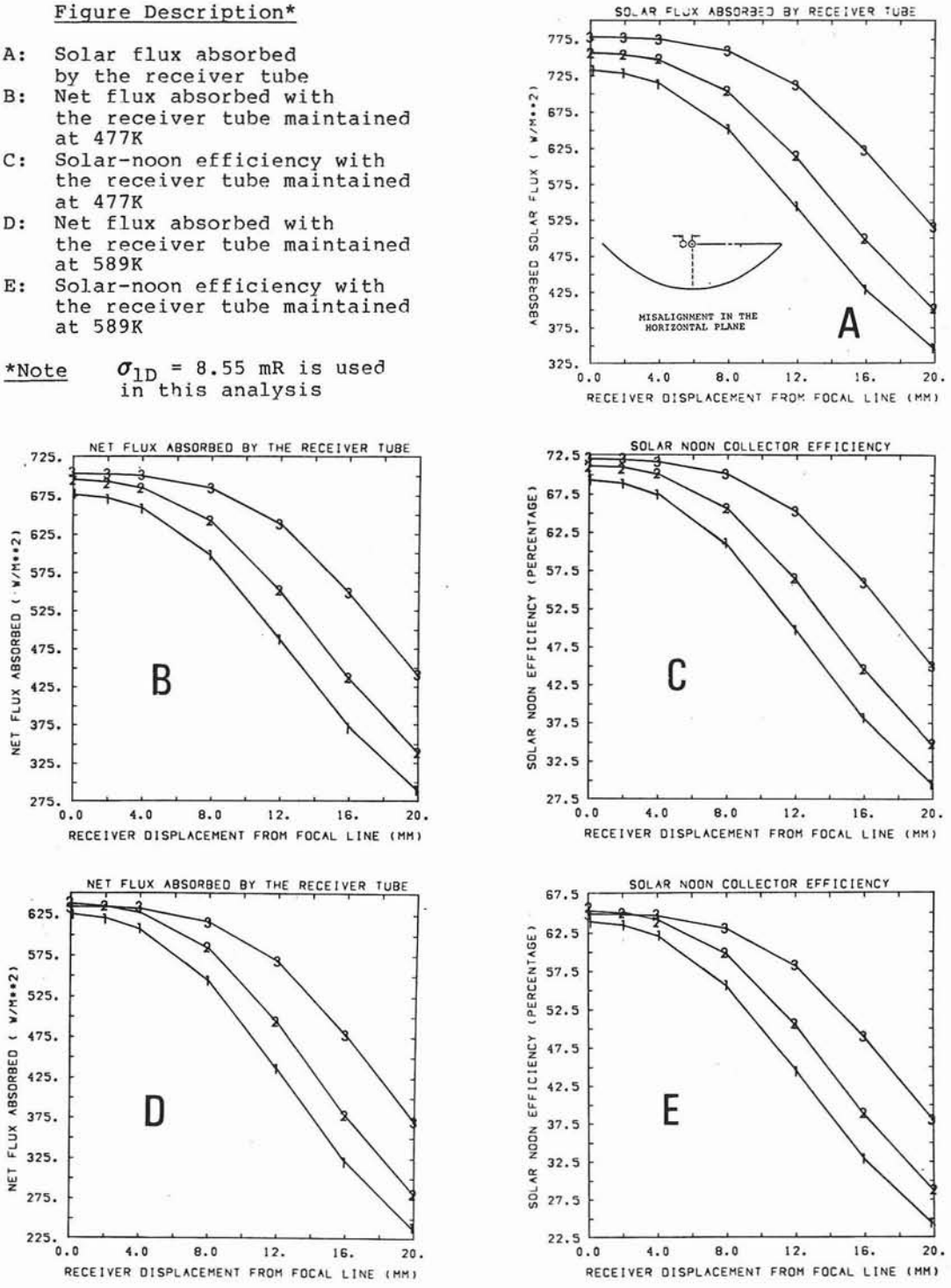

Figure D-7. Horizontal Misalignment of the Receiver Assembly with the One-Dimensional Collector Error Fixed at 8.55 mR--Solar-Noon Results

Figure Description*

A: Solar energy absorbed by the receiver tube
B: Net energy absorbed with the receiver tube maintained at 477K
C: Cumulative efficiency with the receiver tube maintained at 477K
D: Net energy absorbed with the receiver tube maintained at 589K
E: Cumulative efficiency with the receiver tube maintained at 589K

*Note σ_{1D} = 8.55 mR is used in this analysis

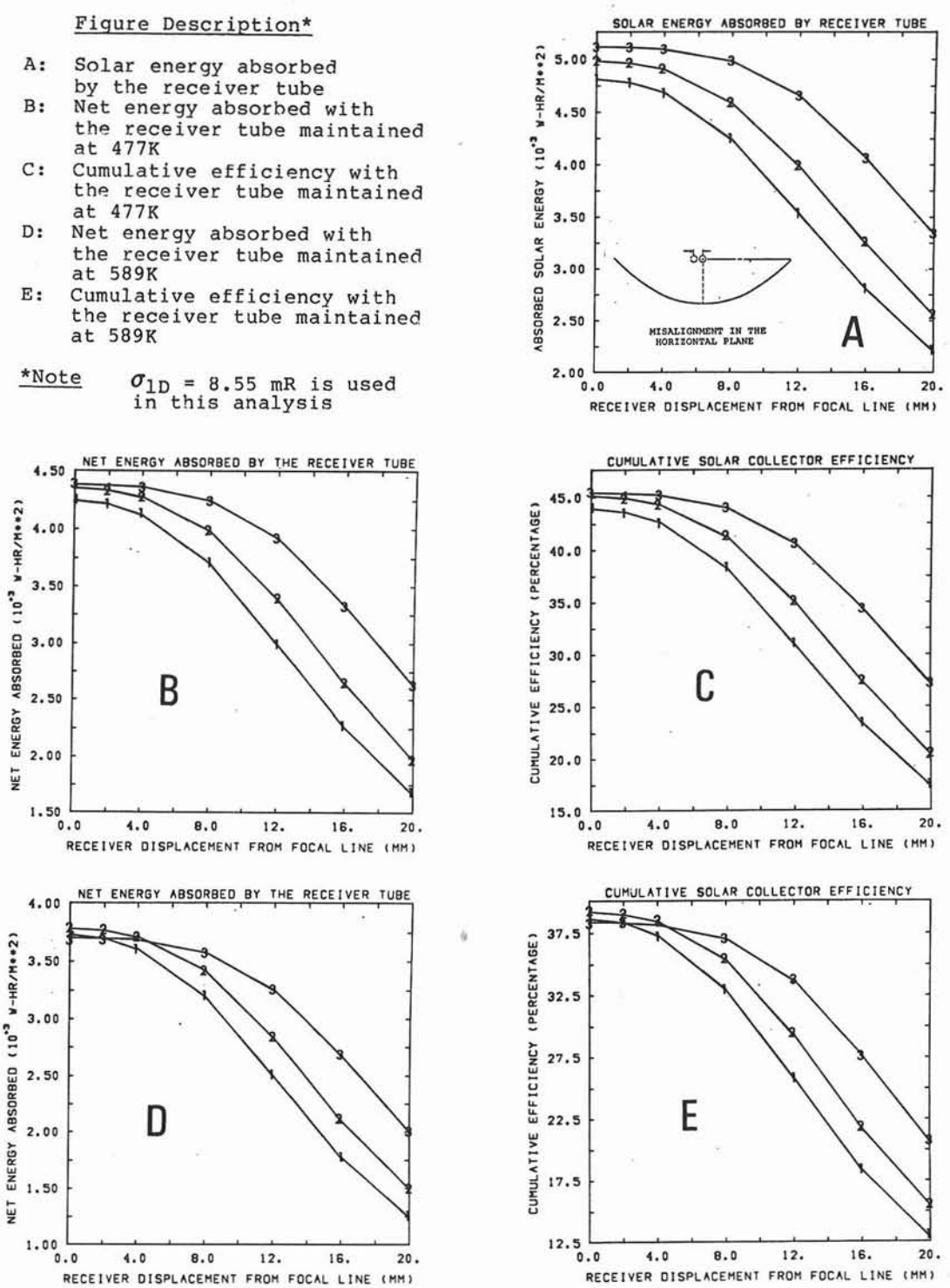

Figure D-8. Horizontal Misalignment of the Receiver Assembly with the One-Dimensional Collector Error Fixed at 8.55 mR--Cumulative Results

(Intentionally left blank)

APPENDIX E

Collector-Trough Tracking Bias

Solar-noon and cumulative performance results are summarized for the baseline parabolic-cylindrical collector, defined in Table I, as a function of collector-trough tracking errors. The analyses use March 15, 1962, weather and insolation conditions, summarized in Figure 8 of the report. Results for two operating temperatures (477K and 589K) and two one-dimensional collector error magnitudes (6.41mR and 8.55mR) are provided for comparative studies.

Data points on the figures designate results from the computer simulation. The following notation is used:

1. 2.223-cm receiver-tube assembly
2. 2.54-cm receiver-tube assembly
3. 3.175-cm receiver-tube assembly

Results presented in the figures of Appendix E are summarized in Table E-I.

TABLE E-I

Collector-Trough Tracking Bias - Summarized Results

Receiver Tube Operating Temperature (K)	One-Dimensional Collector Error (mR)	Type of Result	Figure Showing Results
477 and 589	6.41	Solar Noon	E-1
		Cumulative	E-2
	8.55	Solar Noon	E-3
		Cumulative	E-4

* All other conditions are fixed according to Table I.

Figure Description*

A: Solar flux absorbed by the receiver tube
B: Net flux absorbed with the receiver tube maintained at 477K
C: Solar-noon efficiency with the receiver tube maintained at 477K
D: Net flux absorbed with the receiver tube maintained at 589K
E: Solar-noon efficiency with the receiver tube maintained at 589K

*Note σ_{1D} = 6.41 mR is used in this analysis

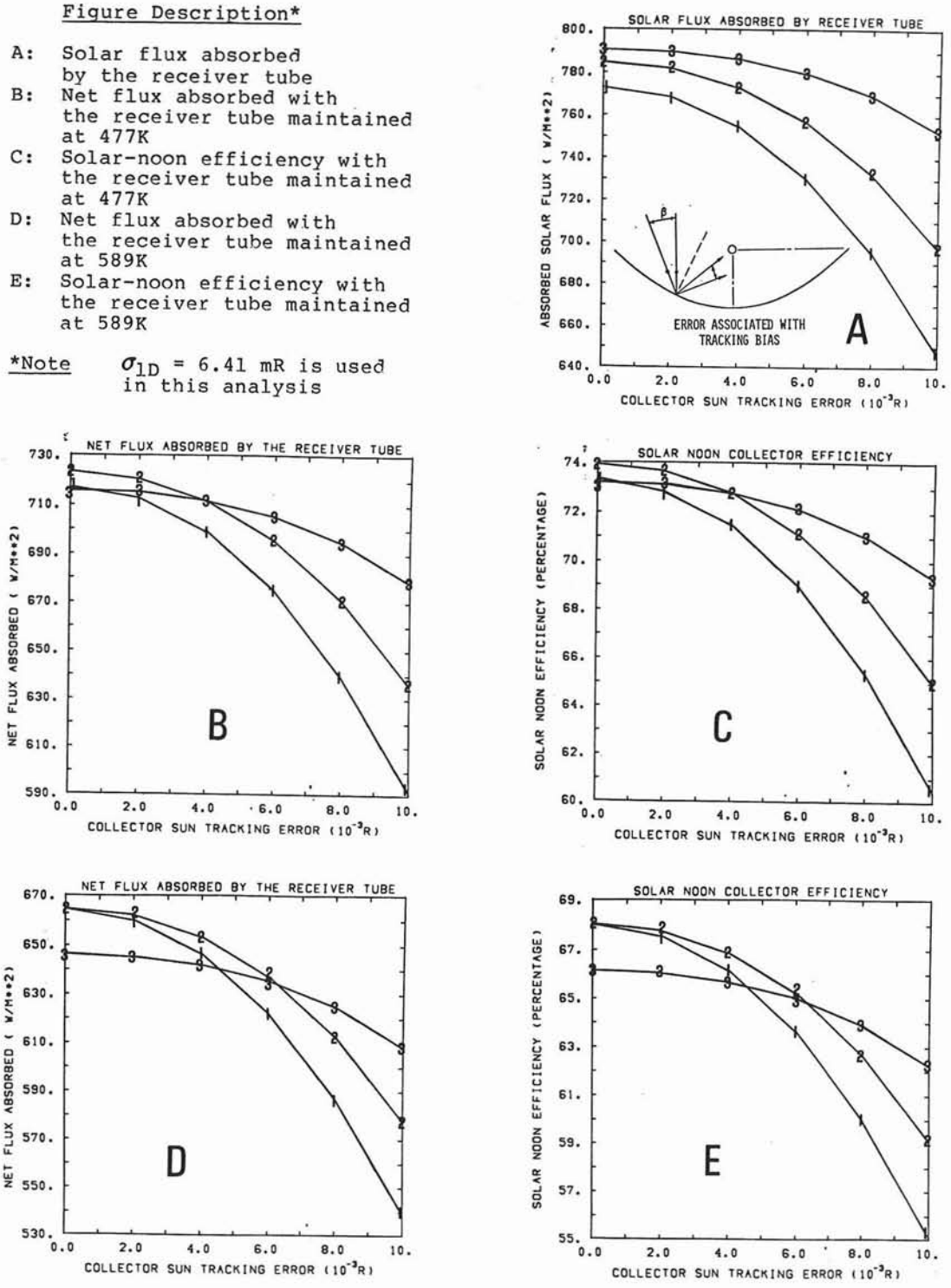

Figure E-1. Tracking Error Variation with the One-Dimensional Collector Error Fixed at 6.41 mR-- Solar-Noon Results

Figure Description*

A: Solar energy absorbed by the receiver tube
B: Net energy absorbed with the receiver tube maintained at 477K
C: Cumulative efficiency with the receiver tube maintained at 477K
D: Net energy absorbed with the receiver tube maintained at 589K
E: Cumulative efficiency with the receiver tube maintained at 589K

*Note σ_{1D} = 6.41 mR is used in this analysis

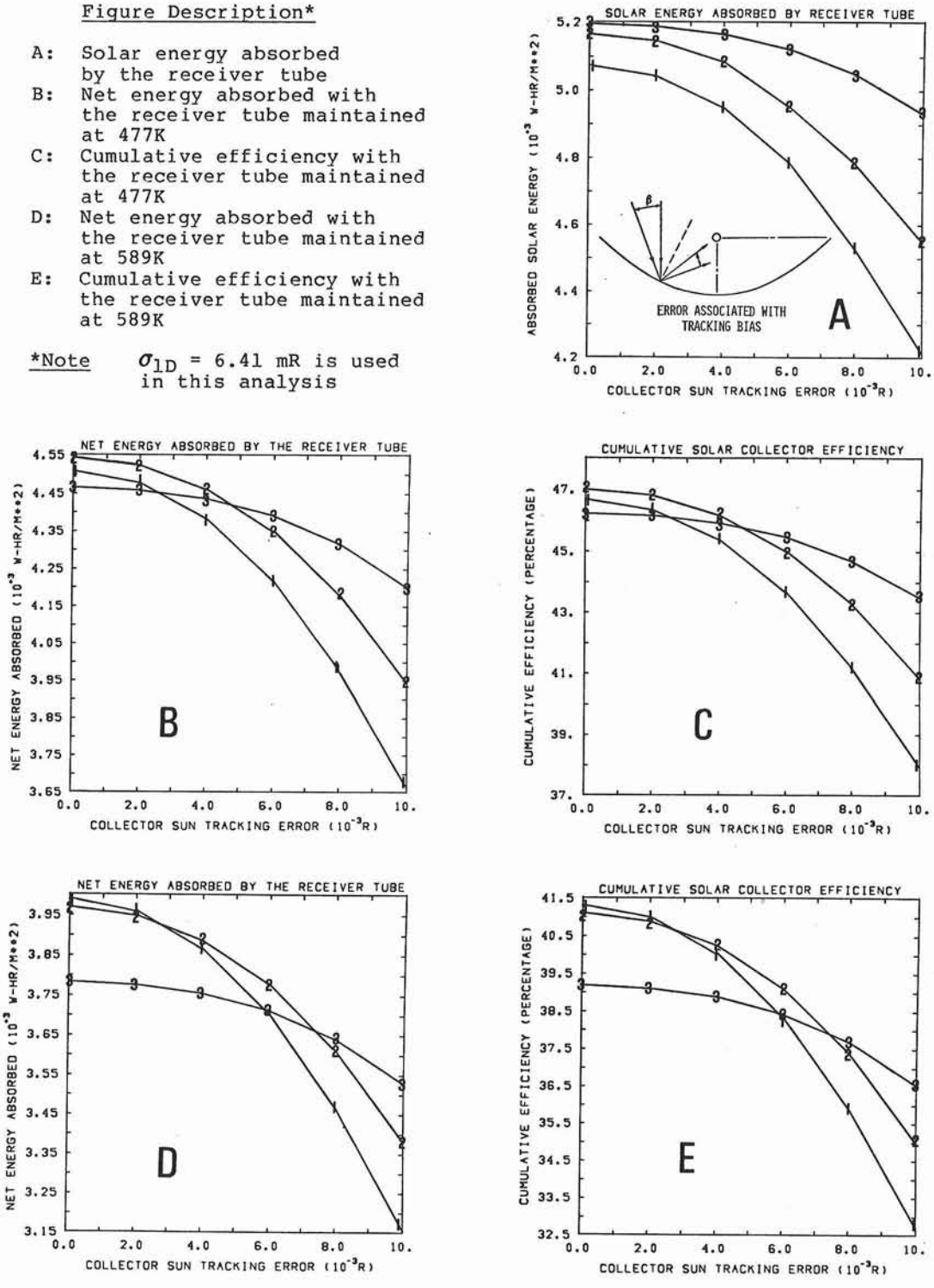

Figure E-2. Tracking Error Variation with the One-Dimensional Collector Error Fixed at 6.41 mR-- Cumulative Results

Figure Description*

A: Solar flux absorbed by the receiver tube
B: Net flux absorbed with the receiver tube maintained at 477K
C: Solar-noon efficiency with the receiver tube maintained at 477K
D: Net flux absorbed with the receiver tube maintained at 589K
E: Solar-noon efficiency with the receiver tube maintained at 589K

*Note σ_{1D} = 8.55 mR is used in this analysis

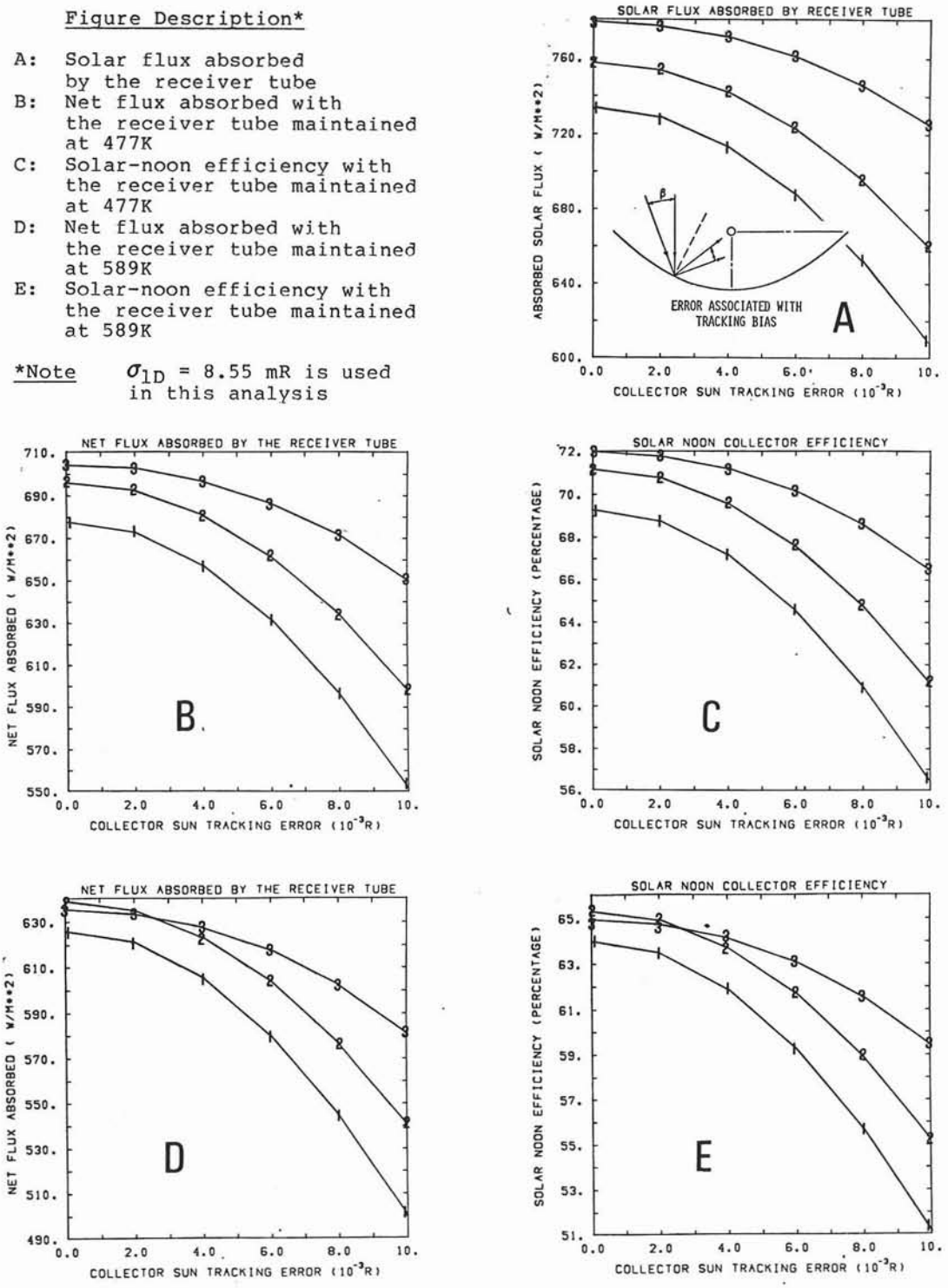

Figure E-3. Tracking Error Variation with the One-Dimensional Collector Error Fixed at 8.55 mR-- Solar-Noon Results

Figure Description*

A: Solar energy absorbed by the receiver tube
B: Net energy absorbed with the receiver tube maintained at 477K
C: Cumulative efficiency with the receiver tube maintained at 477K
D: Net energy absorbed with the receiver tube maintained at 589K
E: Cumulative efficiency with the receiver tube maintained at 589K

*Note σ_{1D} = 8.55 mR is used in this analysis

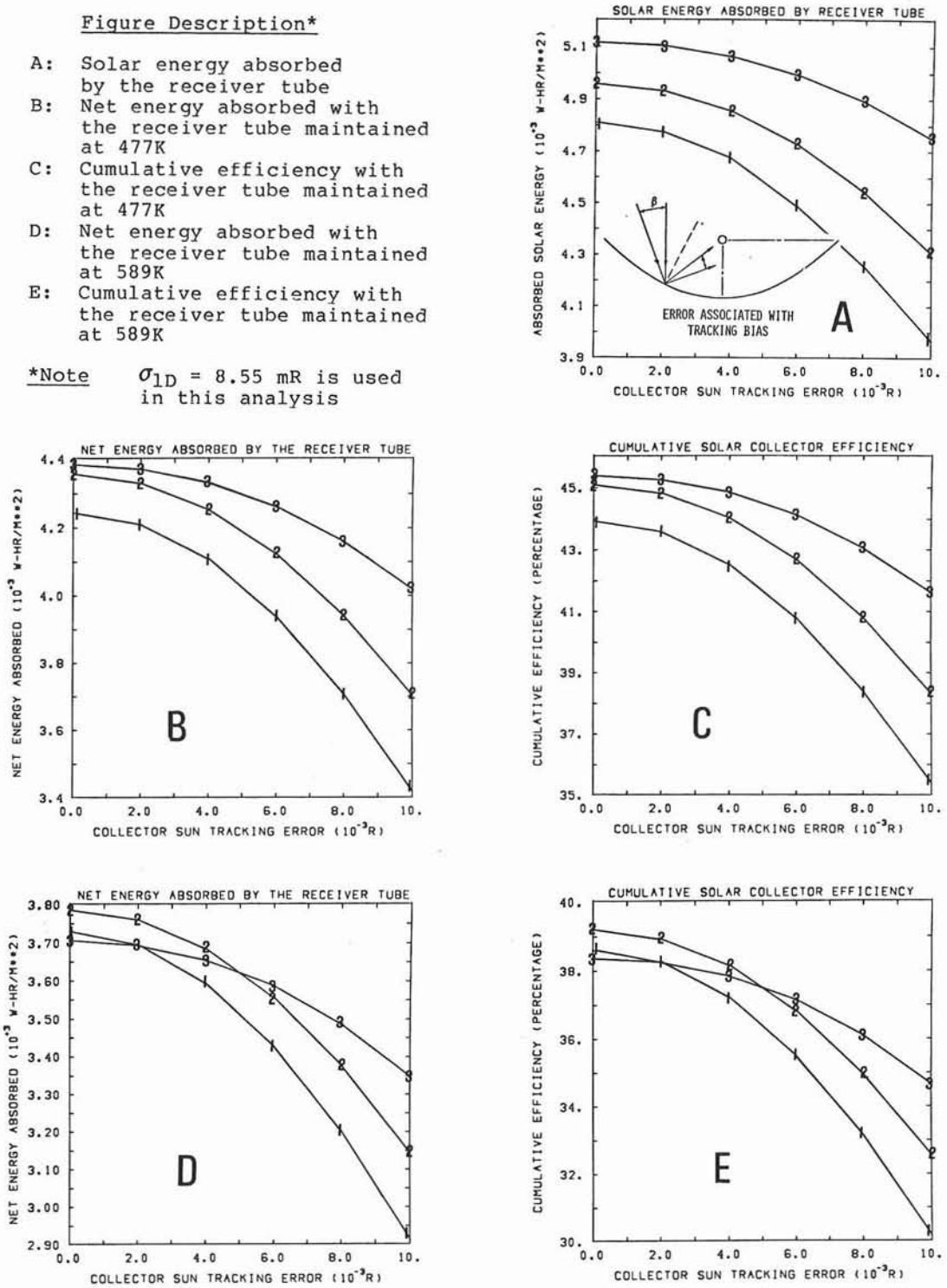

Figure E-4. Tracking Error Variation with the One-Dimensional Collector Error Fixed at 8.55 mR-- Cumulative Results

(Intentionally left blank)

APPENDIX F

Baseline Performance Results for the 2.54-cm Receiver-Tube Assembly

Instantaneous and cumulative baseline performance results for the 2.54-cm receiver tube with the 2-m parabolic-cylindrical collector trough are given for March 15, June 22, and December 21, 1962. Conditions modeled in these analyses are given in Table I, with appropriate weather data summarized in Figures 8, A-1, and A-2, respectively. In addition, results for the variation of (1) receiver tube emissivity, (2) glass transmissivity, trough reflectivity, and receiver solar absorptivity and (3) wind velocity are presented for the 2.54-cm receiver assembly. These studies incorporate weather conditions for March 15, 1962, and baseline conditions of Table I.

Data points on the figures designate results from the computer simulation. The following notation is used:

1. 2.223-cm receiver-tube assembly
2. 2.54-cm receiver-tube assembly
3. 3.175-cm receiver-tube assembly

Results presented in the figures of Appendix F are summarized in Table F-I.

TABLE F-I

2.54-cm Receiver Assembly Collector Design Performance Results*

Type of Analysis	Day of Analysis	Figure Showing Results
Baseline Collector Performance	March 15	F-1
	June 22	F-2
	December 21	F-3
Receiver Tube Emissivity at 589K Varied	March 15	F-4
Collector Solar Radiative Properties Varied	March 15	F-5
Wind Velocity Varied	March 15	F-6

* All other conditions are fixed according to Table I.

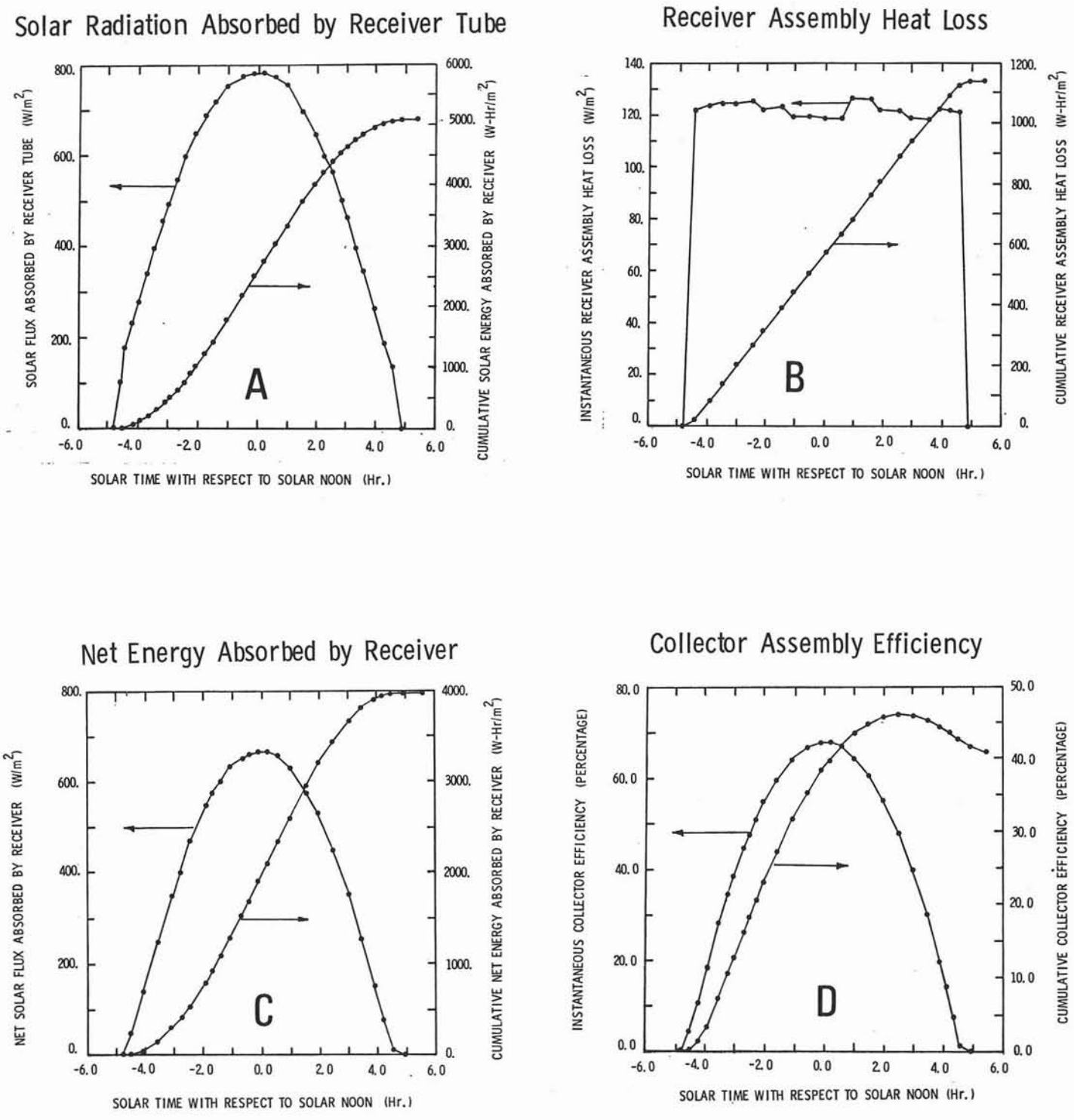

Figure F-1. March 15, 1962 Collector Baseline Performance Results Using the 2.54 cm Receiver Tube Assembly

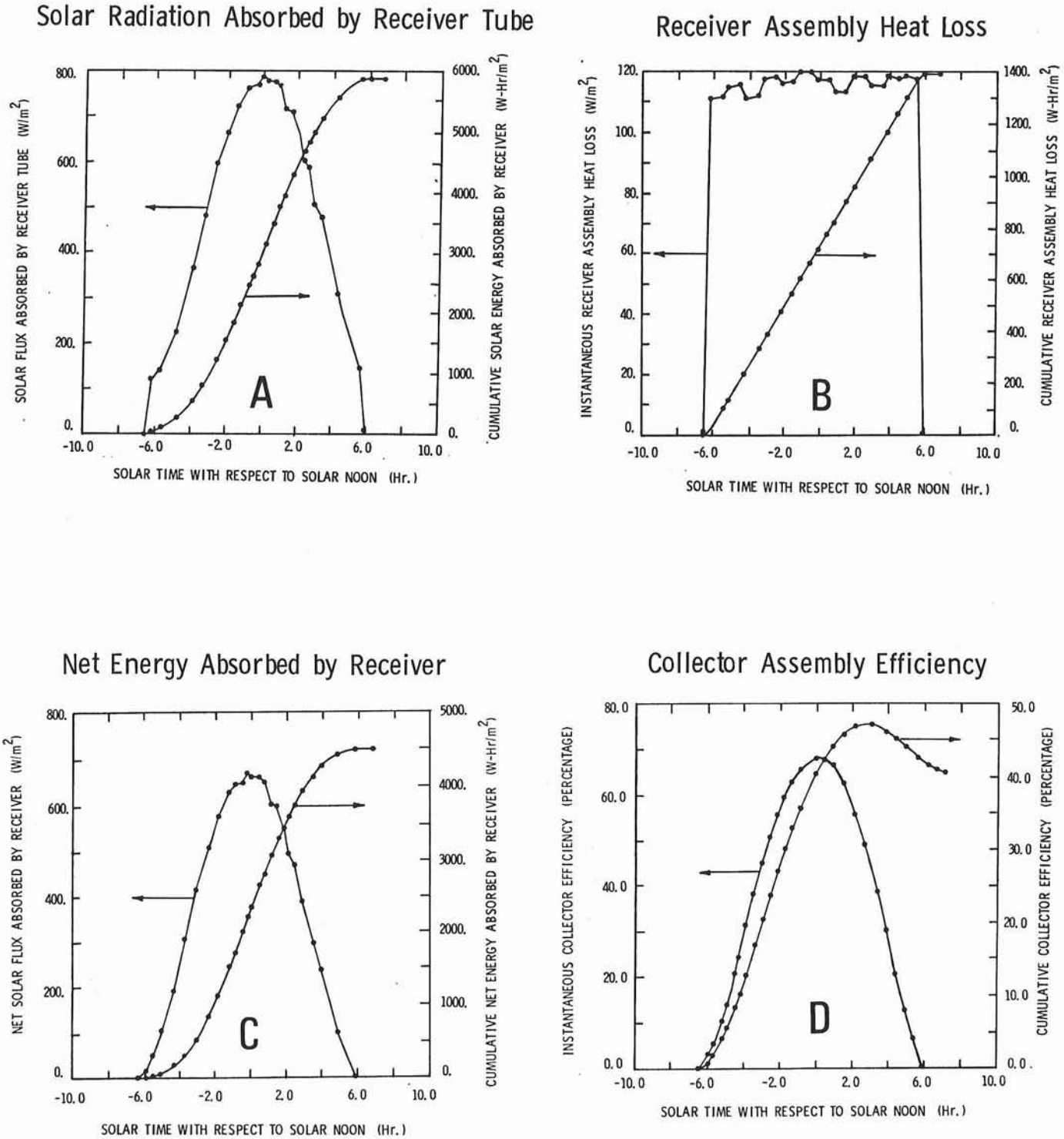

Figure F-2. June 22, 1962 Collector Baseline Performance Results Using the 2.54 cm Receiver Tube Assembly

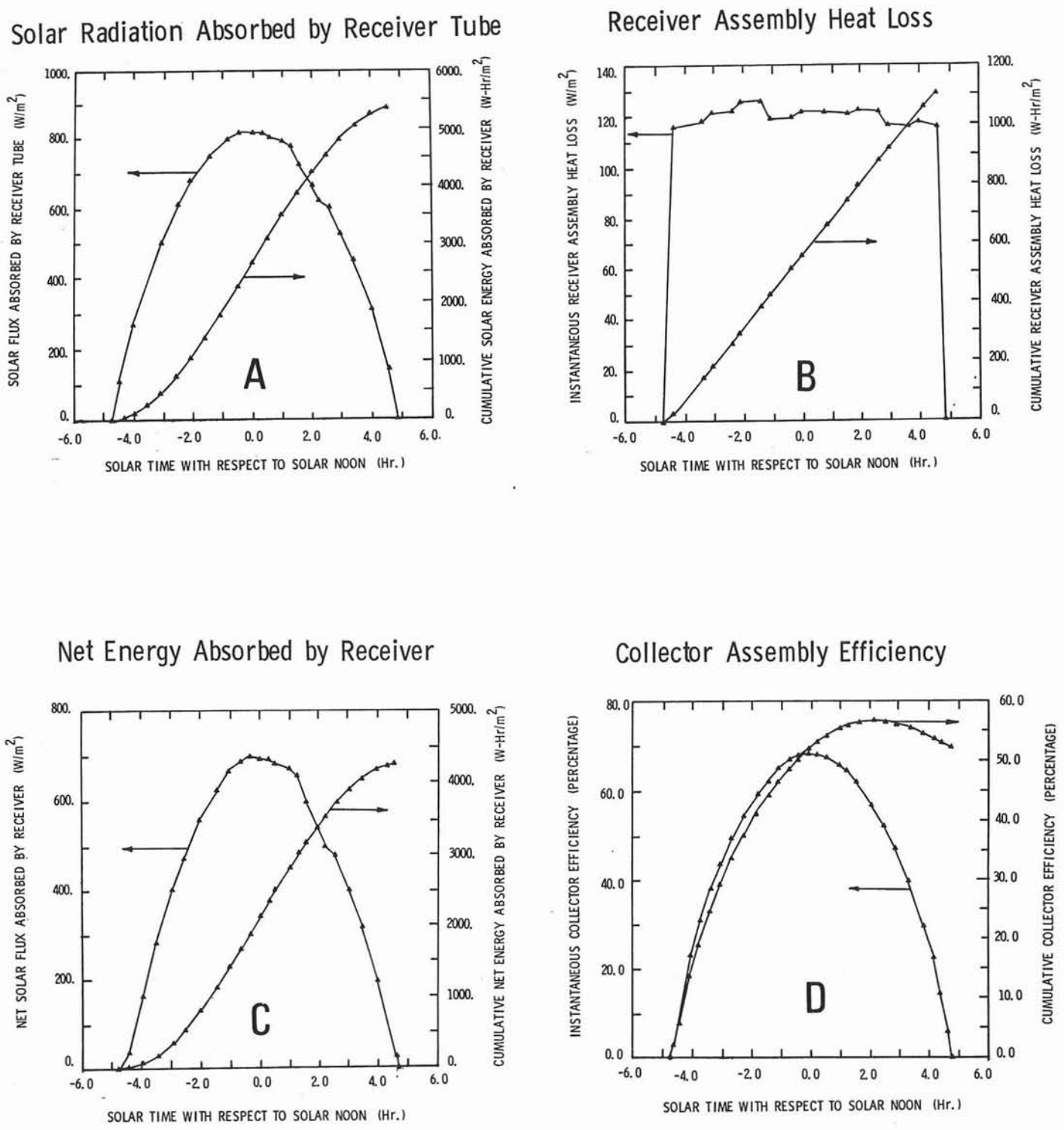

Figure F-3. December 21, 1962 Collector Baseline Performance Results Using the 2.54 cm Receiver Tube Assembly

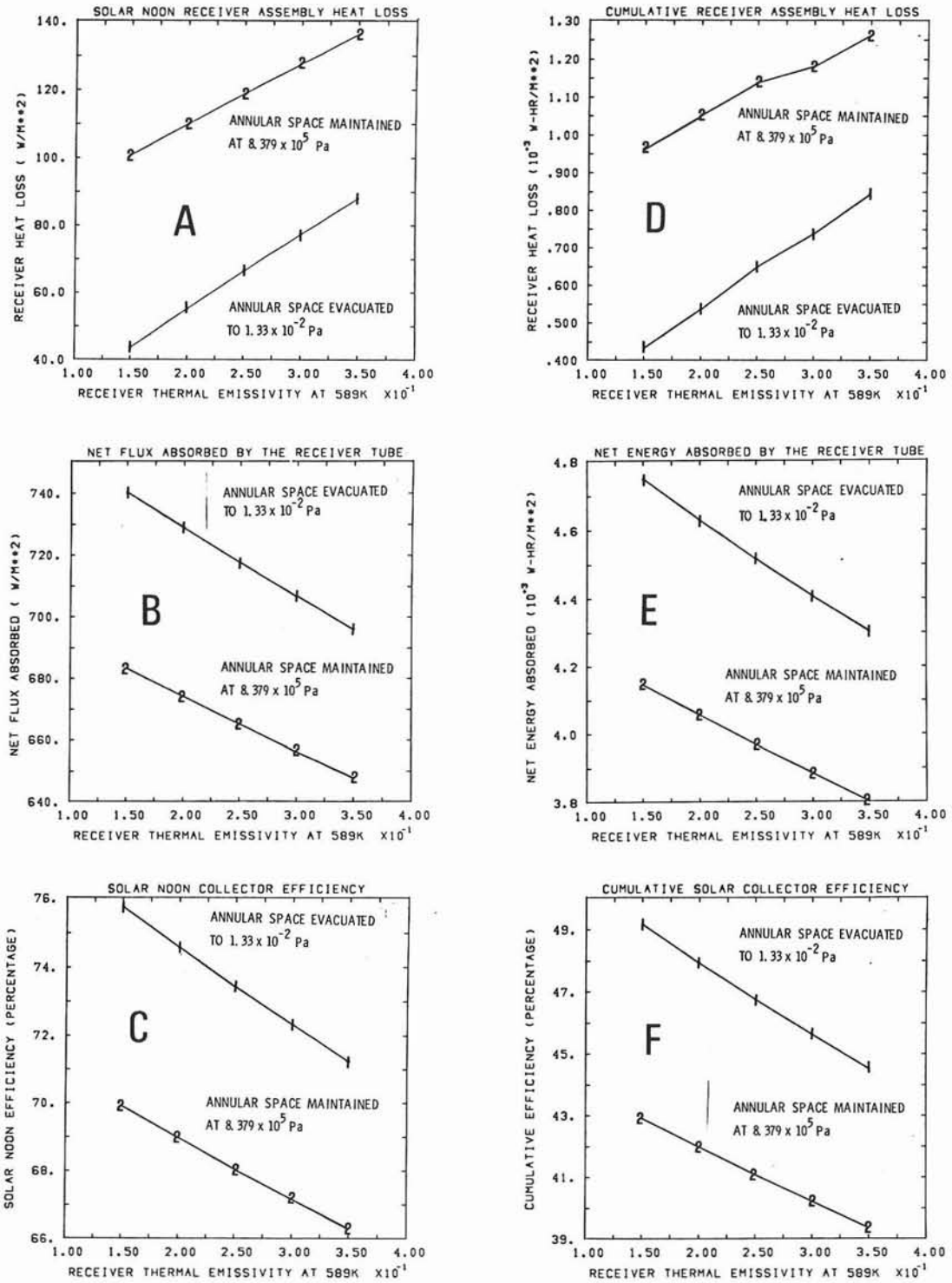

Figure F-4. Variation of Black-Chrome Thermal Emissivity Characteristics with the 2.54 cm Receiver Tube Maintained at 589K-- March 15, 1962 Collector Baseline Performance Results

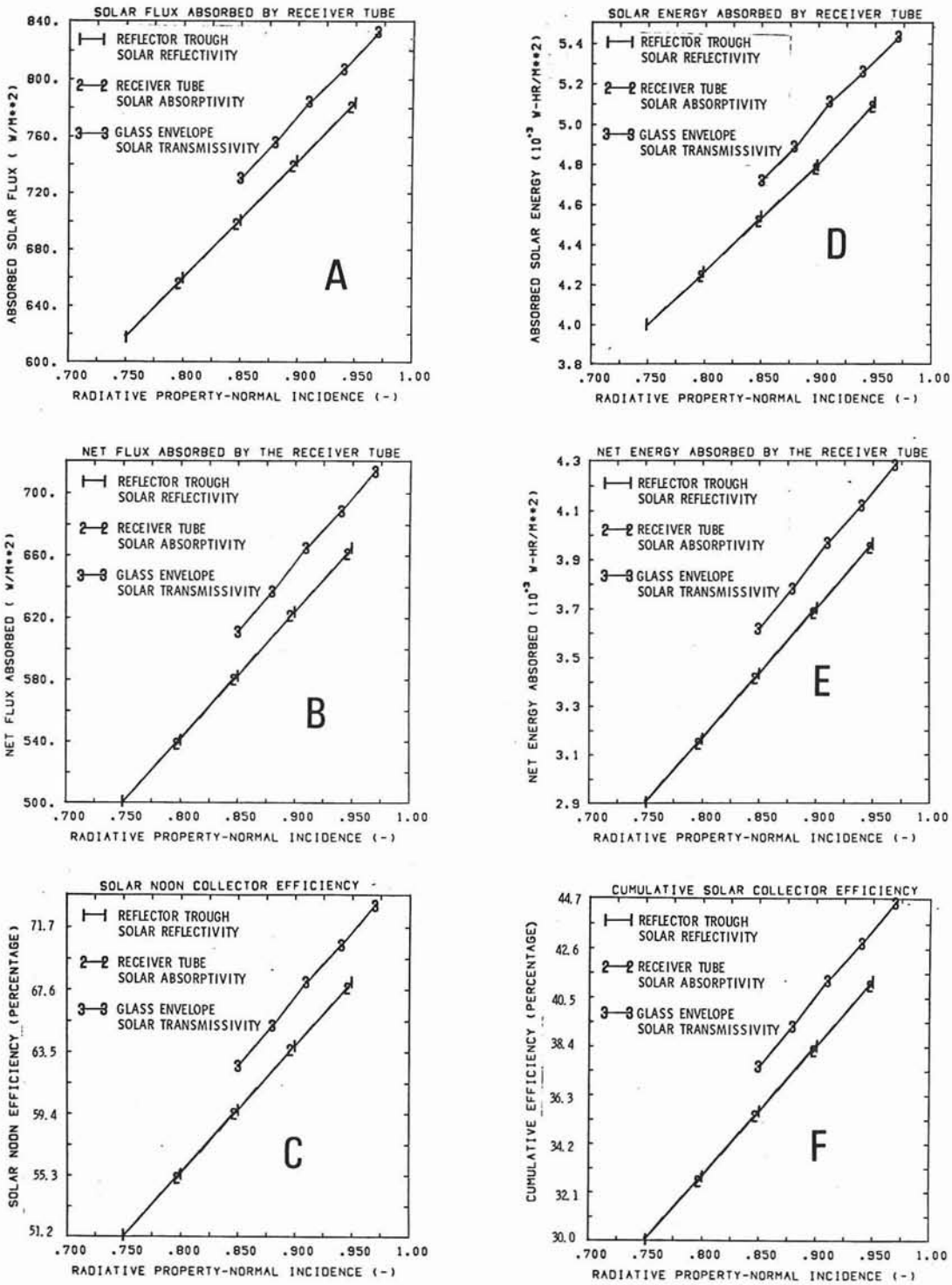

Figure F-5. Variation of the Collector Solar Radiative Properties with the 2.54 cm Receiver Tube Maintained at 589K--
March 15, 1962 Collector Baseline Performance Results

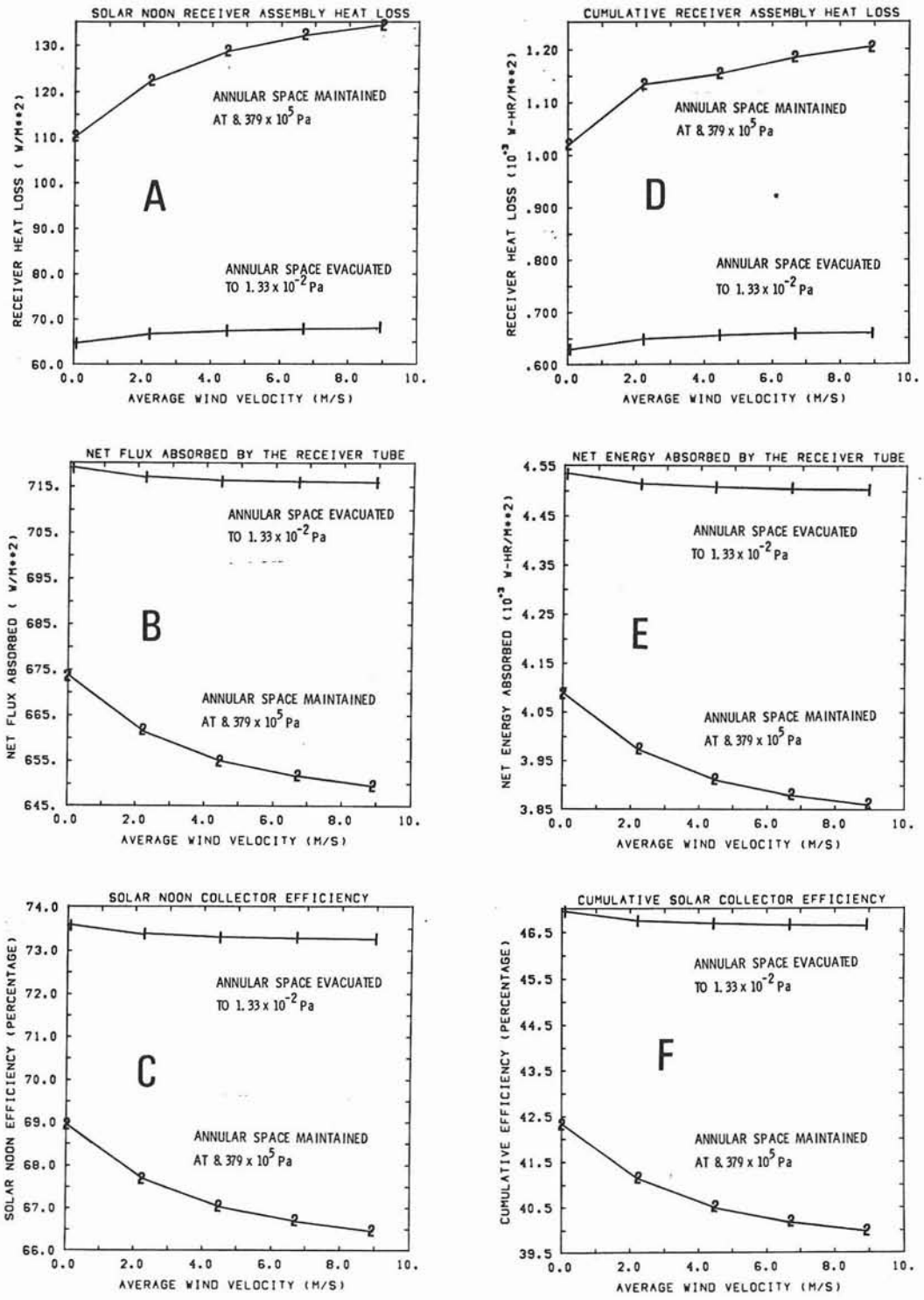

Figure F-6. Variation of All-Day Wind Velocity with the 2.54 cm Receiver Tube Maintained at 589K-- March 15, 1962 Collector Baseline Performance Results

Distribution:
TID-4500-R66, UC-62(268)

Acurex Aerotherm
485 Clyde Avenue
Mountain View, CA 94042
Attn: G. J. Neuner

Budd Company
Fort Washington, PA 19034
Attn: W. W. Dickhart

Ford Aerospace and Communications
3939 Fabian Way
Palo Alto, CA 94303
Attn: H. J. Sund

Ford Glass Division
300 Renaissance Center
P. O. Box 43343
Detroit, MI 48243
Attn: P. Bender

Del Manufacturing Co.
905 Monterey Pass Road
Monterey Park, CA 91754
Attn: M. M. Delgado

Exxon Enterprises
P. O. Box 192
Florham Park, N. J. 07932
Attn: A. L. Shrier

Harrison Radiator Division
General Motors
Lockport, N. Y.
Attn: A. Stocker

Hexcel
11711 Dublin Blvd.
Dublin, CA 94566
Attn: George P. Branch

Jacobs-Del Solar Systems, Inc.
251 South Lake Avenue
Pasadena, CA 91101
Attn: C. F. Roos

Jet Propulsion Laboratory (2)
4800 Oak Grove Drive
Pasadena, CA 91103
Attn: V. C. Truscello
K. Selcuk

McDonnell Douglas Astronautics Co.
5301 Bolsa Avenue
Huntington Beach, CA 92647
Attn: J. Rogan

Solar Energy Research Institute (2)
1536 Cole Blvd.
Golden, CO 80401
Attn: B. Gupta
B. L. Butler
F. Kreith
K. J. Touryan

Solar Kinetics Inc.
P. O. Box 10764
Dallas, TX 75207
Attn: Gus Hutchison

Suntec Systems Inc.
21405 Hamburg Avenue
Lakeville, MN 55044
Attn: J. H. Davison

Technical Center
General Motors
Warren, MI
Attn: J. Britt

Union Carbide Corp.
P. O. Box X
Oak Ridge, Tenn. 37830
Attn: C. G. Lawson

U. S. Department of Energy (2)
Argicultural & Industrial
Process Heat
Conservation & Solar Application
Washington, D. C. 20545
Attn: W. W. Auer
J. Dollard

U. S. Department of Energy (2)
Albuquerque Operations Office
P. O. Box 5400
Albuquerque, NM 87185
Attn: D. K. Nowlin
G. N. Pappas

U. S. Department of Energy (3)
Division of Central Solar Tech.
Washington, D. C. 20545
Attn: M. U. Gutstein
J. E. Rannels
M. E. Resner

U. S. Department of Energy
San Francisco Operations Office
1333 Broadway
Oakland, CA 94612
Attn: W. D. Nettleton

2320 K. Gillespie
2323 C. M. Gabriel
2323 S. B. Martin
3161 J. E. Mitchell
3700 J. C. Strassell
4000 A. Narath
4231 J. H. Renken
4231 F. Biggs
4700 J. H. Scott
4710 G. E. Brandvold
4714 R. P. Stromberg
4719 D. G. Schueler
4720 B. L. Dugan
4721 J. V. Otts
4722 J. F. Banas (25)
4722 R. L. Champion
4722 B. Stiefield
4722 G. W. Treadwell
4723 D. O. Lee
4723 L. L. Lukens
4723 R. R. Peters
4723 W. P. Schimmel
4725 J. A. Leonard
5000 J. K. Galt
5500 O. E. Jones
5510 D. B. Hayes
5512 R. Beraun
5512 M. E. Fewell
5512 R. J. Gross
5512 C. E. Hackett
5512 C. E. Hickox
5512 A. C. Ratzel (15)
5512 C. E. Sisson
5520 T. B. Lane
5530 W. Herrmann
8266 E. A. Aas
8450 R. C. Wayne
3141 T. L. Werner (5)
3151 W. L. Garner (3)
For DOE/TIC
(Unlimited Release)